Appendix A: VSP Data and Interpretations

Walkaway tests were performed at site #1 (line 1A, which was interpreted from modeling to be outside the paleochannel), and site #3 (line 2A) where a paleochannel is suggested (Figure 1). The walkaway test spreads were deployed near the well cluster at site #1. The 96 receivers for the P-wave experiment were laid parallel to Roosevelt, each separated by 0.6 m. The highest signal-to-noise reflection interpretable within the depth range of interest possesses a vertically incident time of about 45 to 50 msec (Figure A1). Comparisons of the geometric shape and arrival time of this proposed reflection with theoretical hyperbolic curves suggest excellent correlation to a reflector at a depth of about 27 to 33 m and an NMO velocity of around 640 m/sec. From velocity check shots (uphole survey) at site #1 the average velocity to 30 m was just over 640 m/sec. It is therefore justified to be cautiously optimistic that this curved arrival is a primary reflection from about 30 m.

The downhole 30.06 possesses the highest signal-to-noise ratio and resolution potential of the three sources tested at site #1 (Figure A1). The 200 Hz analog low-cut filter applied to all the sources dramatically reduces the ground roll and the 100 Hz refraction "ring." The sledge hammer produced a seismogram with nearly equivalent reflection signature and frequency content as the downhole 30.06 when the 200 Hz analog low-cut filter was applied (Figure A2). The dominant negative characteristics of the sledge hammer were the ratio of air-coupled wave to reflection energy, the potential for inconsistent source energy, surface coupling, and the slight degradation of resolution potential due to stacking. The auger gun was much too energetic and possessed a lower reflection frequency bandwidth, likely as a direct result of the higher level of energy release (Knapp and Steeples, 1986) (Figure A3). Reflections from beneath the Castle Hayne are very evident on auger gun data regardless of acquisition filters. An increase in upper corner frequency of the reflection bandwidth, higher dominant frequency, and a more minimum phase source wavelet was more evident on shot gathers from the downhole 30.06 than either the sledge hammer or auger gun after the application of a digital filter (Figures A4, A5, and A6). This is especially true of the records that were recorded with a 200 Hz analog filter. Analog filtering seems to provide slightly higher resolution potential than nearly equivalent digital filtering. This pre-A/D spectral shaping allows the full dynamic range of the 15-bit seismograph to exploited. Analysis of compressional wave tests at site #1 lead to the recommendation that production data be acquired with the downhole 30.06 fired into shallow holes and recorded with 200 Hz analog low-cut filters, 100 Hz geophones, a source and receiver spacing of 0.6 m, and 24-fold redundancy.

Testing at site #3 (line 2A) was not as extensive as at site #1 due mainly to the results and recommendations developed from testing at site #1 (the auger gun was not tested at this site). The increased time and source-to-receiver offset of the direct and refracted wave cross-over at site #3 in comparison to site #1 is evidence of either a thicker low velocity near-surface layer or a dramatic decrease

in compressional wave velocity. Consistent with site #1, the ratio of air-coupled wave to reflections is lower with the downhole 30.06 (Figure A7) than the sledge hammer (Figure A8). A well-developed reflection with a zero offset time of about 50 msec is evident on seismograms from all three sources. Examination of reflections on digitally filtered 200 Hz analog low-cut filter data leaves little doubt that the downhole 30.06 possesses the highest resolution and signal-to-noise ratio potential of the sources tested at this site (Figures A9 and A10). The ratio of air-coupled wave to reflection energy is a very important criteria at this site when considering that a large portion of the near-vertically incident reflection energy returning from reflectors within the depth range of interest will arrive after the air-coupled wave. Based on the optimum reflection recording window, the ineffectiveness of digital filtering to enhance reflections arriving after ground roll or air-coupled waves on sledge hammer data, the need for maximum coherency of the shallowest reflections, a low signal-to-noise ratio on sledge hammer data, and the extremely small optimum reflection window for reflection returning from depths less than 25 m, the downhole 30.06, 0.6 m receiver shot and receiver spacing, and 200 Hz analog low-cut filter were selected as optimum for this site and target.

Shear waves were tested at site #1 in hopes of improving the resolution potential. This potential for improved resolution of shear wave data over compressional wave data is directly related to the slower phase velocity of shear (S) waves in comparison to compressional (P) waves in the same sediments. Few sources with truly high quality broadband horizontally polarized shear wave production have been identified (Miller et al., 1992). For this test a modified wood block (steel plates on the ends to avoid deformation and spikes for ground coupling) was aligned perpendicular to the survey line and struck on the ends with a 7.3 kg sledge hammer. Source impacts from both directions were collected onto each shot gather according to source-to-receiver offset. Shear wave receivers were deployed with orientations sensitive to motion perpendicular to the survey line. The data were gathered together according to common shot location with the polarity of the right-to-left shot reversed. This display format allows visual separation of the polarized nature of S-waves and permits easy separation of the shear waves from compressional waves. Little in the way of confidently interpretable reflected energy is present on S-wave gathers regardless of analog filter settings (Figures A11, A12, A13, and A14). Some suggestion of curved arrivals is visible within very narrow time/offset windows. An abundance of Love wave and mode converted energy is evident. The very limited apparent bandwidth and low signal-to-noise ratio is likely responsible for the inability of S-wave energy to produce high-confidence interpreted reflections on seismograms. The lack of any confident reflection arrival forced discontinuation of S-wave testing and eliminated S-waves as a viable approach to image the proposed bedrock channel.

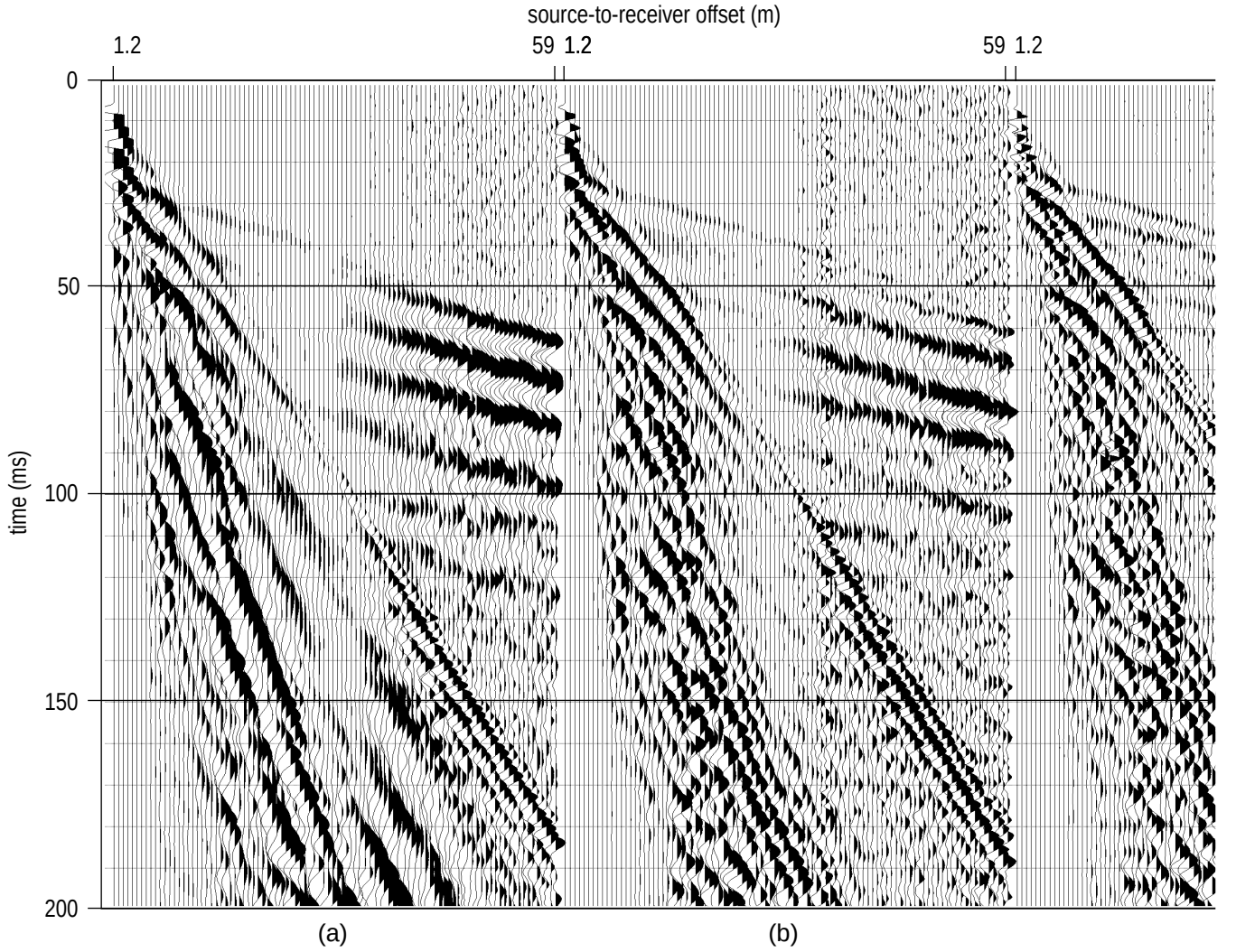

Figure A1a. Walkaway field files from site #1 using downhole 30.06 recorded with (a) no analog low-cut filter, (b) 100 Hz, and (c) 200 Hz.

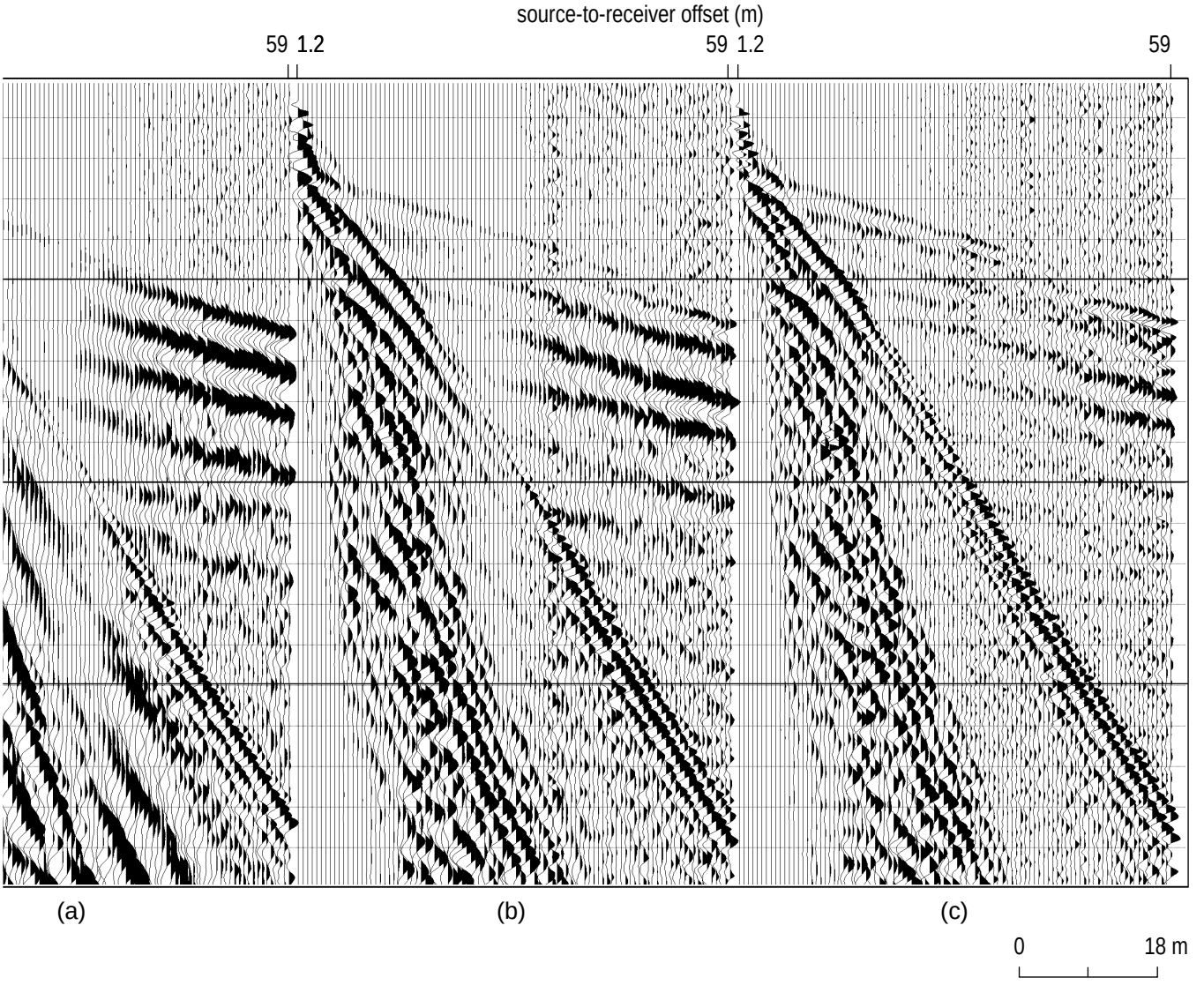

Figure A1b.

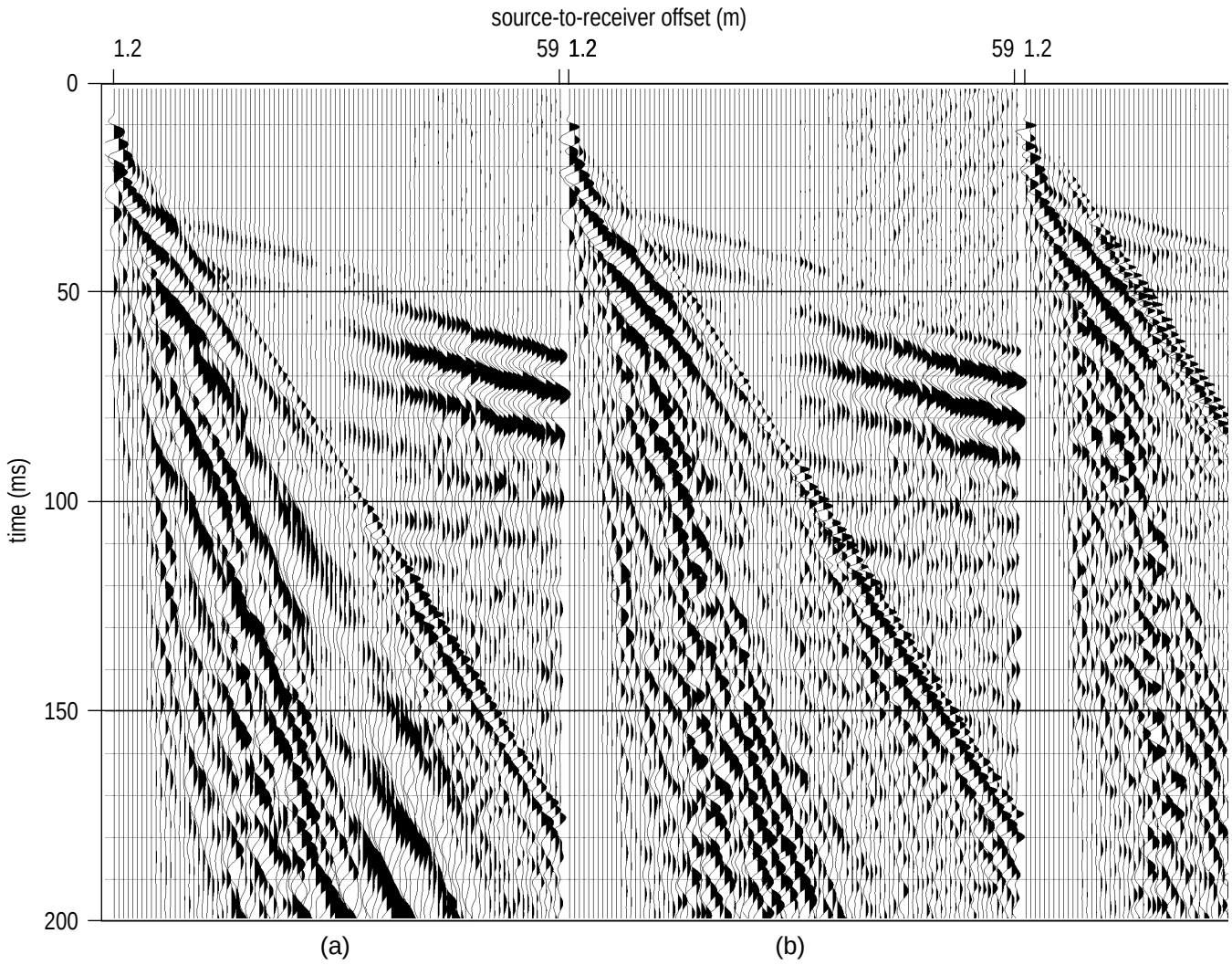

Figure A2a. Walkaway field files from site #1 using sledgehammer recorded with low-cut filter (a) out, (b) 100 Hz, and (c) 200 Hz.

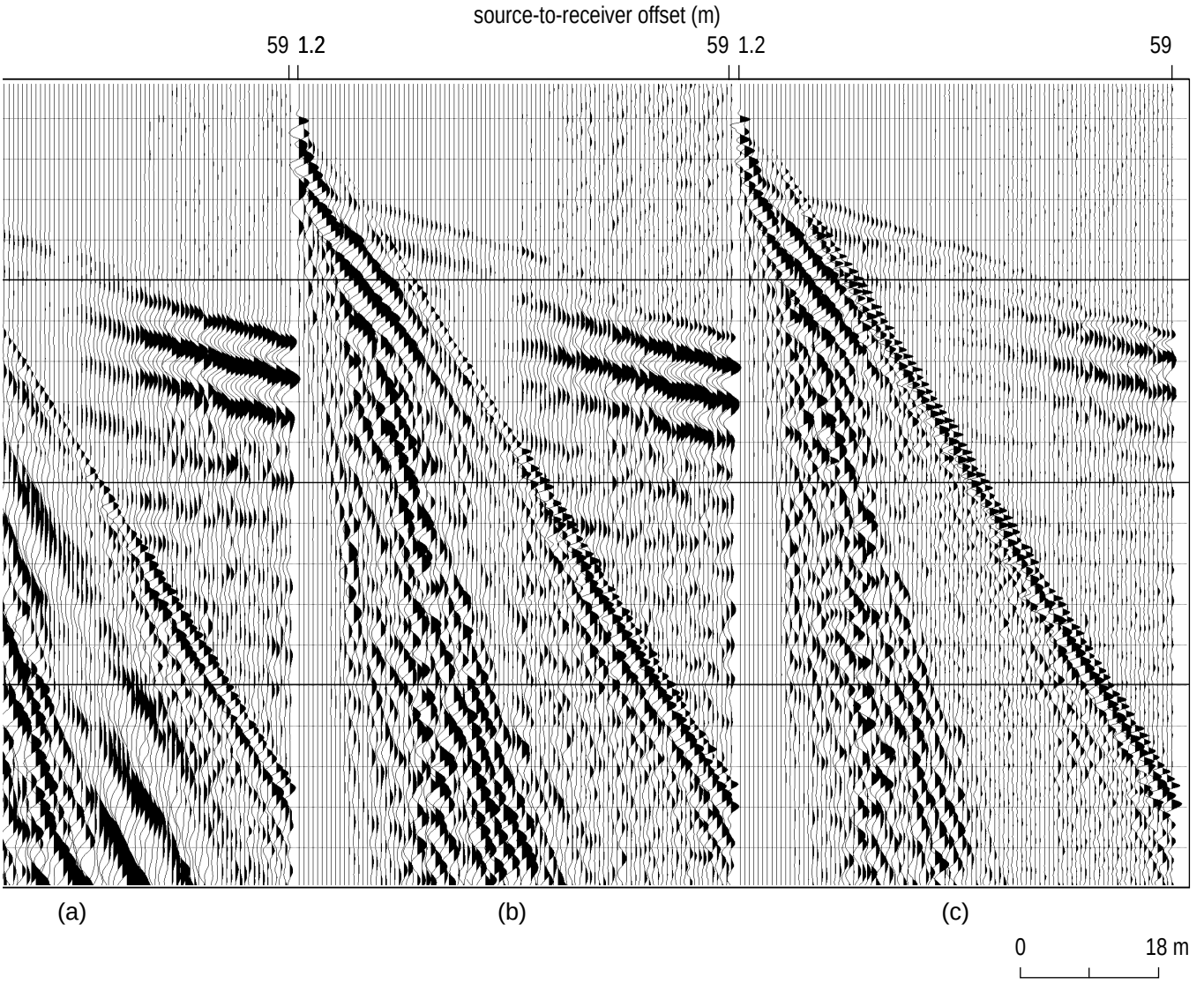

Figure A2b.

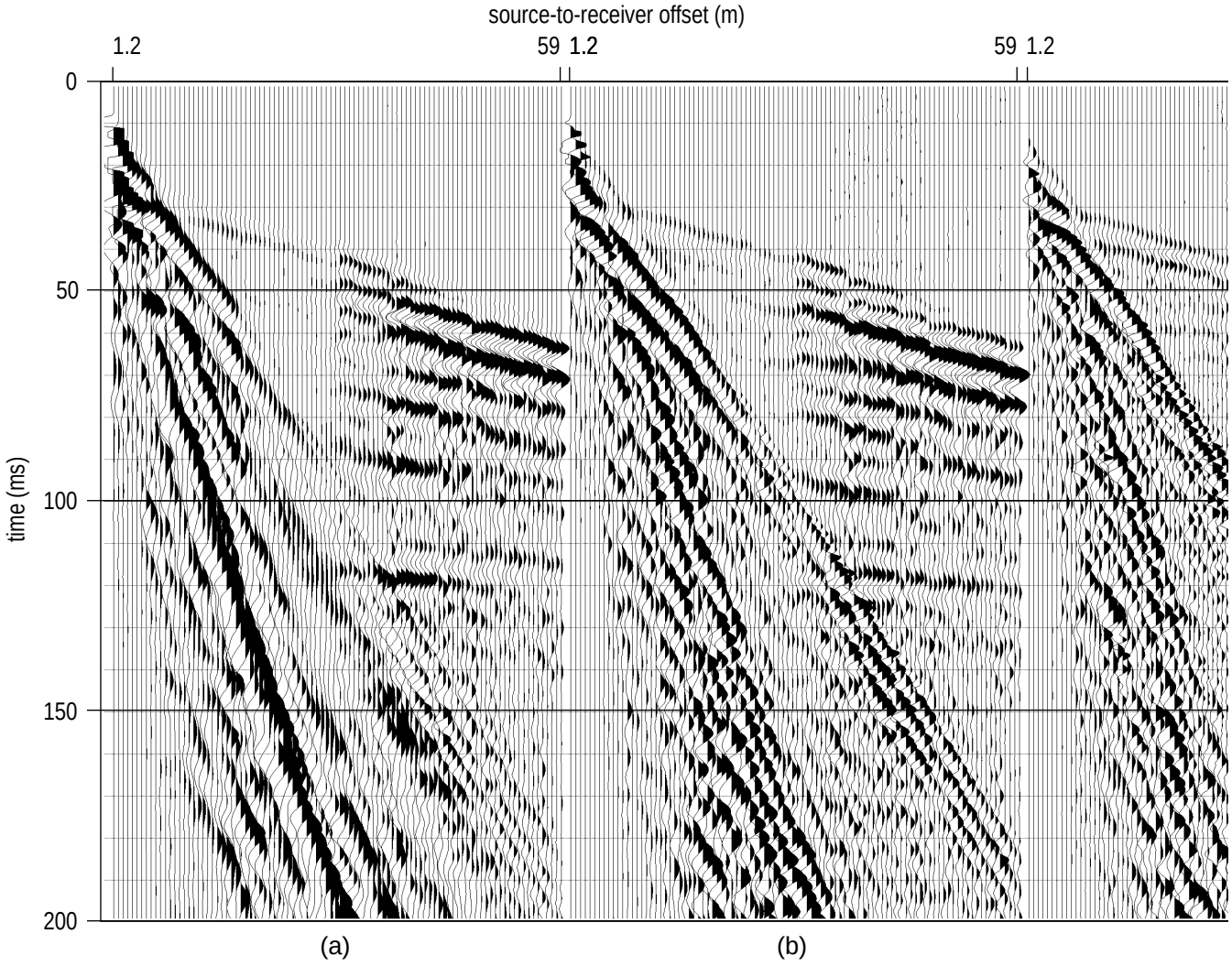

Figure A3a. Walkaway field files from site #1 using 12-gauge auger gun recorded with low-cut filter (a) out, (b) 100 Hz, and (c) 200 Hz.

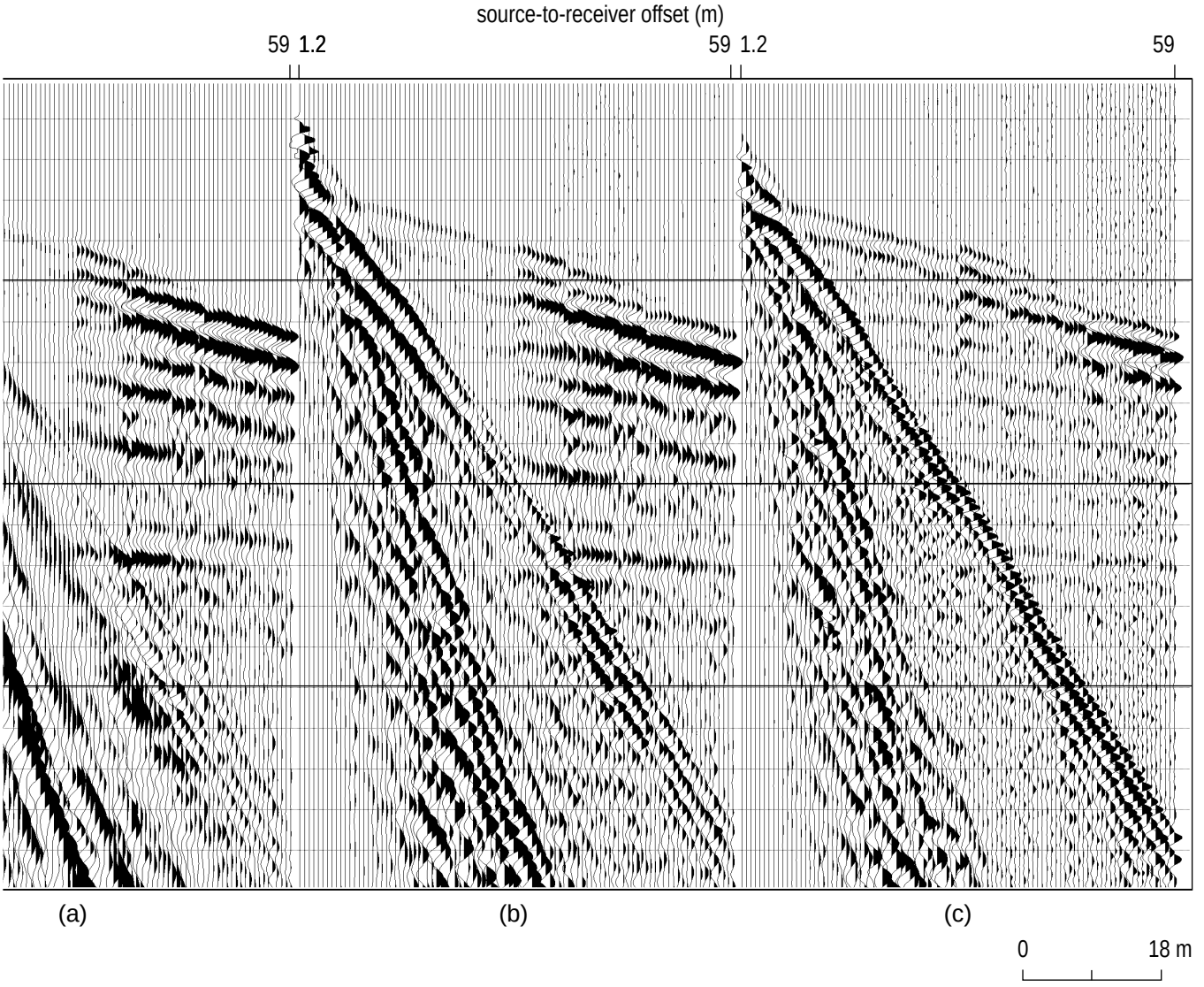

Figure A3b.

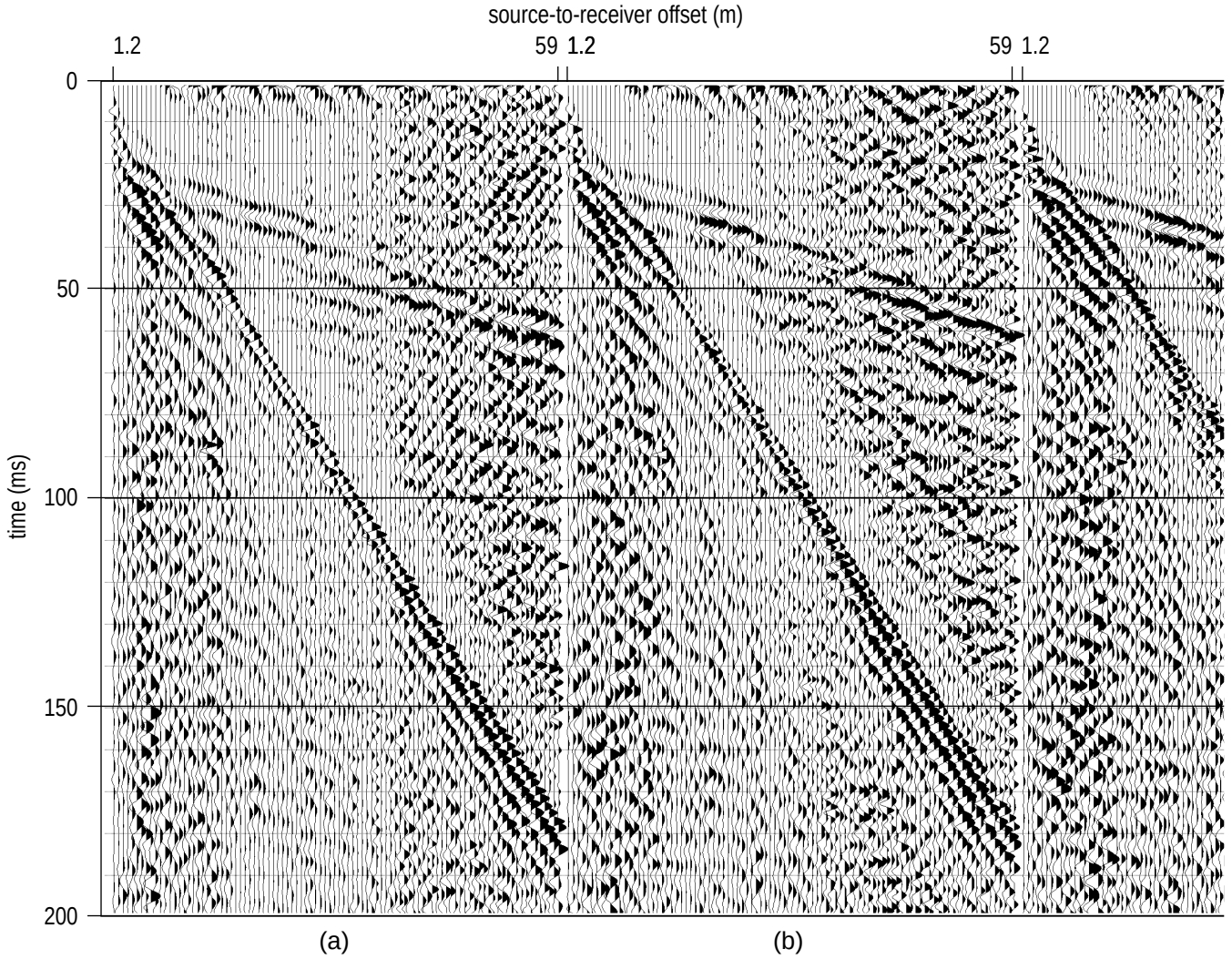

Figure A4a. A 100-200-400-600 digital filter applied to files from Figure A1.

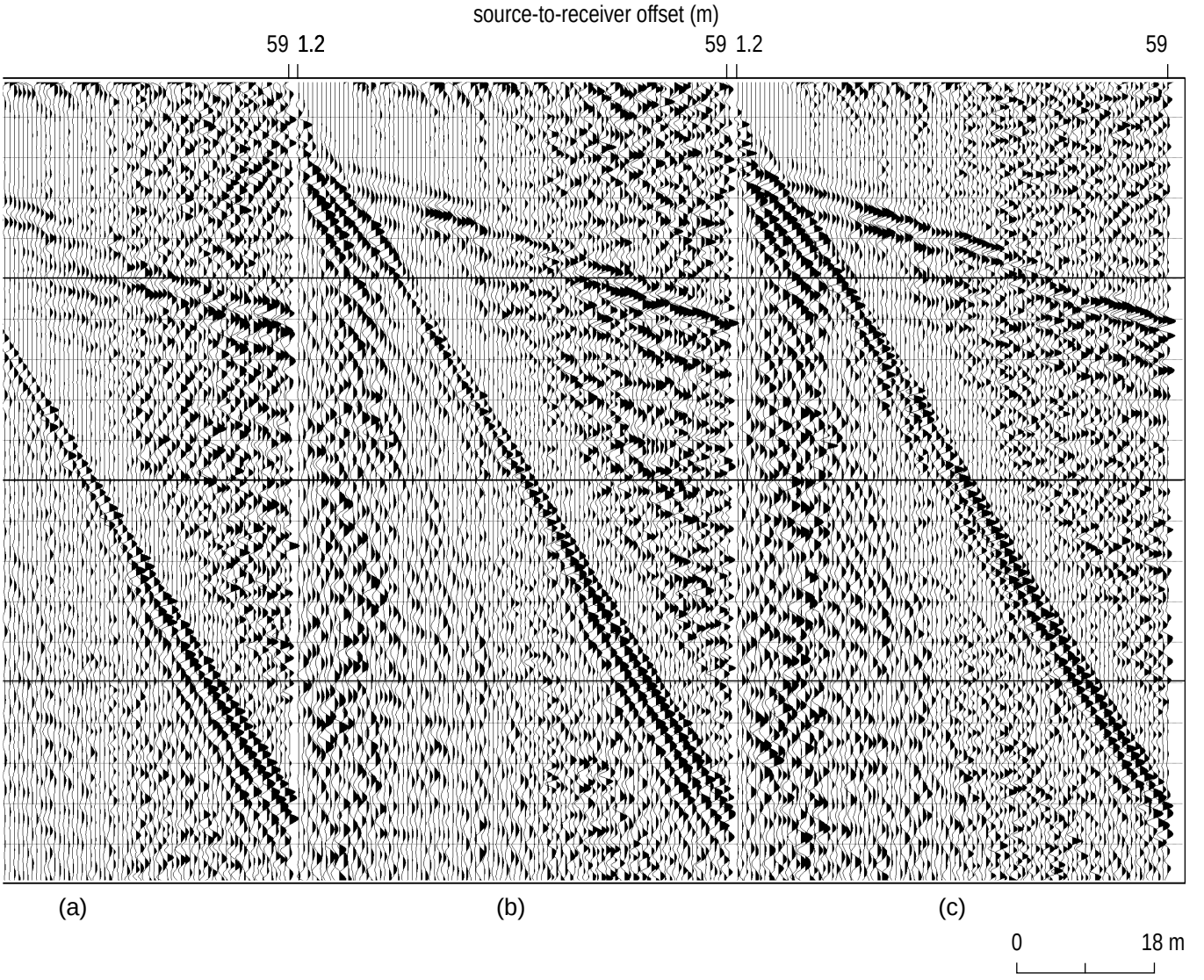

Figure A4b.

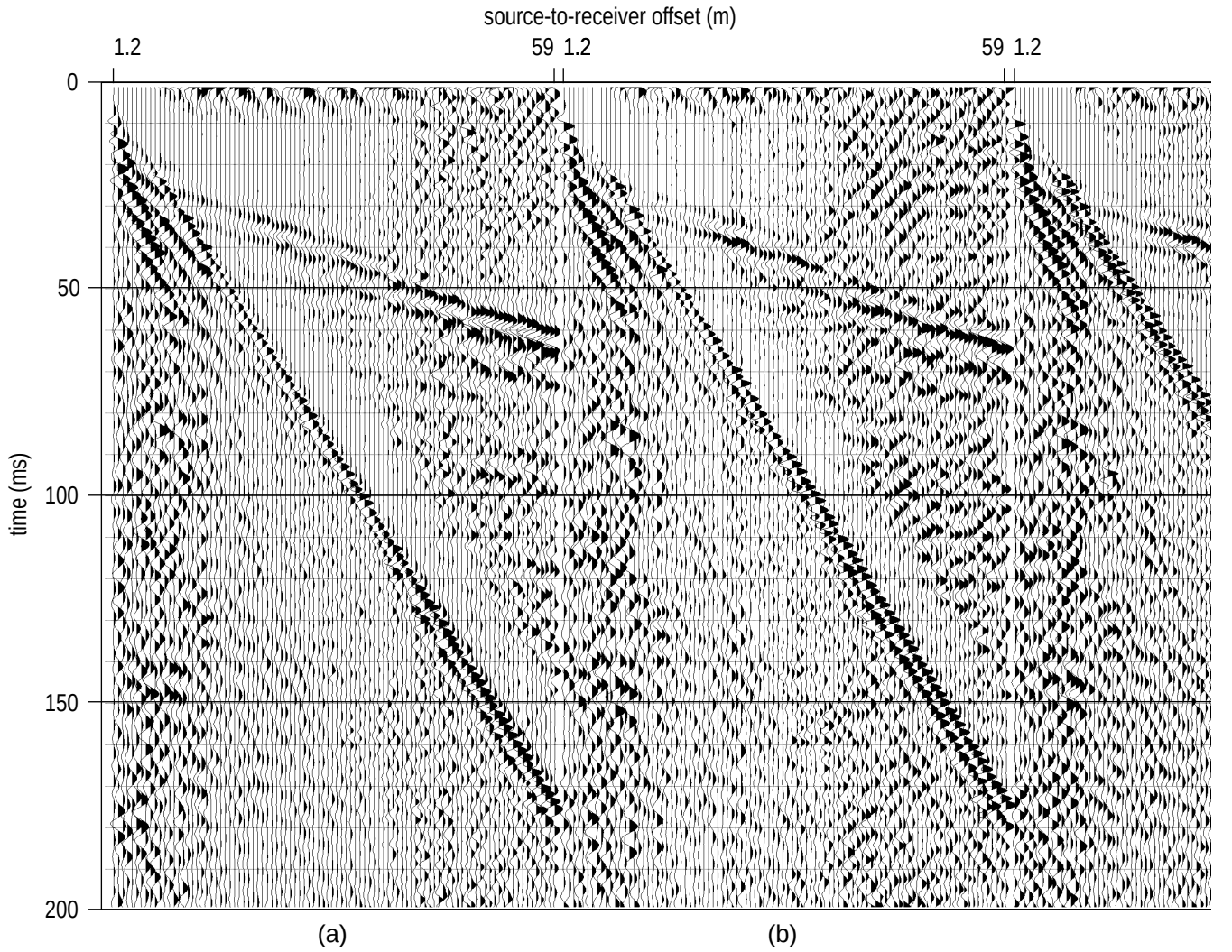

Figure A5a. A 100-200-400-600 digital filter applied to files from Figure A2.

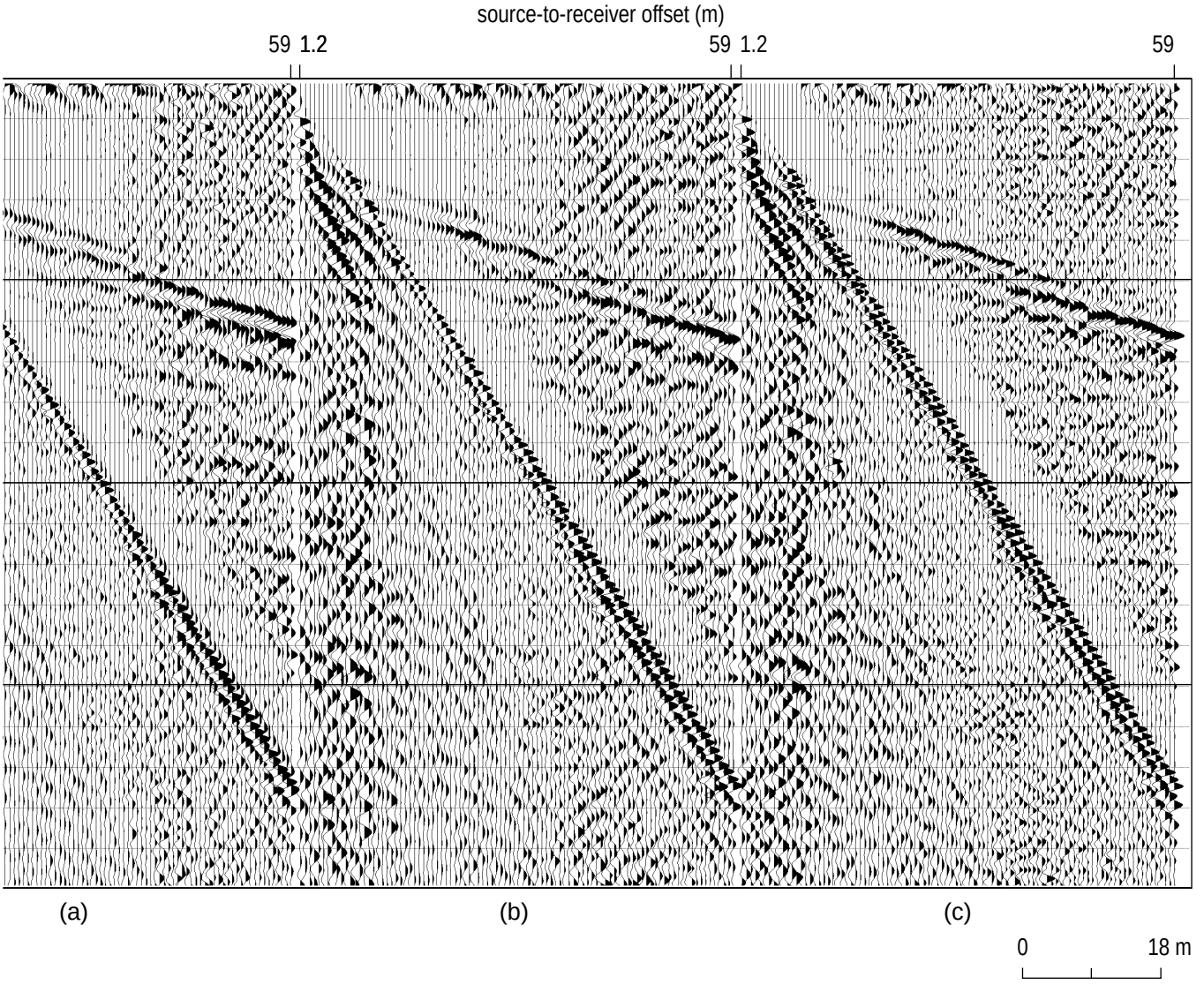

Figure A5b.

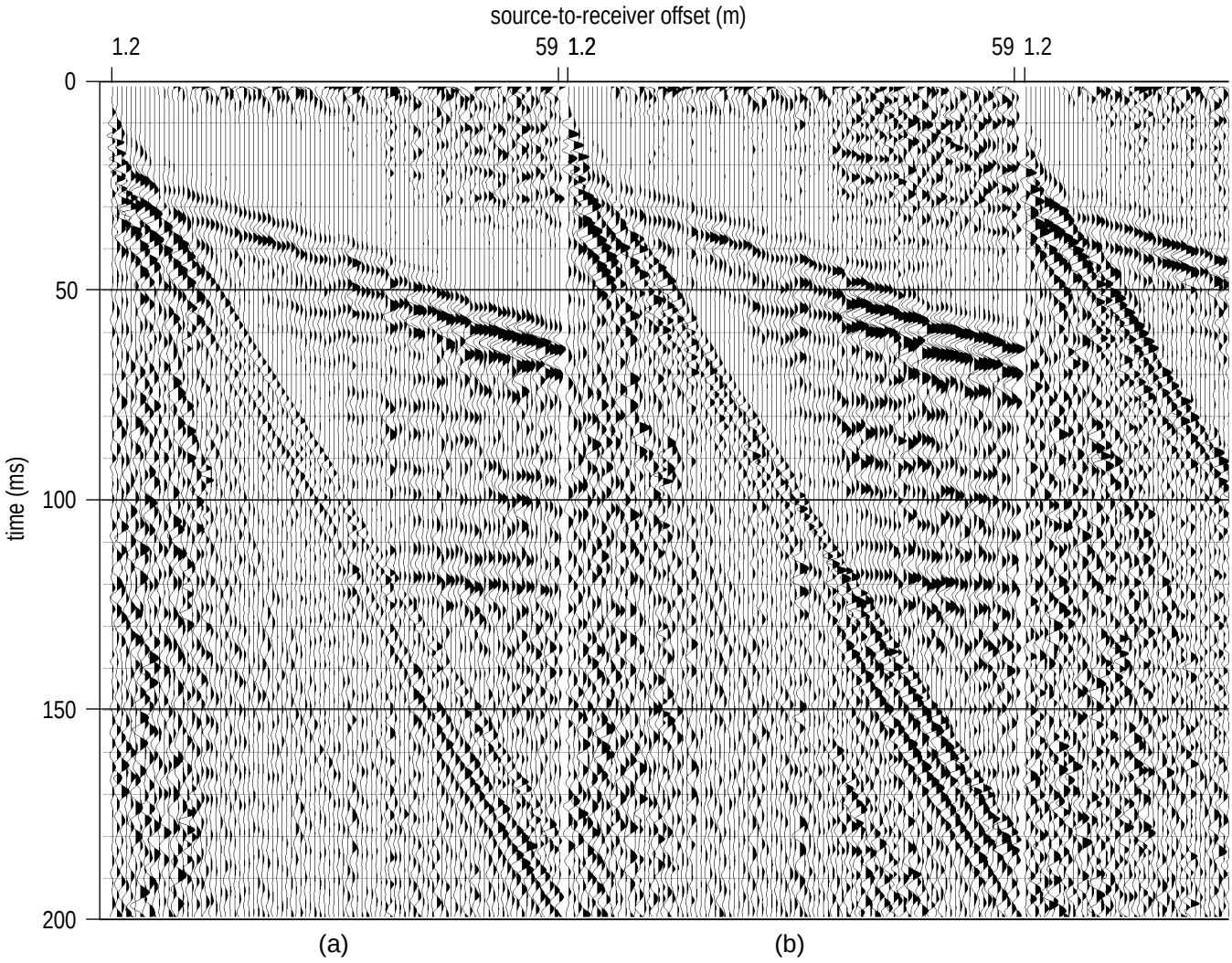

Figure A6a. A 100-200-400-600 digital filter applied to files from Figure A3.

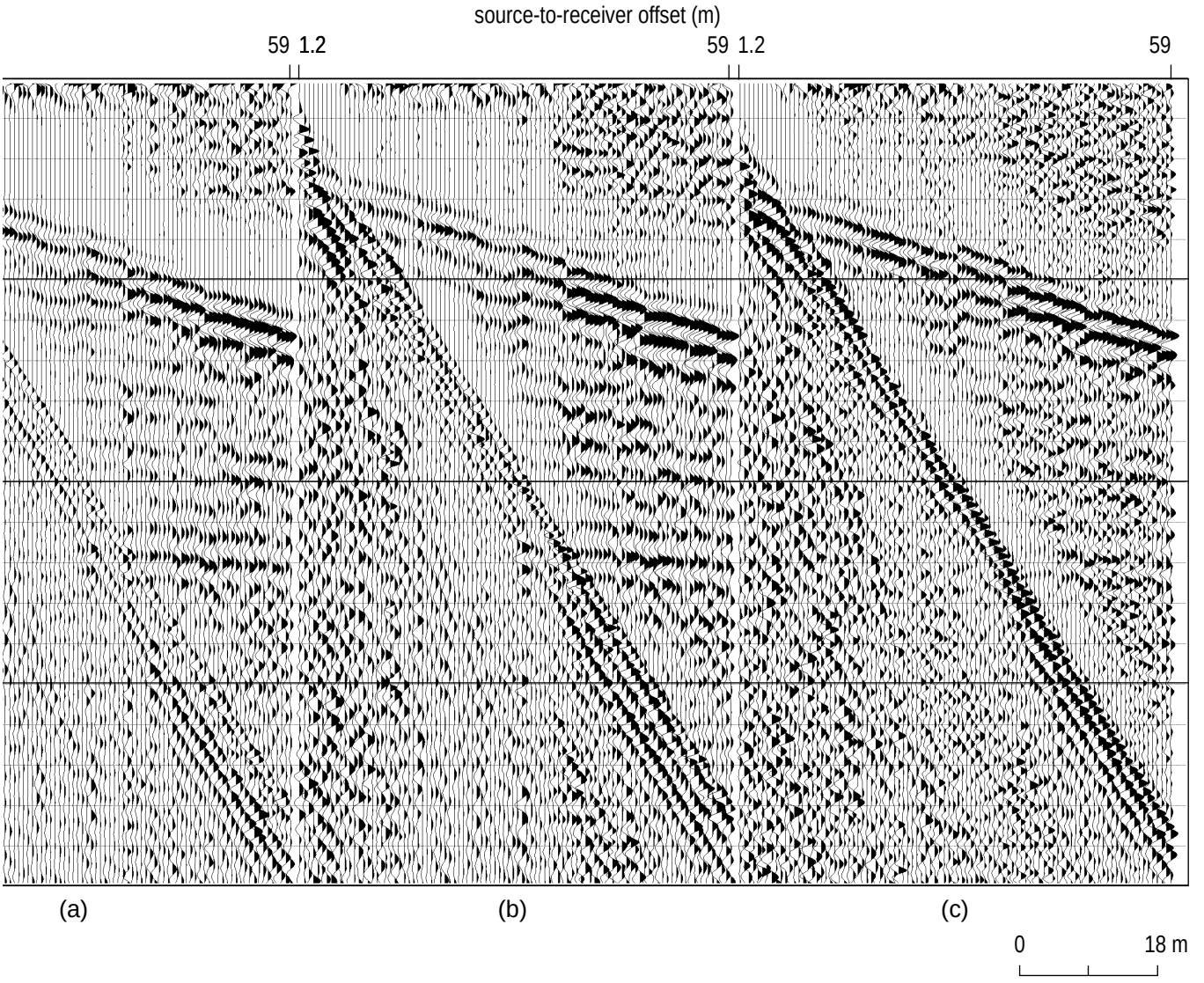

Figure A6b.

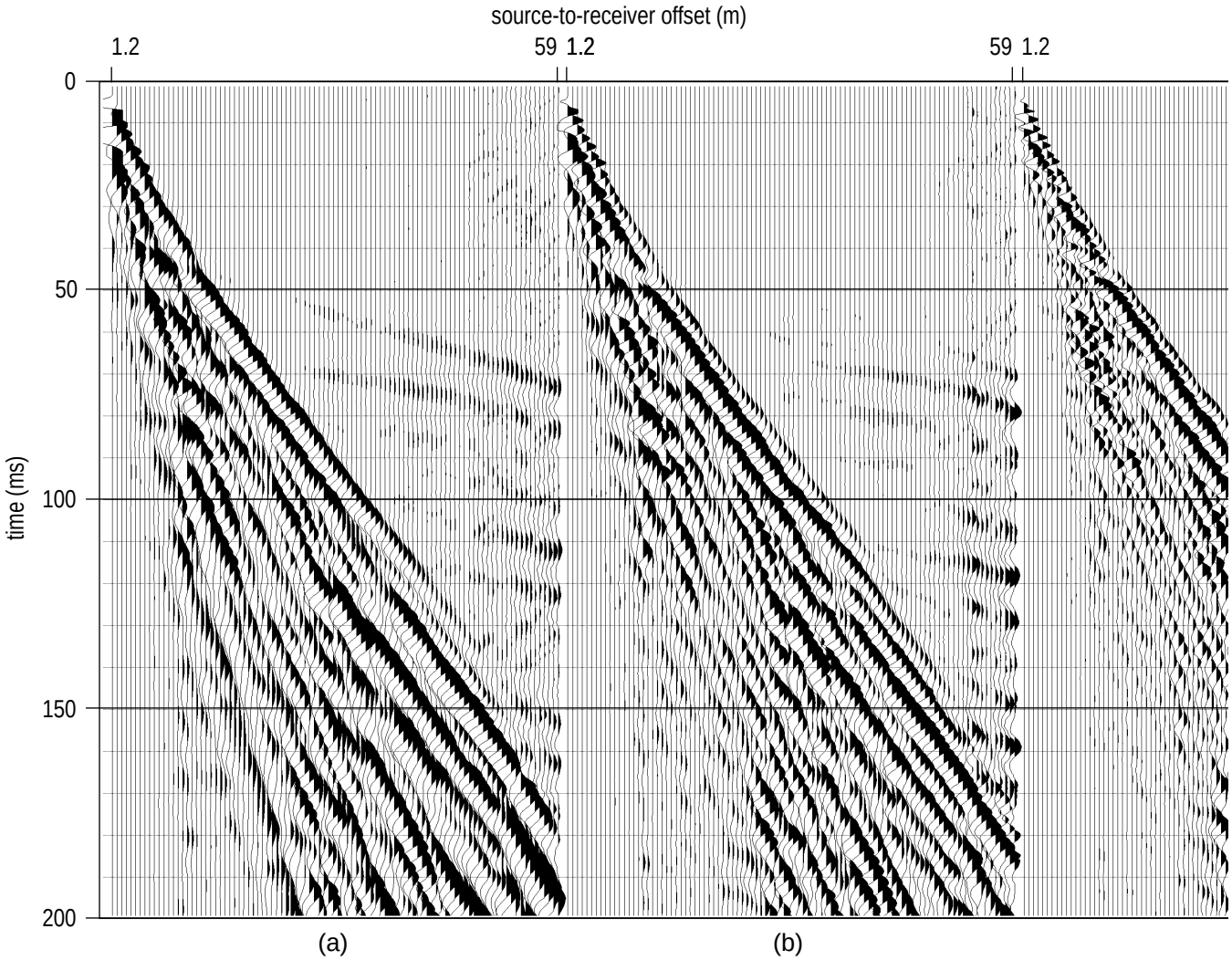

Figure A7a. Walkaway field files from site #3 using downhole 30.06 recorded with (a) no analog low-cut filter, (b) 100 Hz, and (c) 200 Hz.

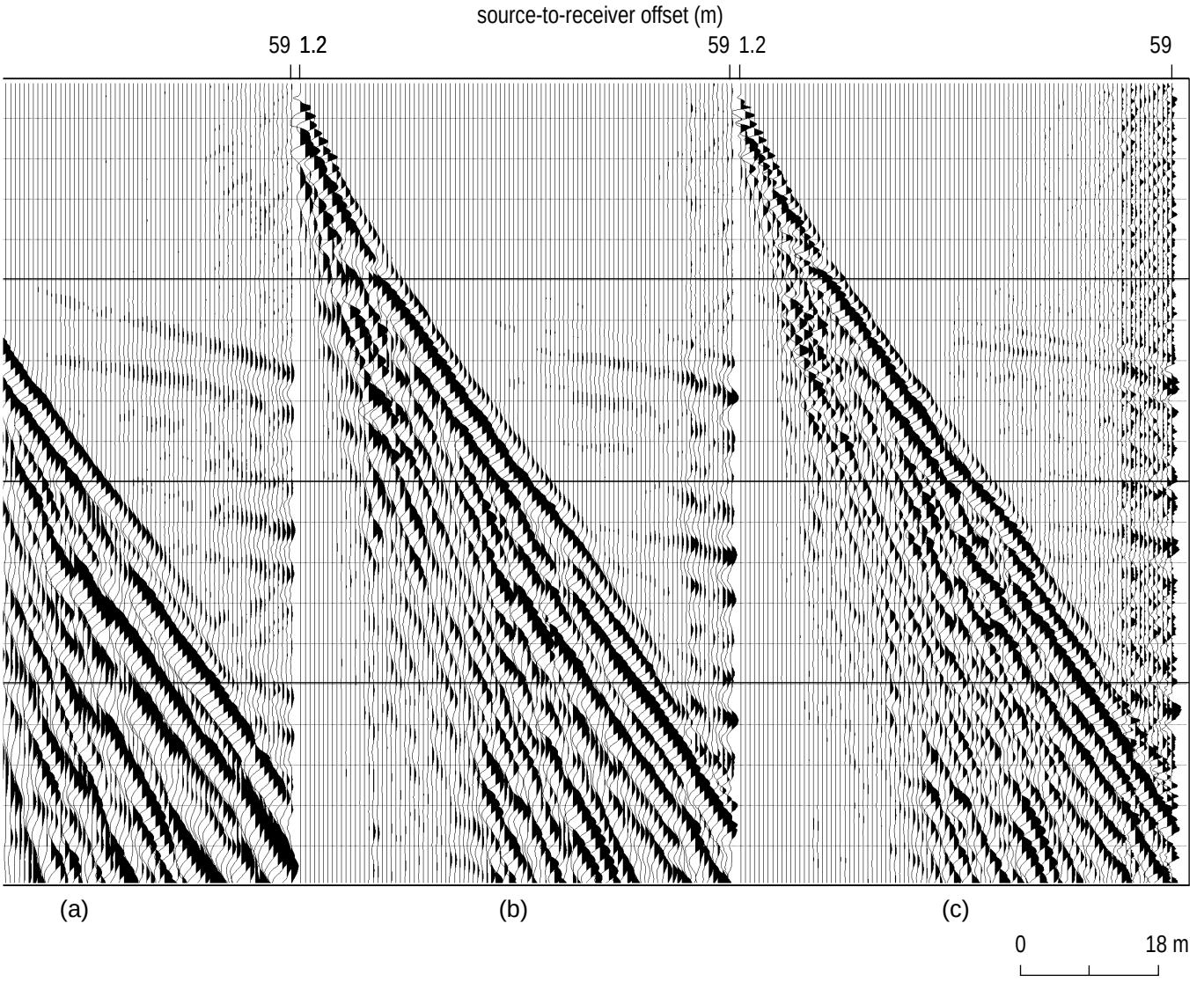

Figure A7b.

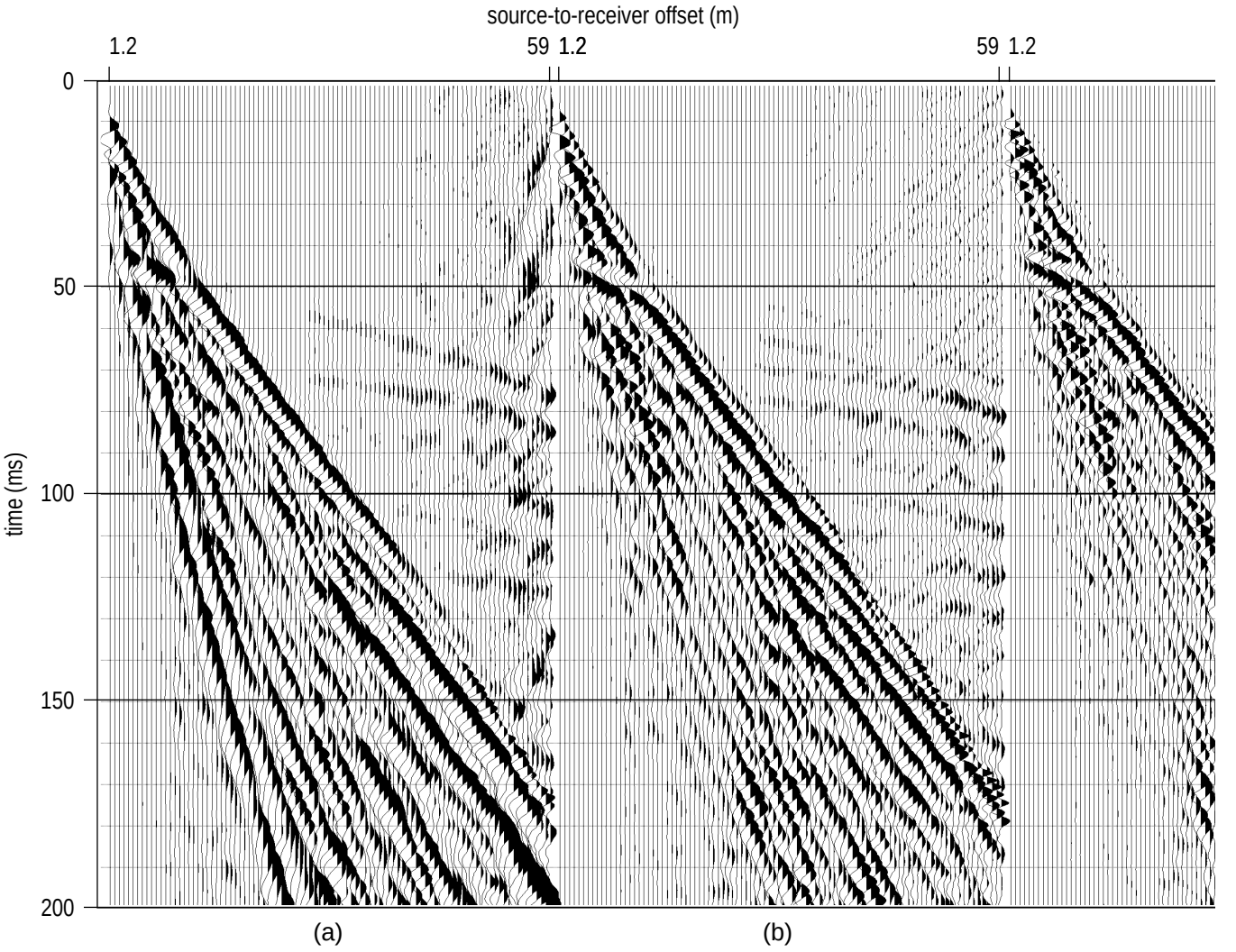

Figure A8a. Walkaway field files from site #3 using sledgehammer recorded with low-cut filter (a) out, (b) 100 Hz, and (c) 200 Hz.

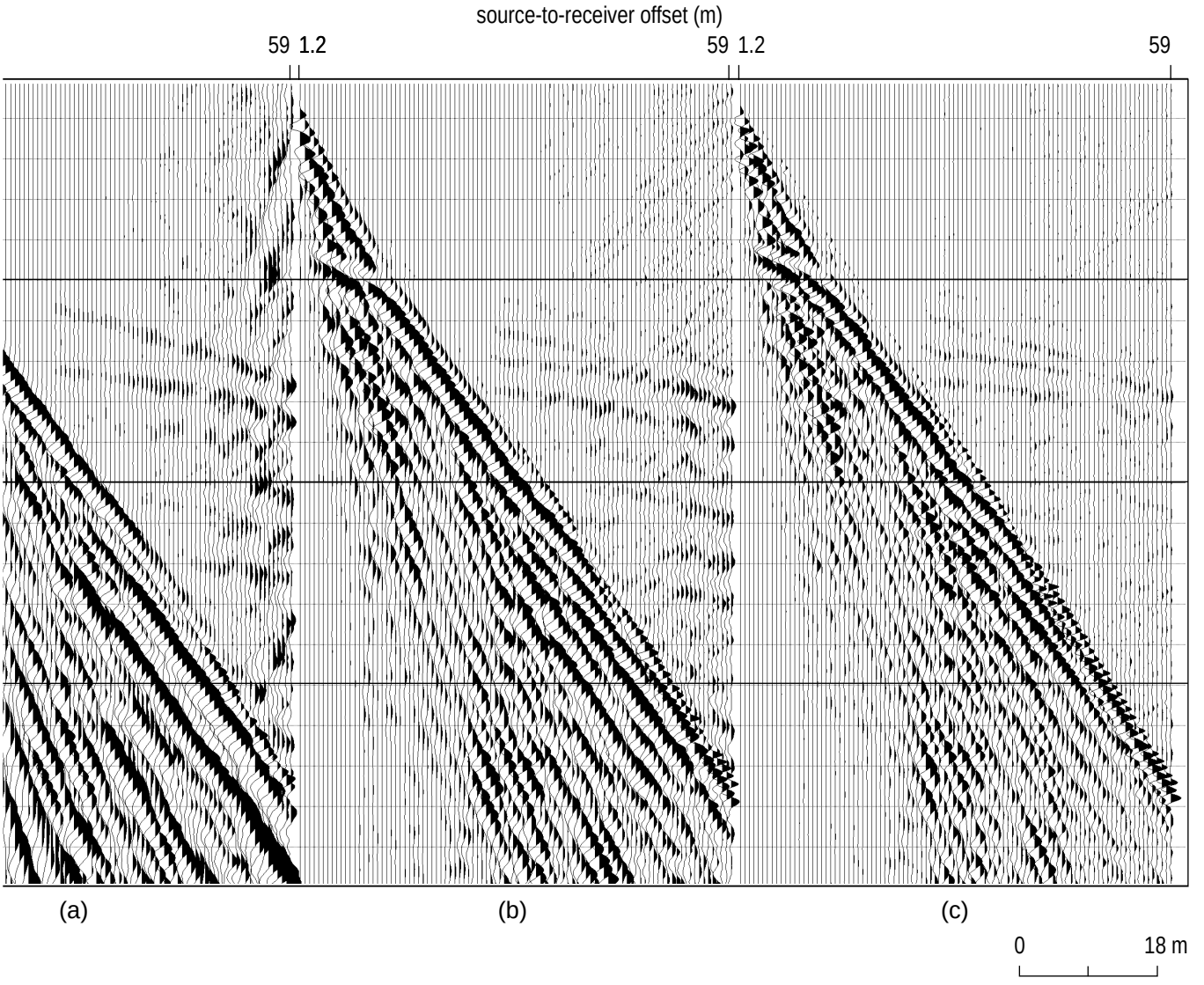

Figure A8b.

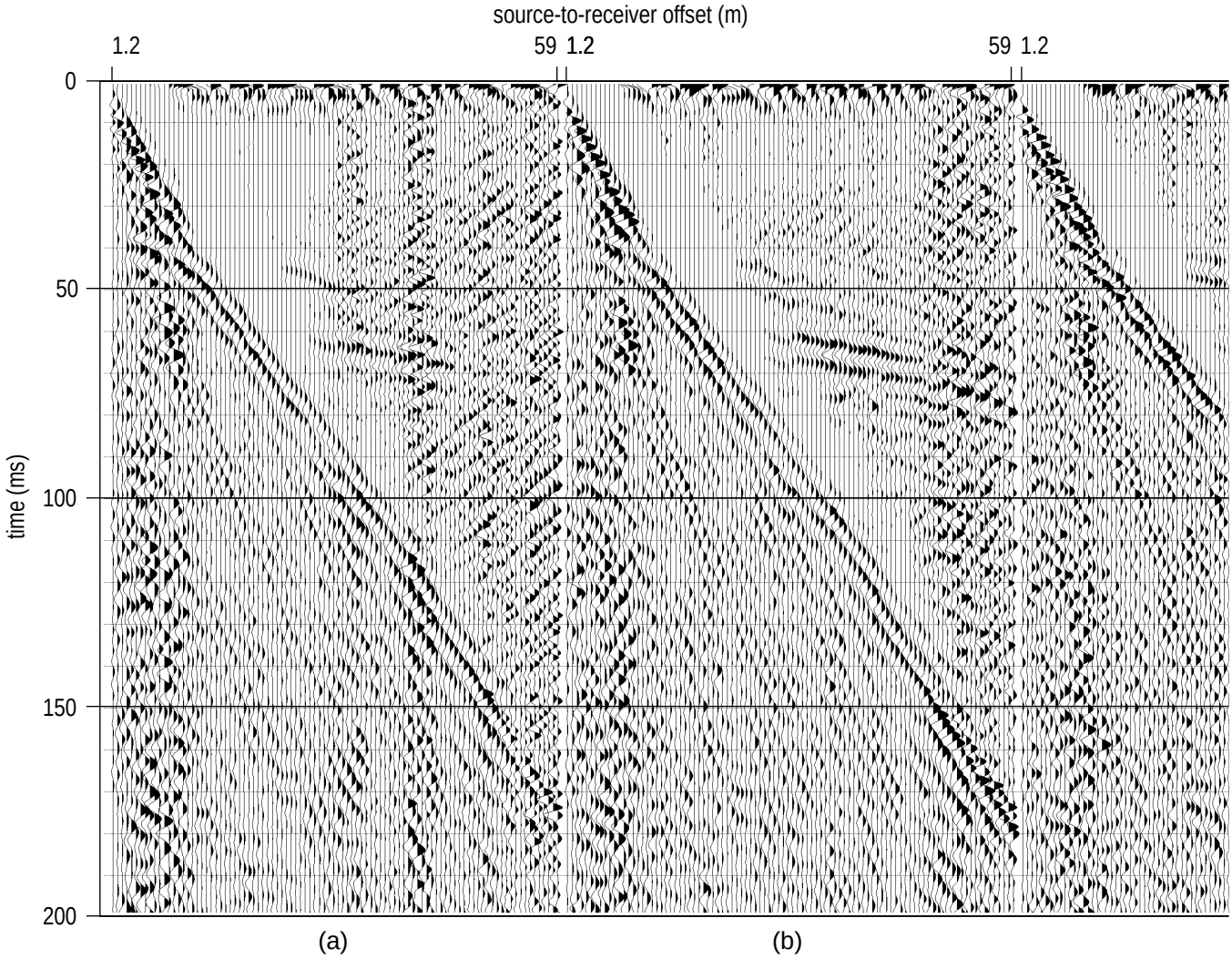

Figure A9a. A 100-200-400-600 digital filter applied to files from Figure A7.

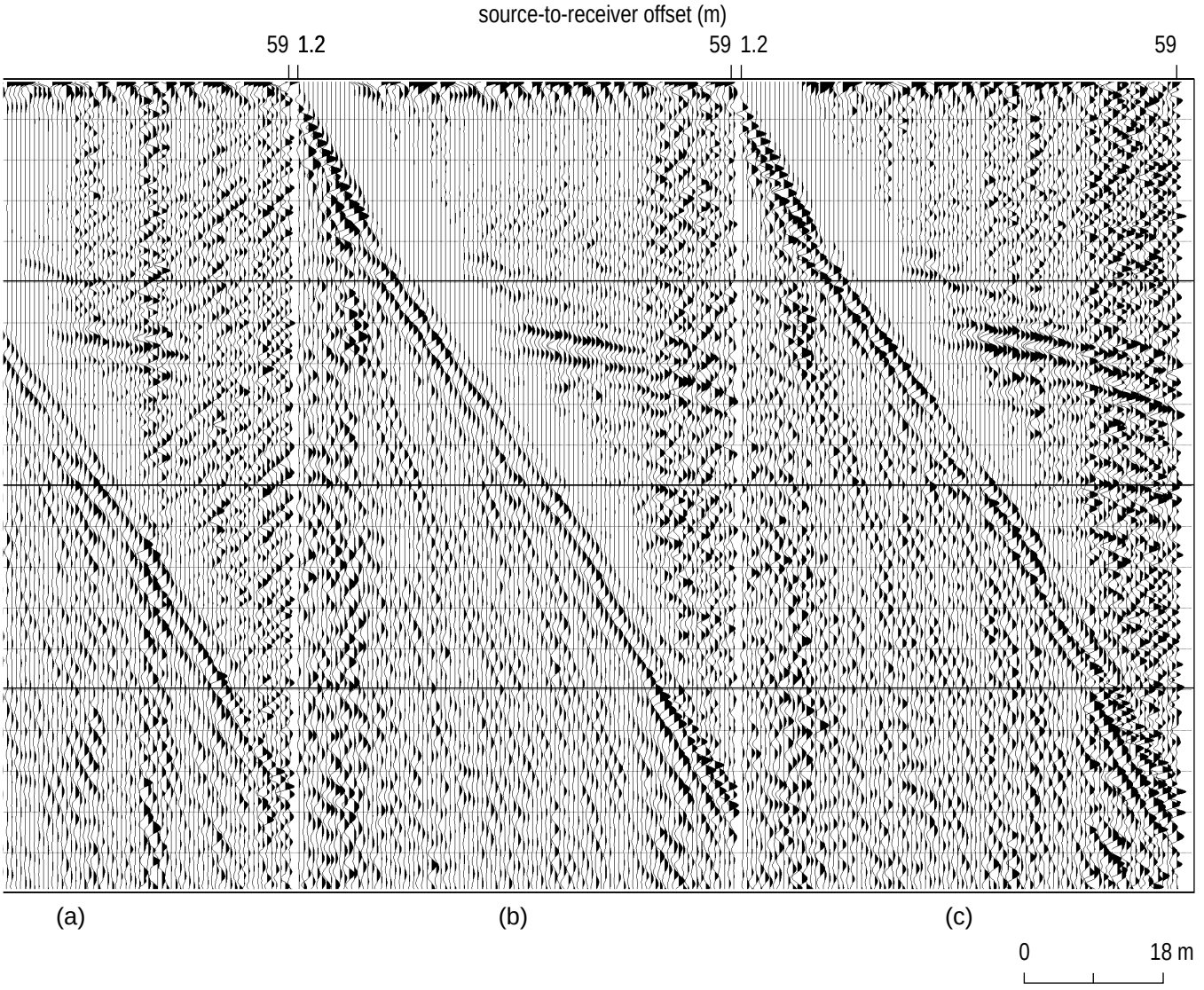

Figure A9b.

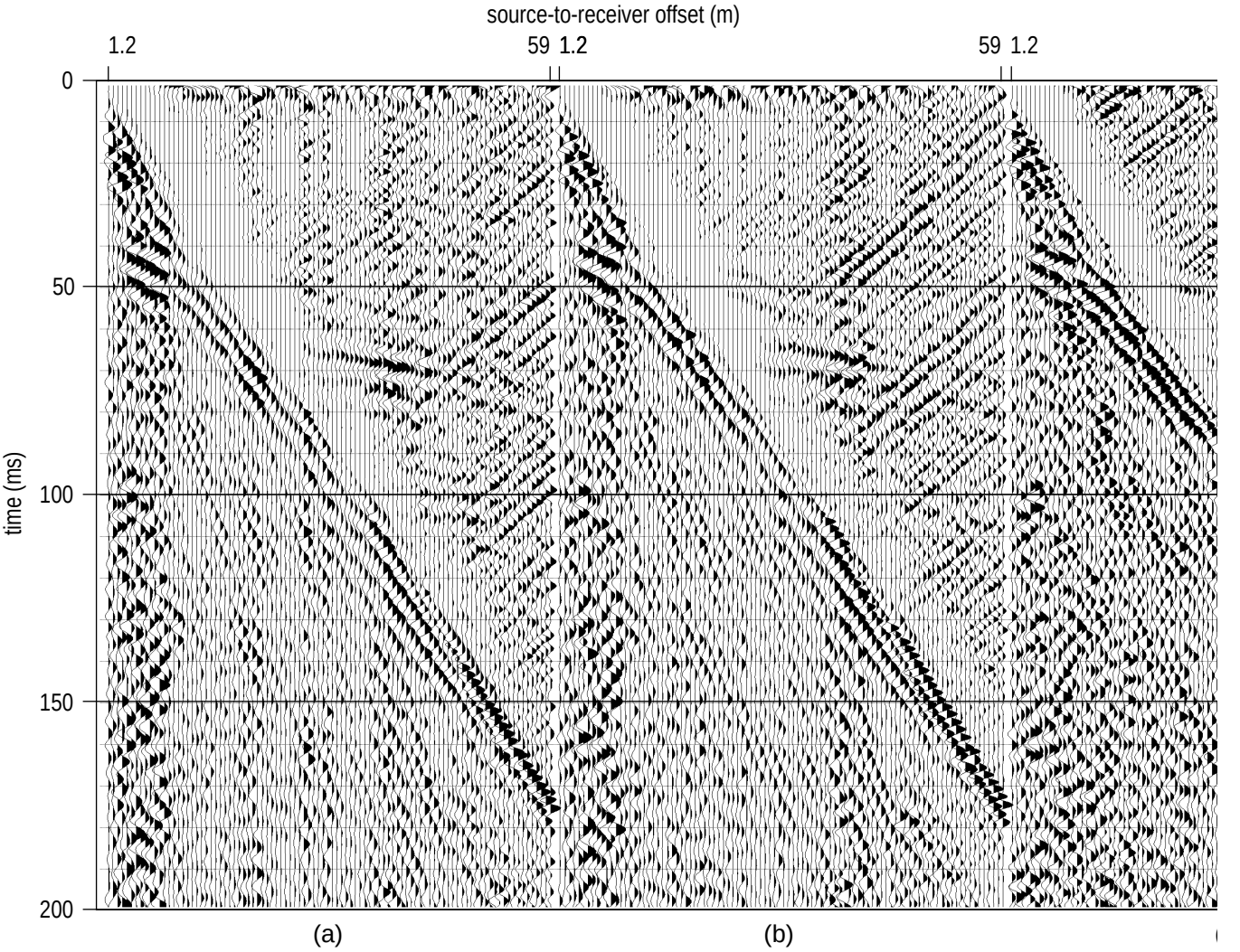

Figure A10a. A 100-200-400-600 digital filter applied to files from Figure A8.

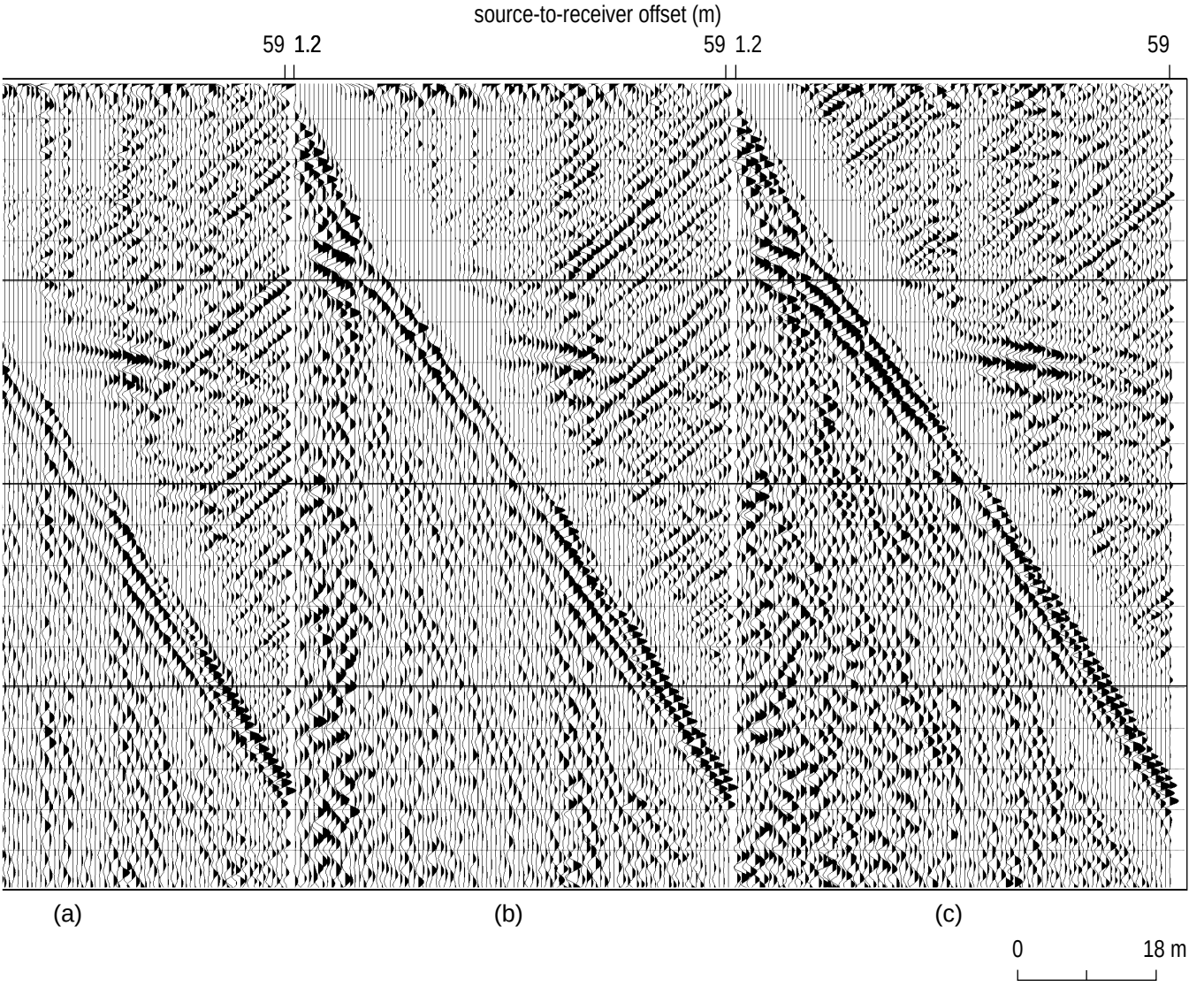

Figure A10b.

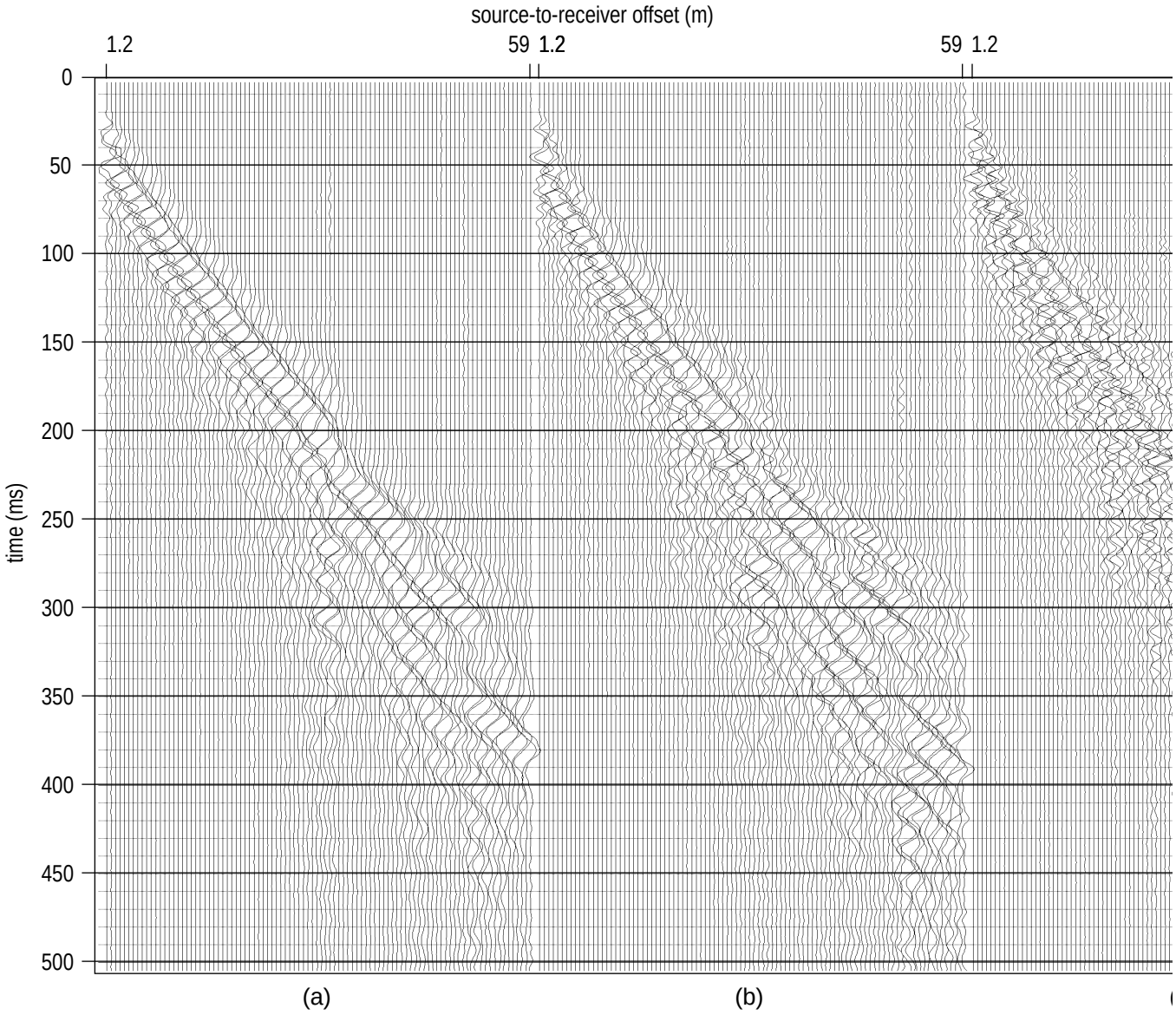

Figure A11a. Combined forward and reverse polarity S-wave field files with every other wiggle trace reversed to allow visual inspection of polarization and coherence of potential reflection events. The S-wave mini block source was recorded with analog low-cut filters (a) out, (b) 50 Hz, and (c) 100 Hz.

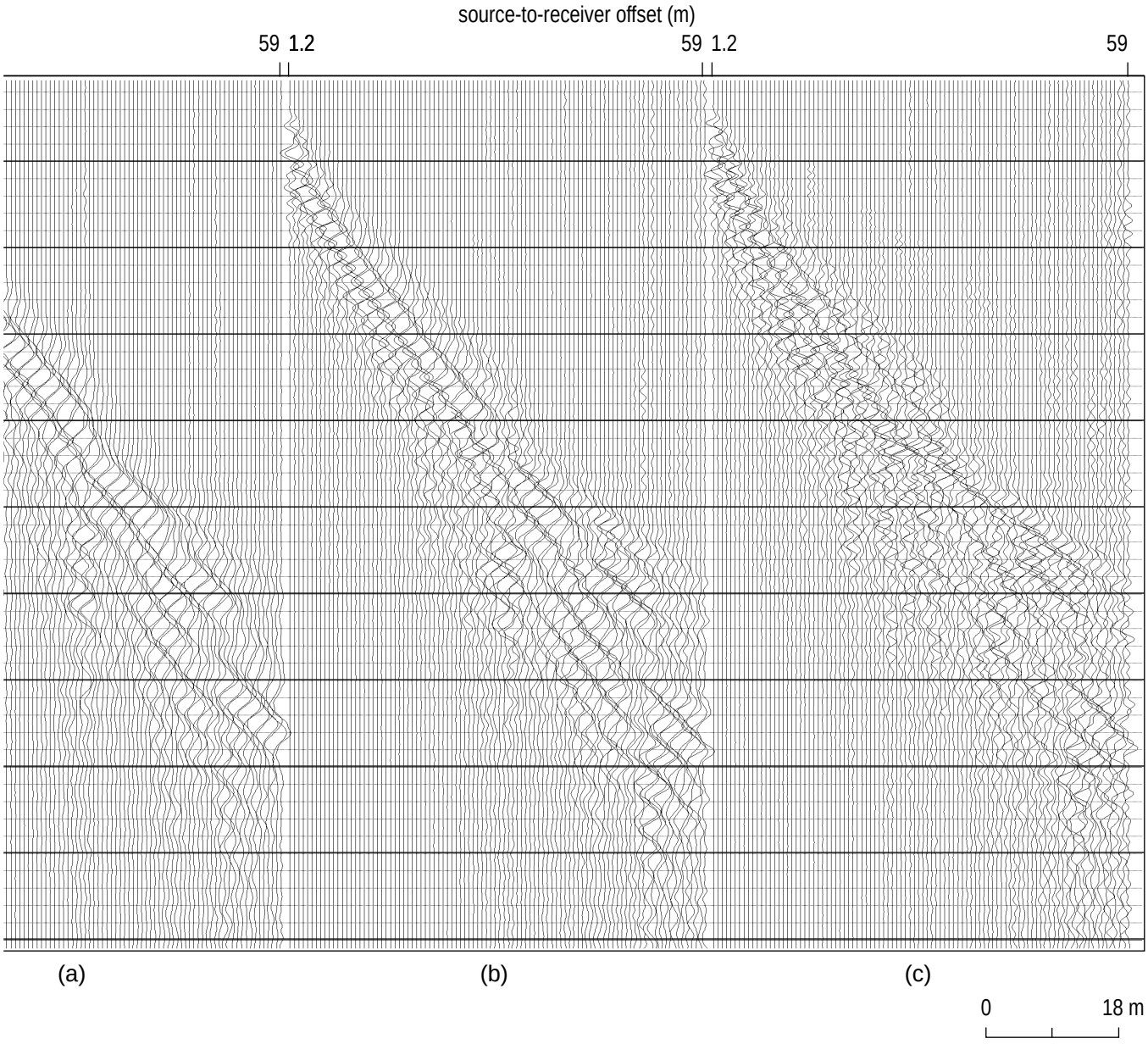

Figure A11b.

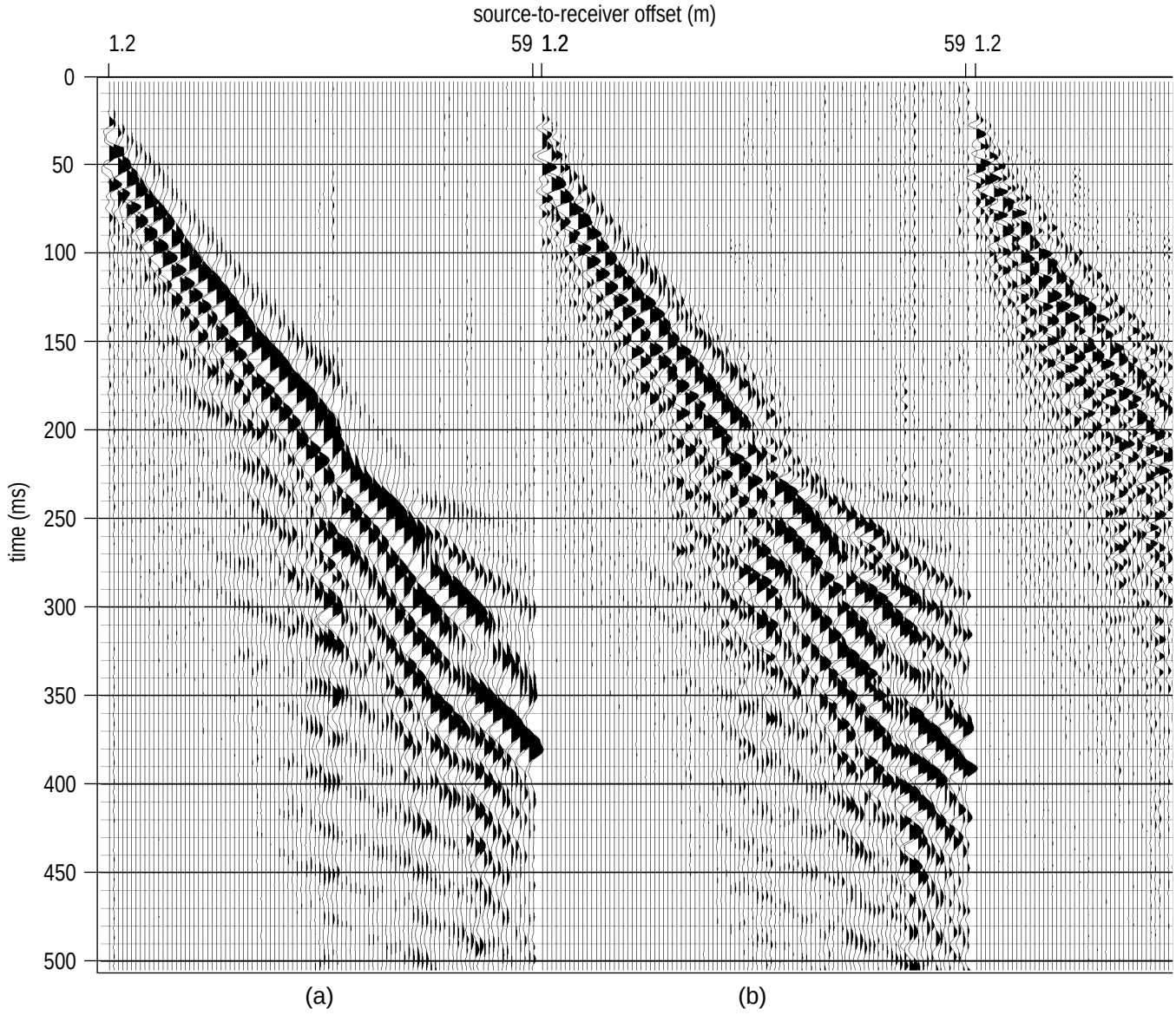

Figure A12a. Combined forward and reverse polarity S-wave field files with every other variable wiggle trace reversed to allow visual inspection of polarization and coherence of potential reflection events. The only potential reflection that can be identified with any degree of confidence has a zero offset time of about 180 msec. The S-wave mini block source was recorded with analog low-cut filters (a) out, (b) 50 Hz, and (c) 100 Hz.

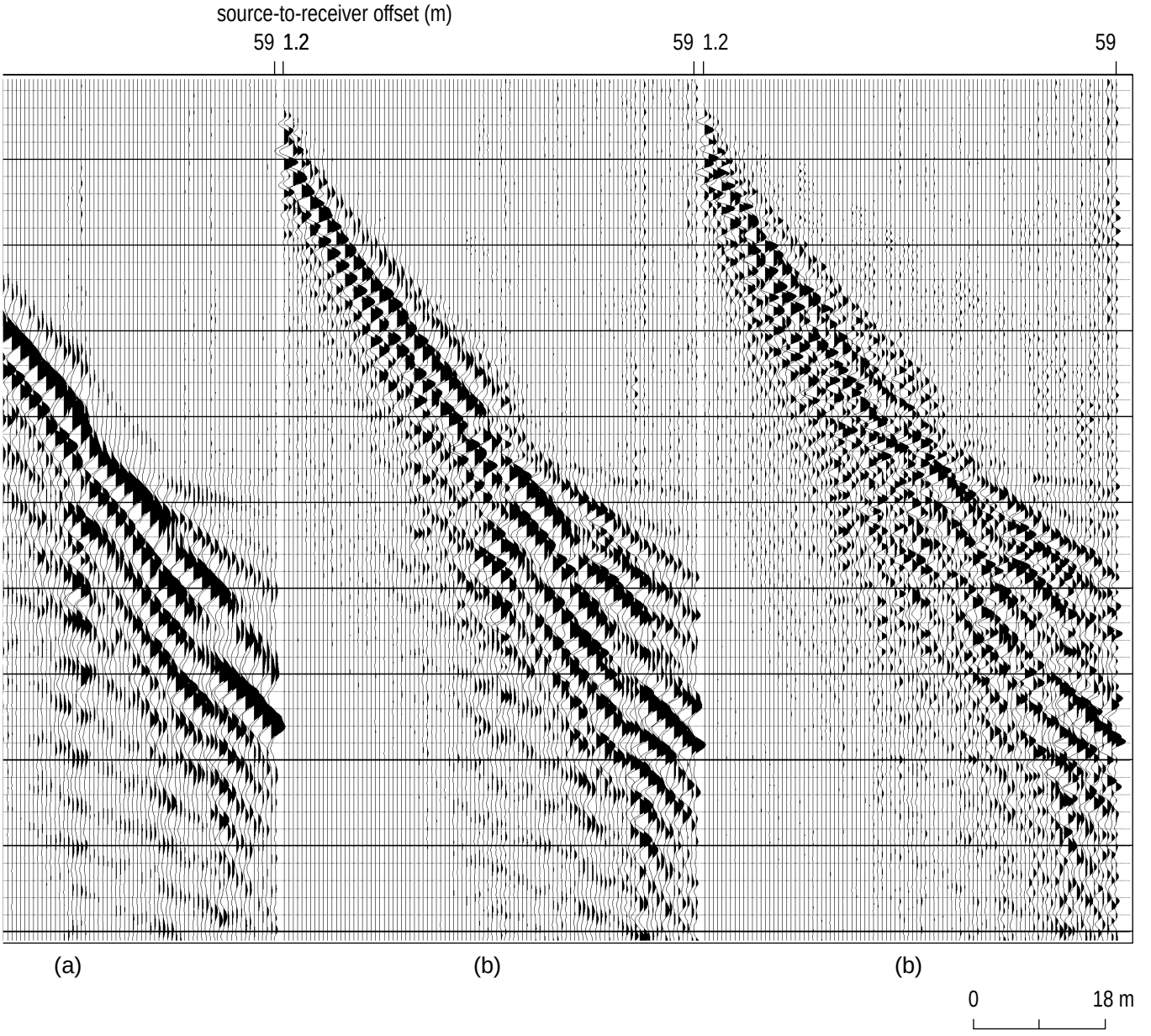

Figure A12b.

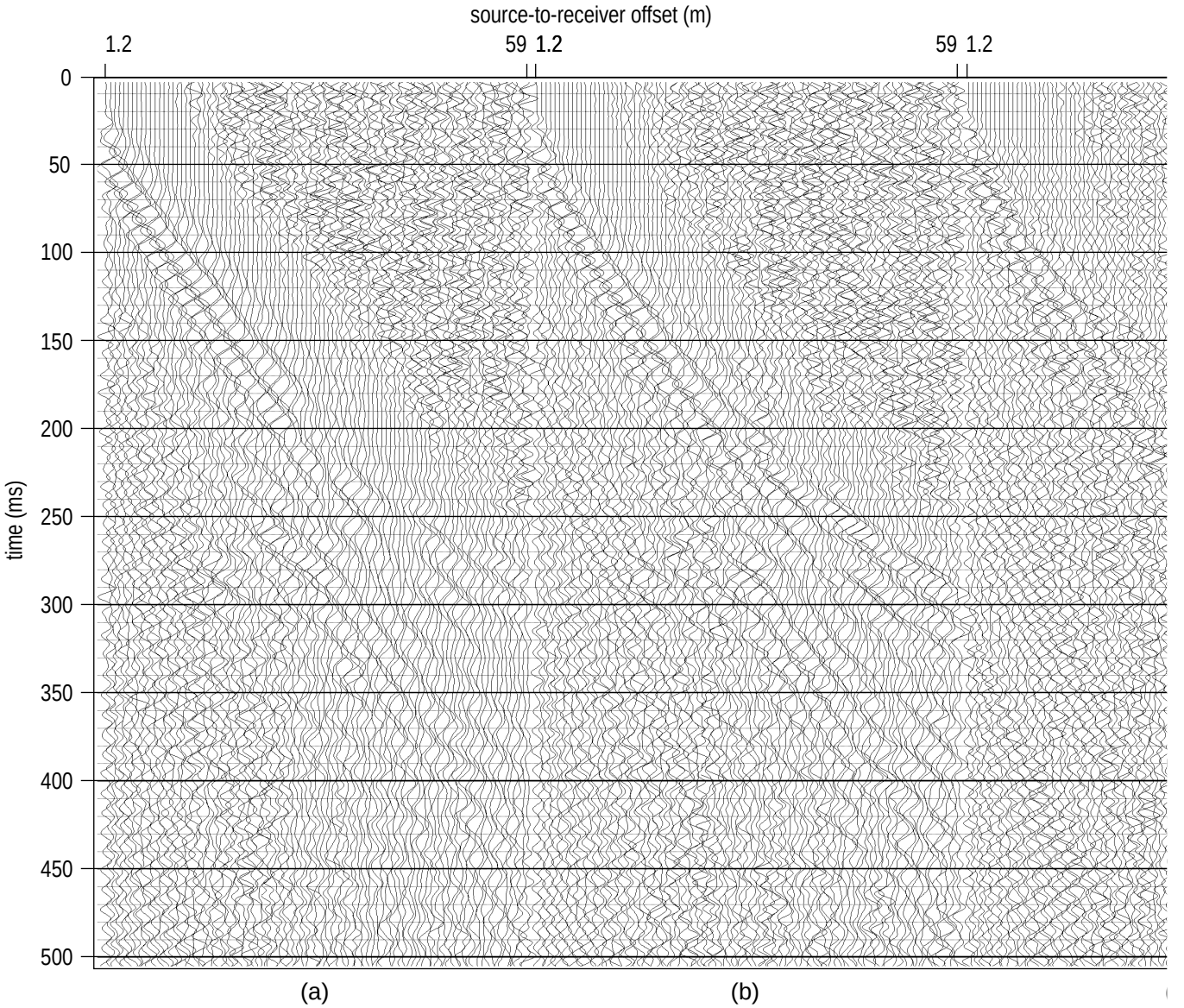

Figure A13a. S-wave shot gather of Figure A11 with a 25-50, 125-250 Hz digital filter and 100 msec AGC scale applied. Digital filtering did little to enhance potential reflection events evident with this display format.

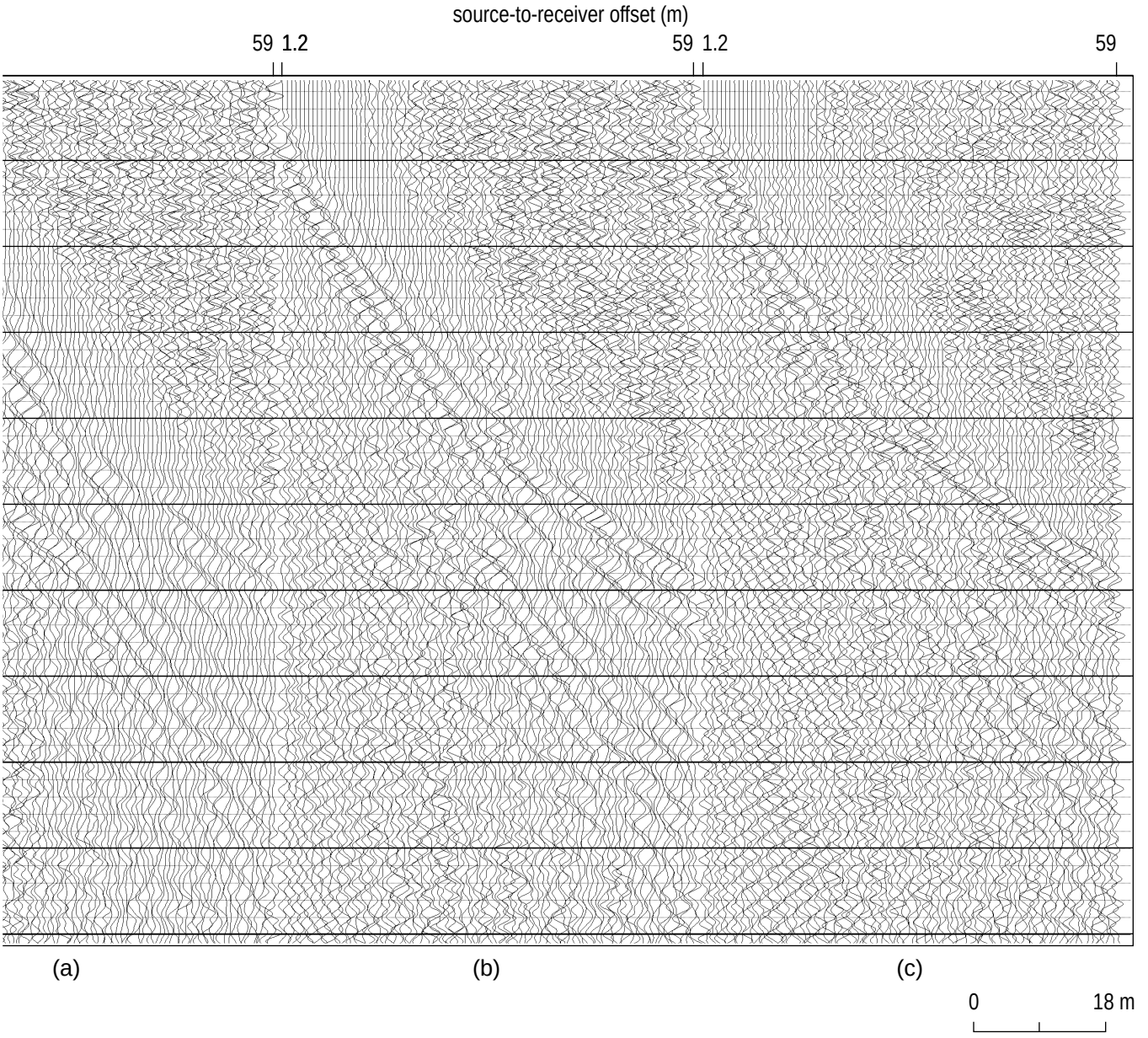

Figure A13b.

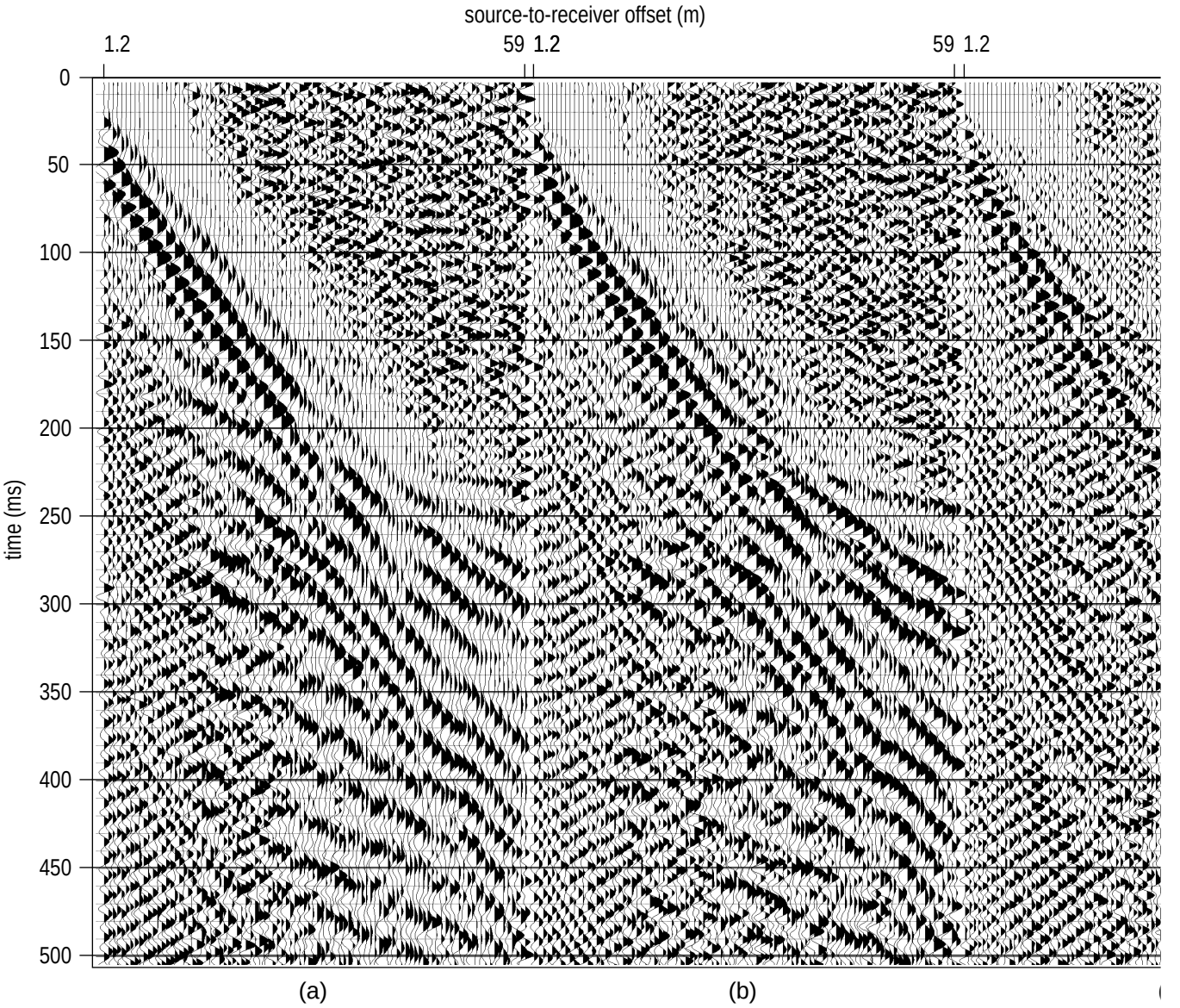

Figure A14a. S-wave shot gather of Figure A12 with a 25-50, 125-250 Hz digital filter and 100 msec AGC scale applied. Digital filtering did little to enhance potential reflection events evident on raw data. Some suggestion of reflections on data acquired with no analog low-cut are interpretable with vertical incident times between 150 and 250 msec.

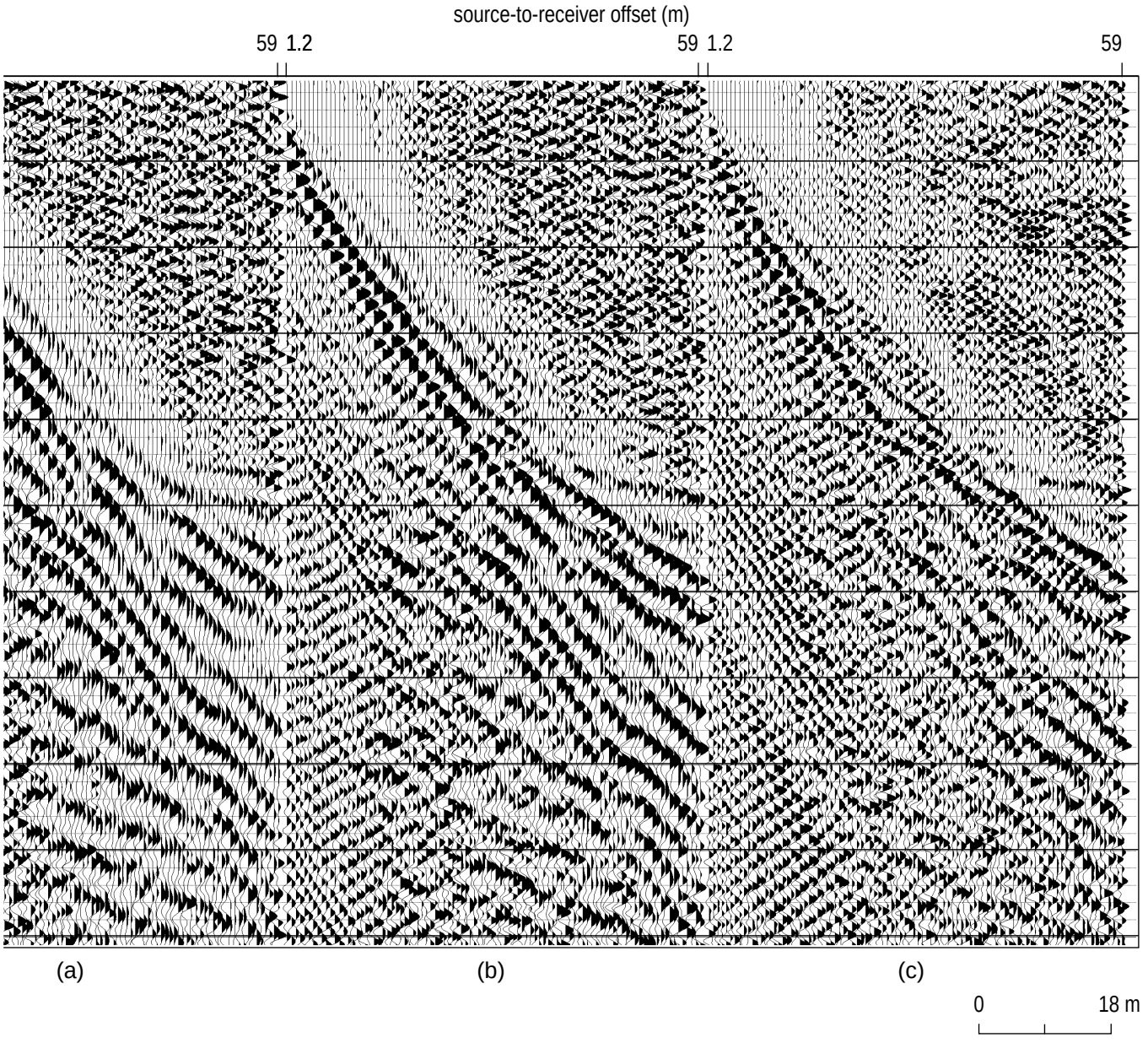

Figure A14b.

Appendix B: VSP Data and Interpretations

1. Velocity model. The first break traveltime is picked up to generate interval velocity and average velocity models in these three wells. Precaution should be made in interpretation of these velocity models. Errors in picking the first break traveltime are transferred into the velocity models, especially the interval velocity model. The relative errors in the interval velocity models could be as high as ±20% of the true value. The errors in the average velocity models are normally less than ±5% of the true average velocities, which are much less than those in the interval velocity models.

Velocity models from depth 0 m to 10 m (VSP 1), to 18 m (VSP 2), and to 12 m (VSP 3) are also derived from downhole geophone data. The overlaps between velocity models derived from hydrophone data and downhole geophone data (from depth 8 m to 10 m of VSP 1, 4 m to 18 m of VSP 2, and 8 m to 12 m of VSP 3) could be used to evaluate the accuracy of the velocity models. The relative differences in two average velocities are less than 5% for VSP 1 and VSP 2 and less than 10% for VSP 3.

2. Reflection events. In processed data of VSP 1, although it is relatively difficult to identify shallow reflection events compared with VSP 2 and VSP 3, we can still pick reflection events at depths of 18 m in 9 m source-well-offset gathers and at depths of 33 m in 15 m source-well-offset gathers. These two events are correlated to the gamma ray well log (STRAT-VSP1). Another strong reflection event at a depth of 73 m can be easily determined in 18 m to 30 m source-well-offset gathers.

In processed data of VSP 2, two strong shallow reflection events can be identified at depths of 17 m and 37 m in 10 m source-well-offset gathers. These two events are correlated to the gamma ray well log (STRAT-VSP2). The 17 m event could also be seen in 6 to 18 m source-to-well-offset gathers. Several strong reflection events at depth below 70 m can be easily determined in 15 to 45 m source-well-offset gathers.

In processed data of VSP 3, two shallow reflection events can be identified at depths of 17 m and 33 m in 10 m source-well-offset gathers and others. These two events are correlated to the gamma ray well log (STRAT-VSP3). Several strong reflection events at depths below 70 m can be easily determined in 12 to 58 m source-well-offset gathers.

3. Corridor stacking. Several gathers are picked to generate the corridor stacking section: 15 m source-well-offset gather of VSP 1, 10 m source-well-offset gather of VSP 2, and 10 m source-well-offset gather of VSP 3.

Table B1
VSP Processing

1. AGC scale	50 msec time window)
2. Bandpass filter	(50/100/300/450 trapezoidal, dominant frequency 190 Hz)
3. F-K filter	(reject direct wave 0.25 ms/trace to 1.5 ms/trace; eject downgoing tube wave 2.3 ms/trace to 4.4 ms/trace; reject upcoming tube wave -4.4 ms/trace to -2.3 ms/trace)
4. Bandpass filter	(50/100/300/450 trapezoidal, remove F-K artifacts)
5. Edit	(first arrival mute to remove wrap around noise of fk filter)
6. Static correction	(datum correction to the well head; i.e., two way travel time)
7. Corridor stacking	(30 to 150 msec trace summing, only reflections will be horizontal)

Table B2
Depth vs Time

Depth (m)	Two-way Time (ms) VSP 1	VSP 2	VSP 3	Depth (m)	Two-way Time (ms) VSP 1	VSP 2	VSP 3
1.5	3.8	3.9	4.2	31.9	49.3	48.6	55.0
3.0	7.8	7.7	8.2	33.5	50.9	50.7	56.2
4.6	11.6	11.6	12.1	35.0	52.3	52.4	57.9
6.1	14.9	14.7	15.7	36.5	54.1	54.2	59.2
7.6	18.2	17.3	20.2	38.0	55.9	55.9	61.1
9.1	21.3	19.6	23.2	39.5	57.8	57.6	63.1
10.6	23.4	21.6	26.0	41.1	59.3	59.4	64.8
12.2	25.7	23.9	28.5	42.6	61.4	61.0	66.2
13.7	27.5	26.0	31.7	44.1	62.6	62.5	67.9
15.2	29.6	28.2	33.7	45.6	64.2	64.0	69.8
16.7	31.2	30.2	35.4	47.2	66.0	65.7	71.7
18.3	33.0	32.1	37.7	48.7	67.3		72.9
19.8	34.9	34.0	9.9	50.2			74.0
21.3	37.0	35.7	42.0	51.7			76.1
22.8	38.8	37.6	43.7	53.2			77.6
24.3	40.3	39.5	45.7	54.8			78.9
25.9	42.1	41.0	47.6	56.3			81.0
27.4	43.9	42.7	49.6	57.8			82.5
28.9	45.3	44.3	51.2	59.3			84.2
30.4	47.4	46.4	53.0	60.8			86.1

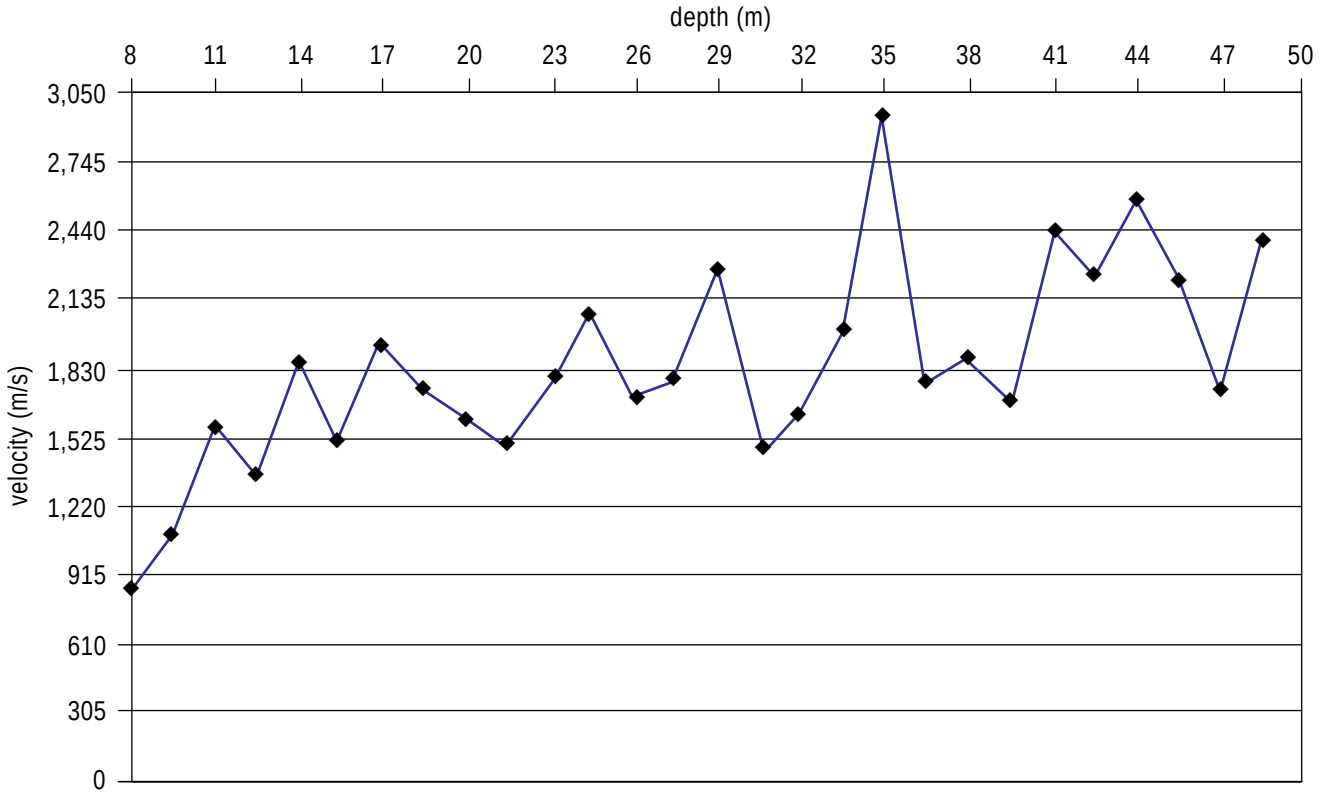

Figure B1. Interval velocity plot of VSP #1 using the hydrophone receiver.

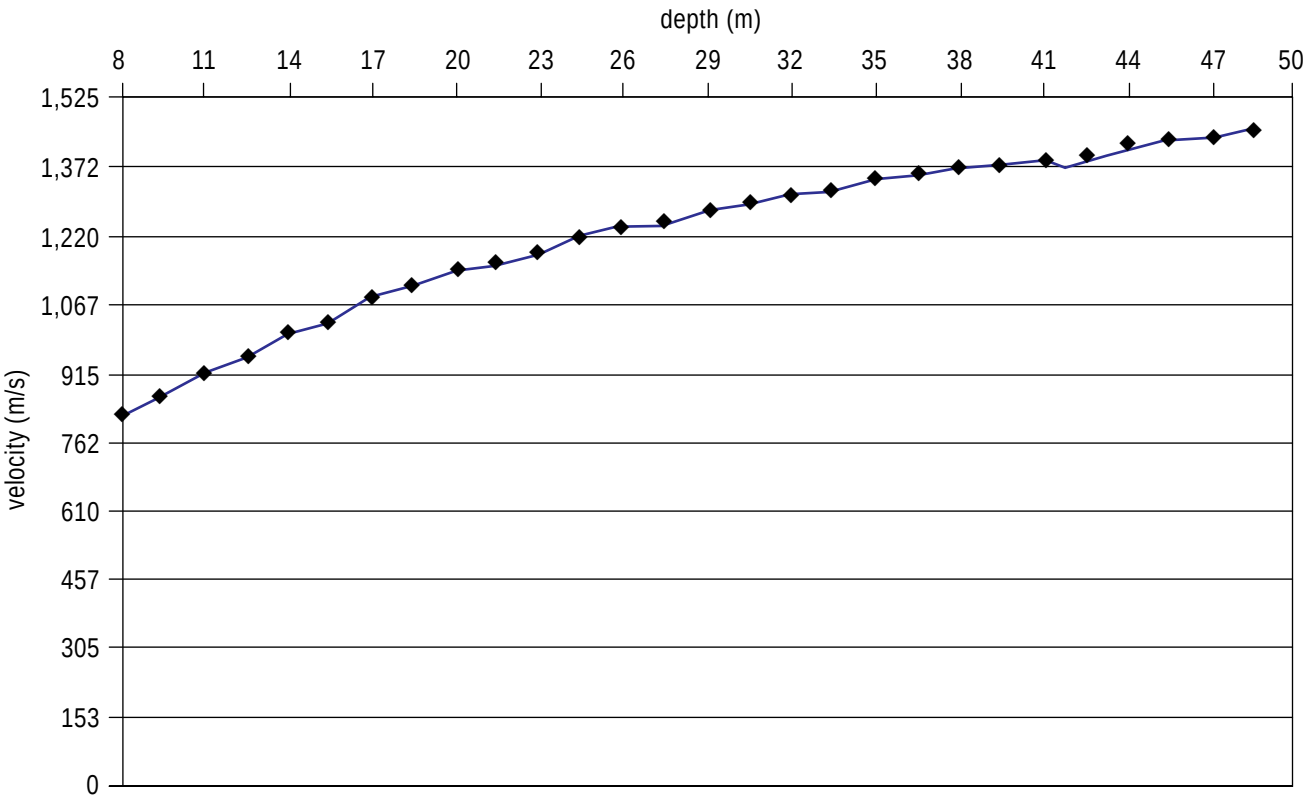

Figure B2. Average velocity plot of VSP #1 using the hydrophone receiver.

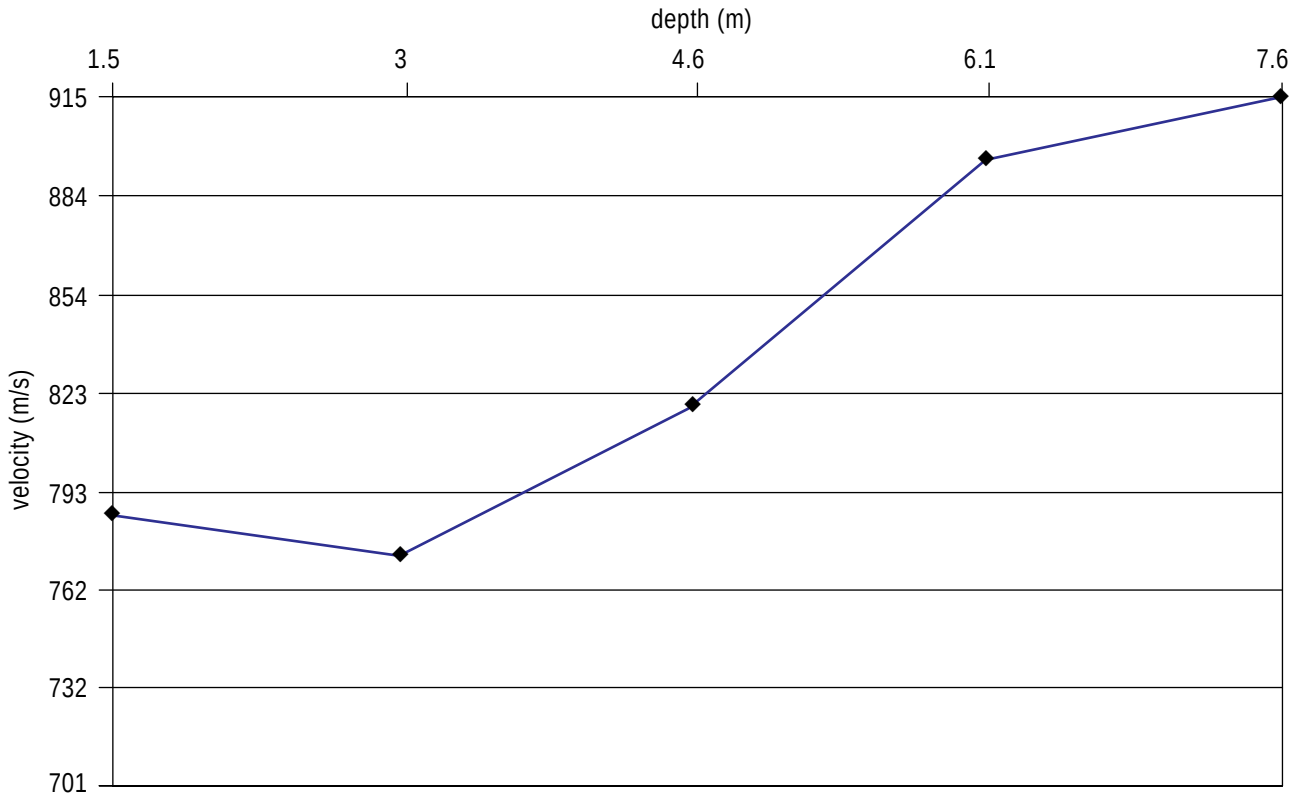

Figure B3. Interval velocity plot of VSP #1 using the hole-lock geophone.

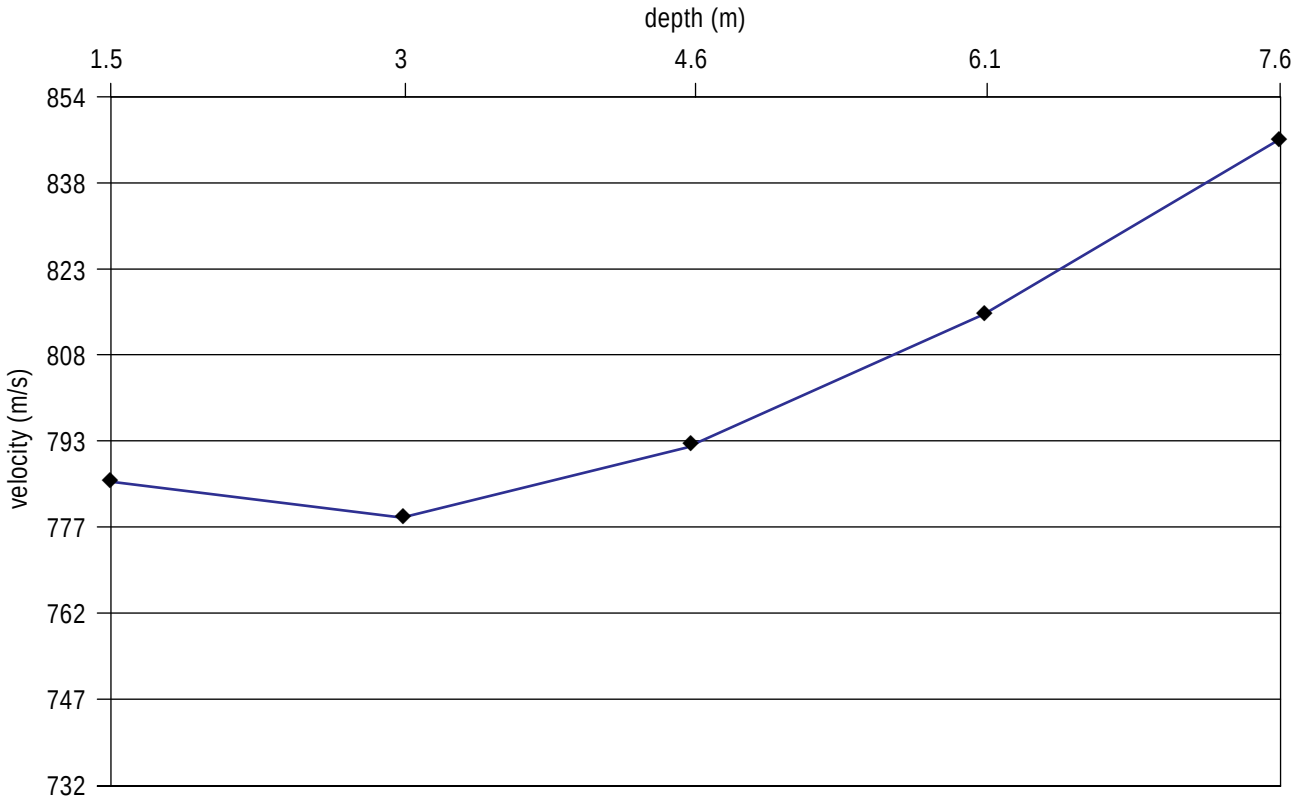

Figure B4. Average velocity plot of VSP #1 using the hole-lock geophone.

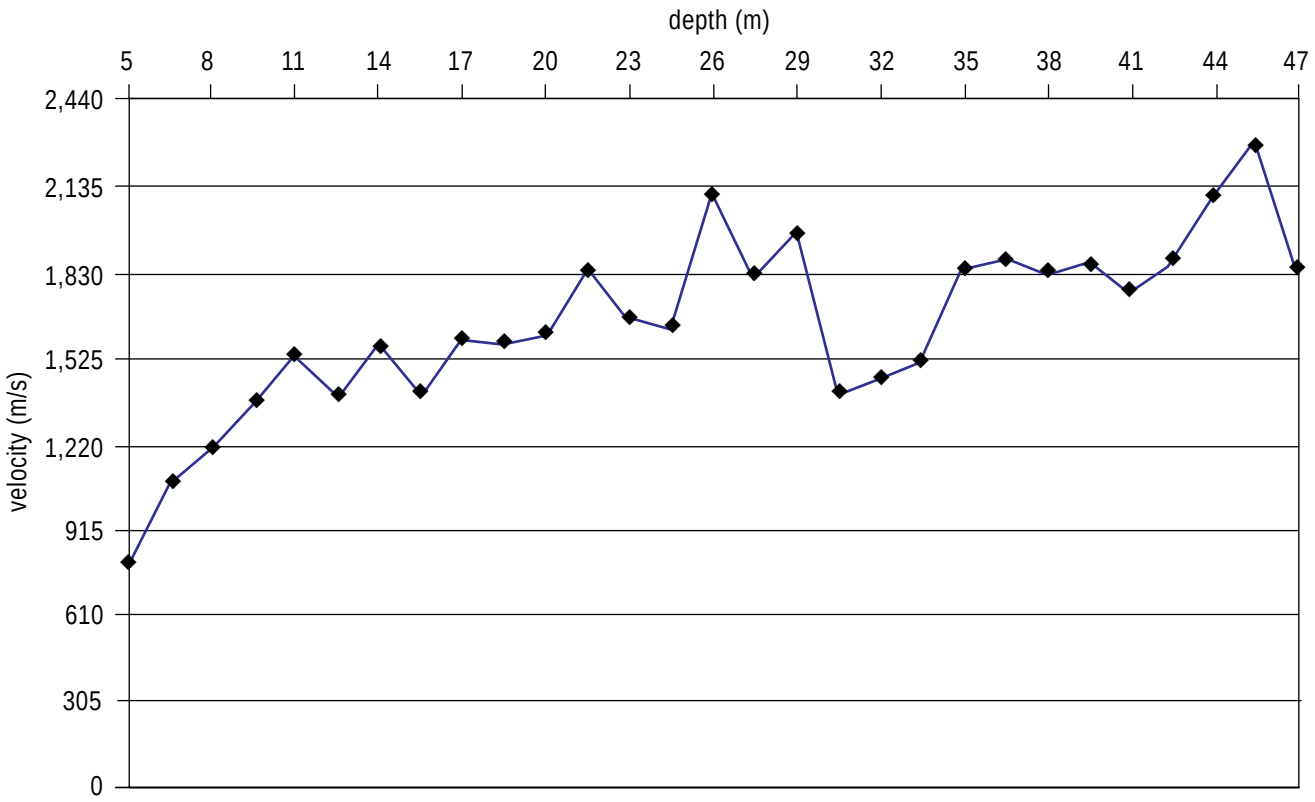

Figure B5. Interval velocity plot of VSP #2 using the hydrophone receiver.

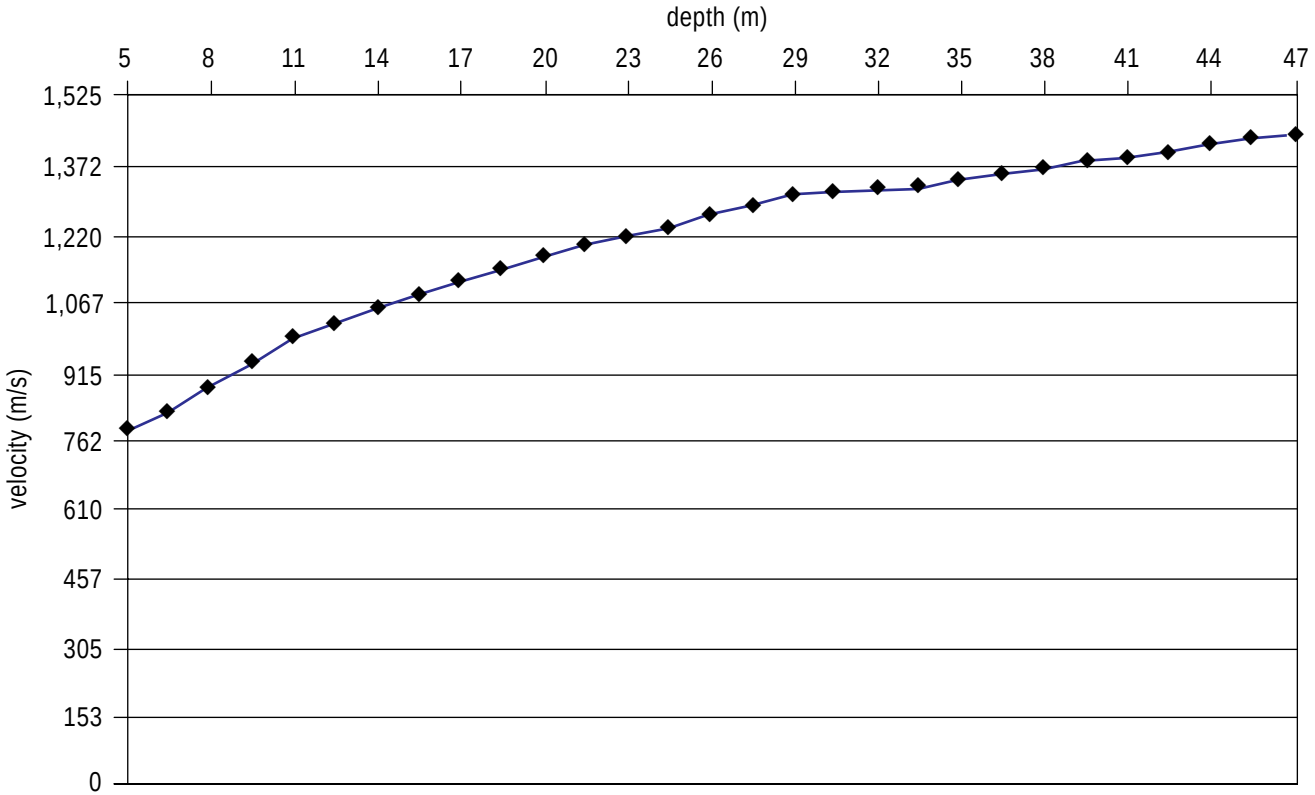

Figure B6. Average velocity plot of VSP #2 using the hydrophone receiver.

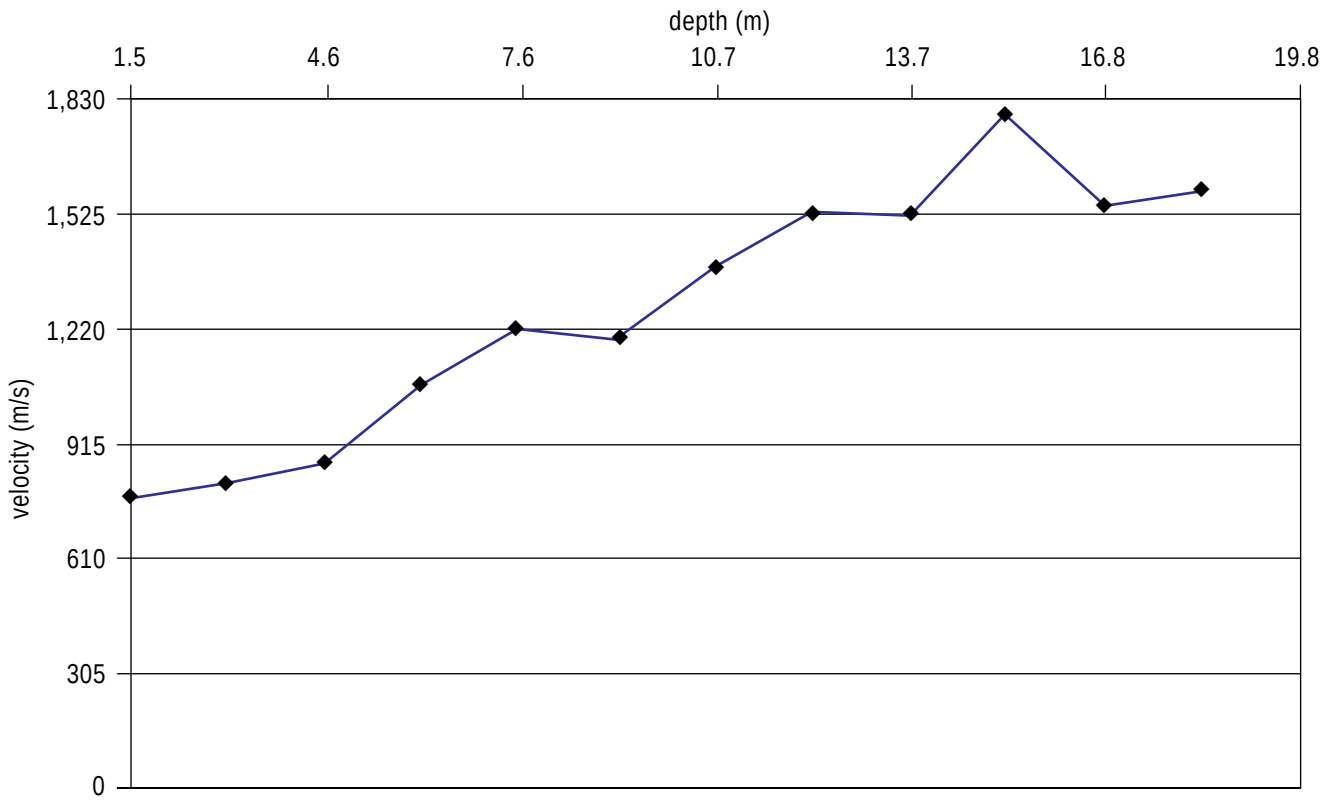

Figure B7. Interval velocity plot of VSP #2 using the hole-lock geophone.

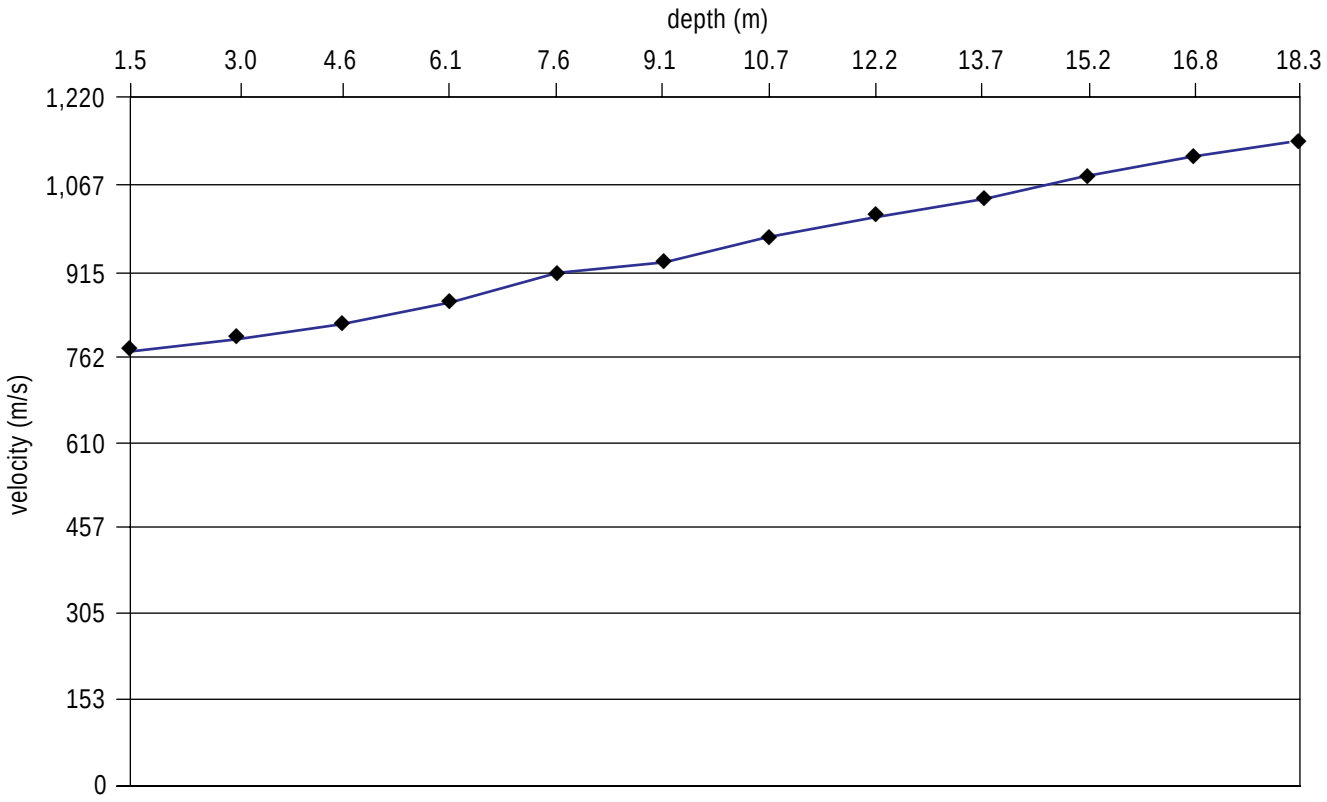

Figure B8. Average velocity plot of VSP #2 using the hole-lock geophone.

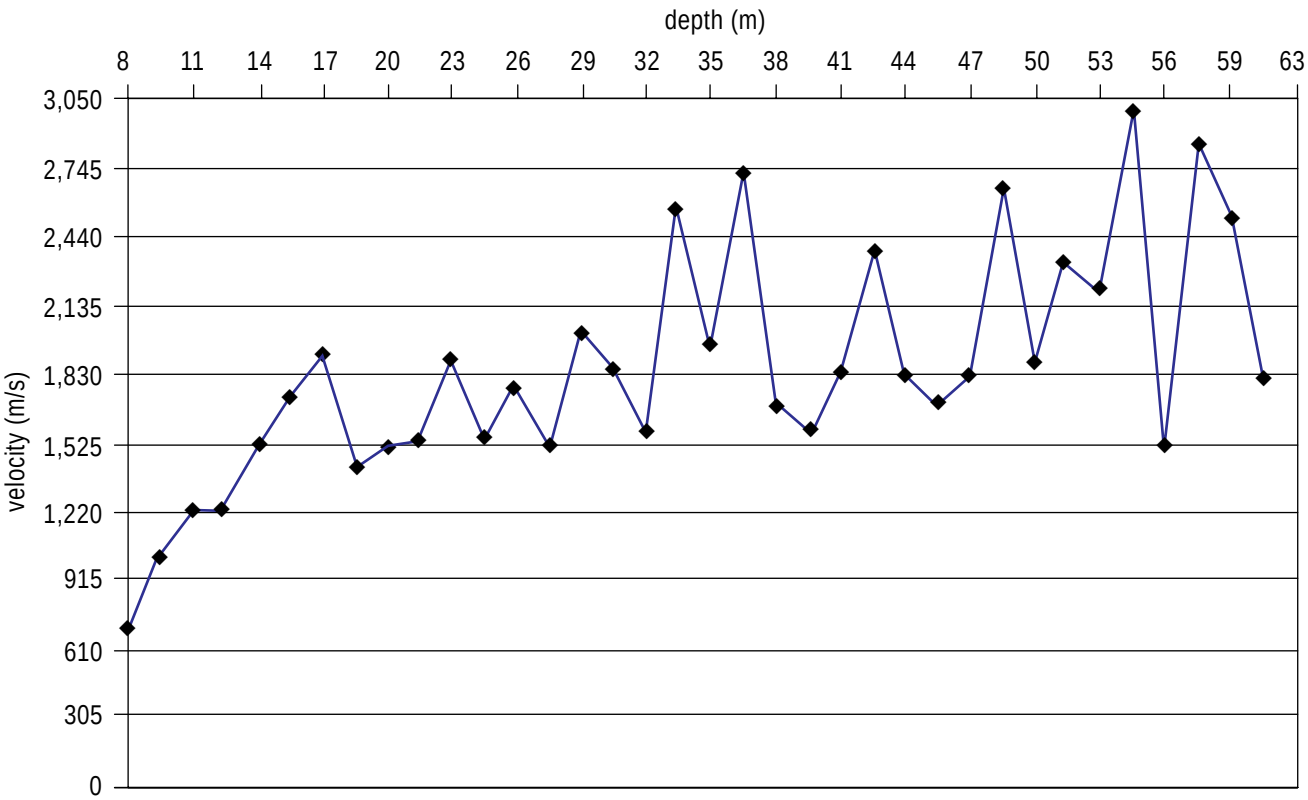

Figure B9. Interval velocity plot of VSP #3 using the hydrophone receiver.

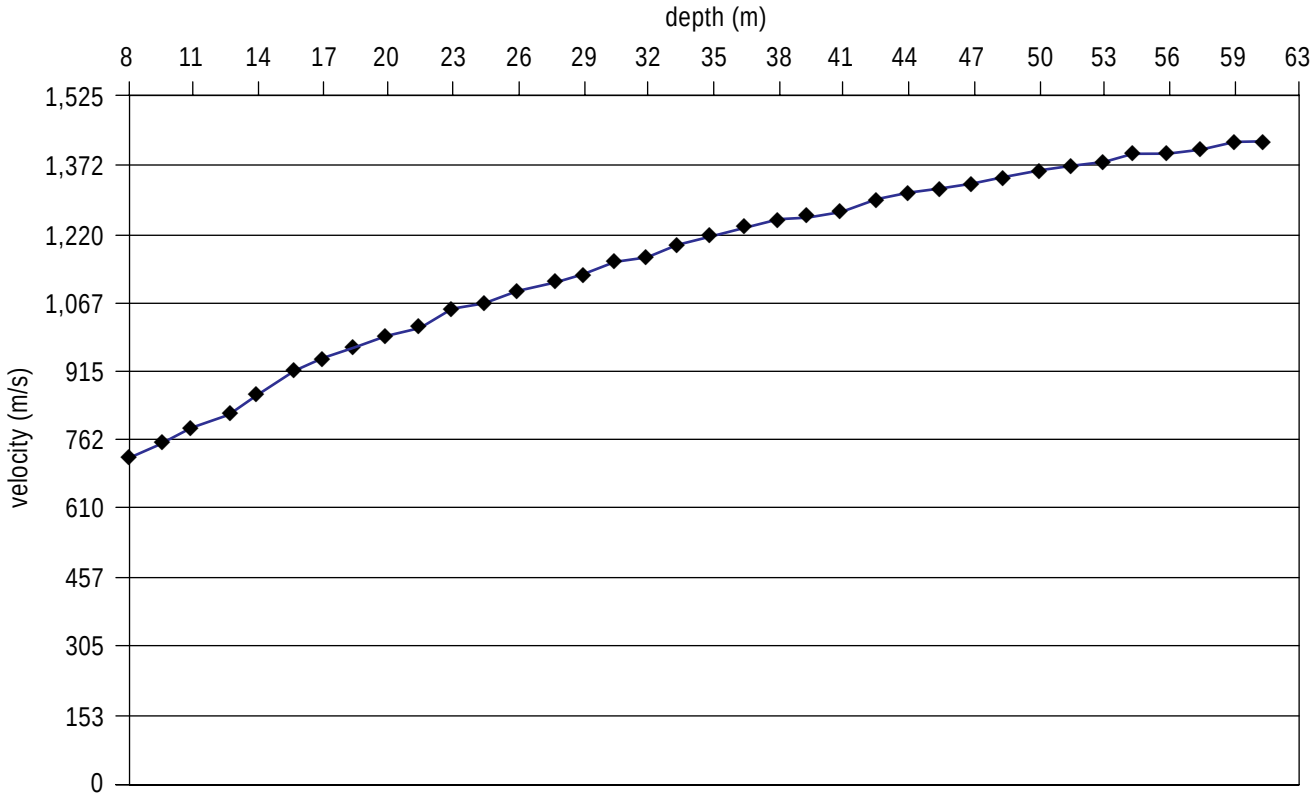

Figure B10. Average velocity plot of VSP #3 using the hydrophone receiver.

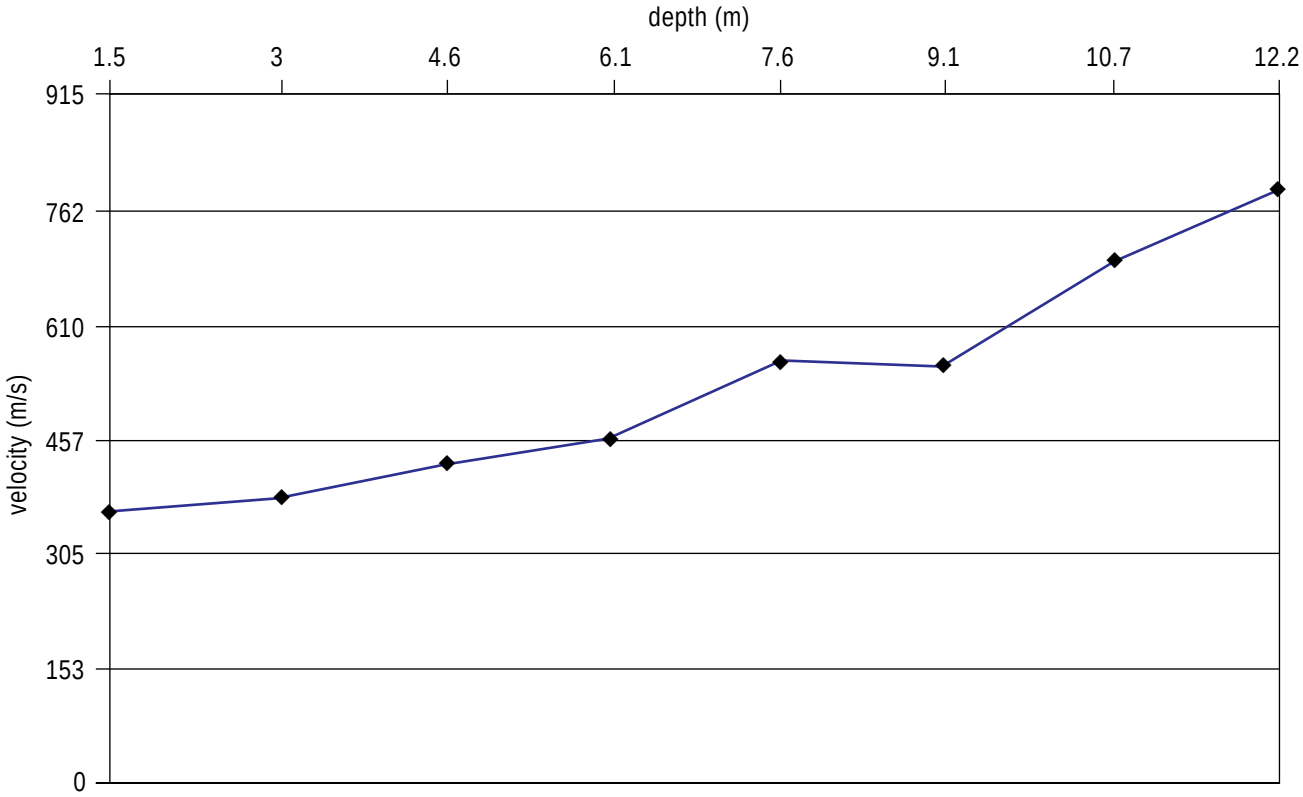

Figure B11. Interval velocity plot of VSP #3 using the hole-lock geophone.

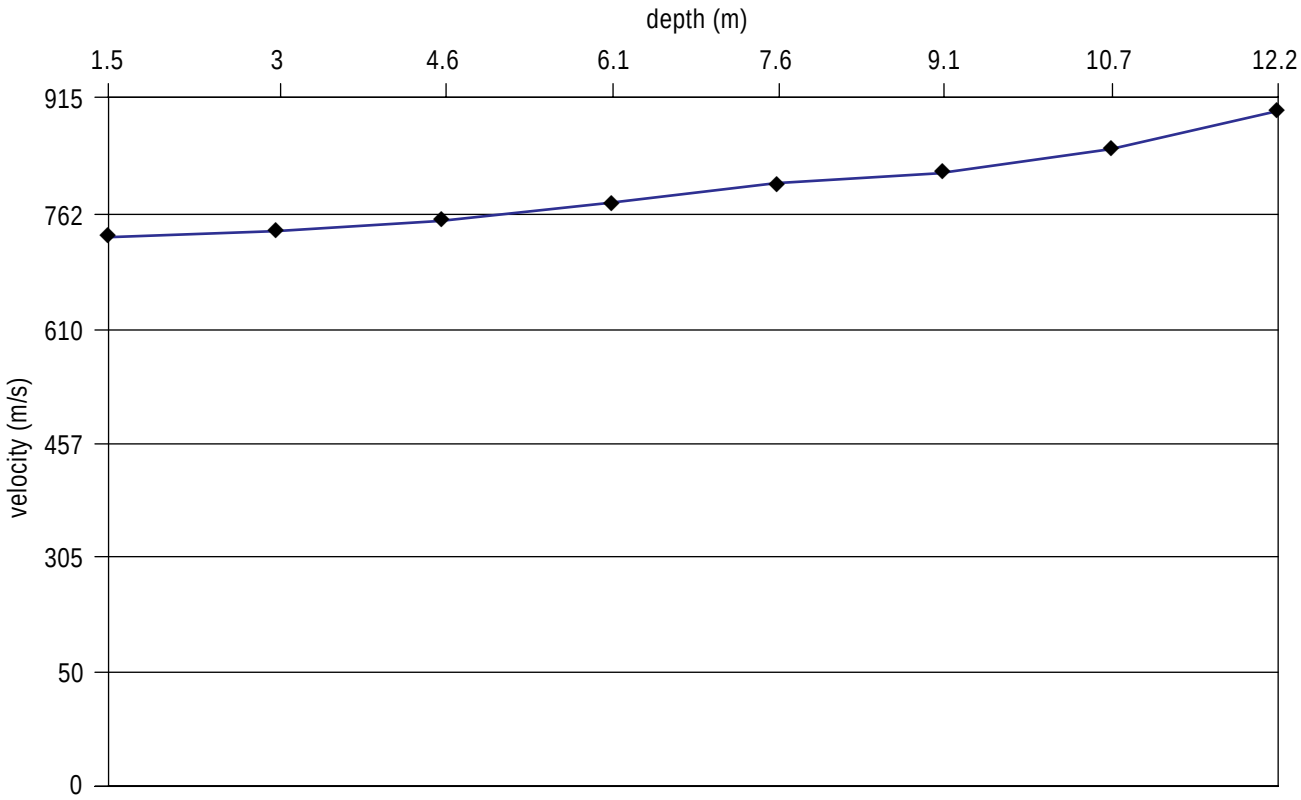

Figure B12. Average velocity plot of VSP #3 using the hole-lock geophone.

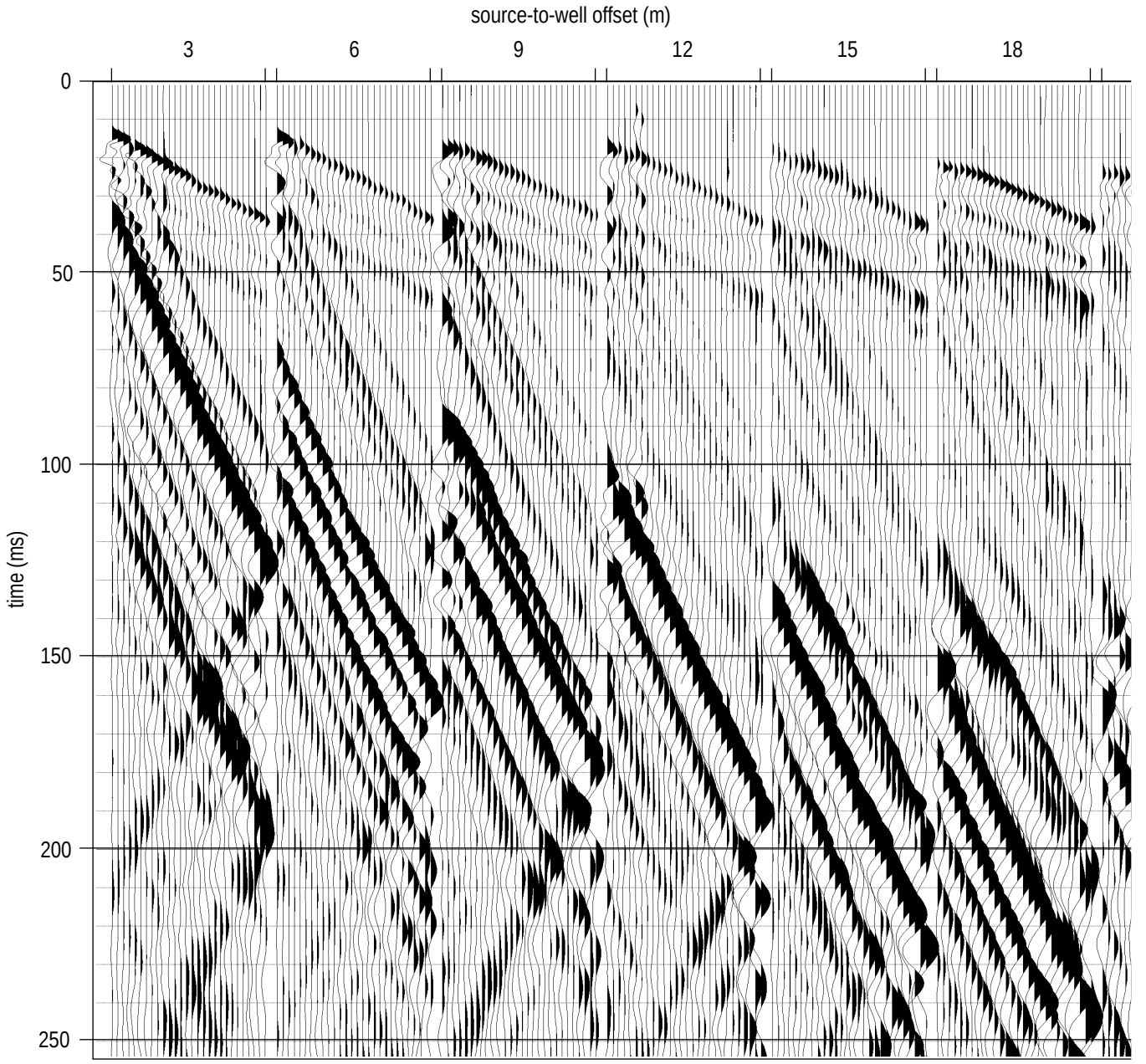

Figure B13a. VSP #1 raw hydrophone data. There are a total of 28 traces in each source offset gather with depths from 8 m to 48 m.

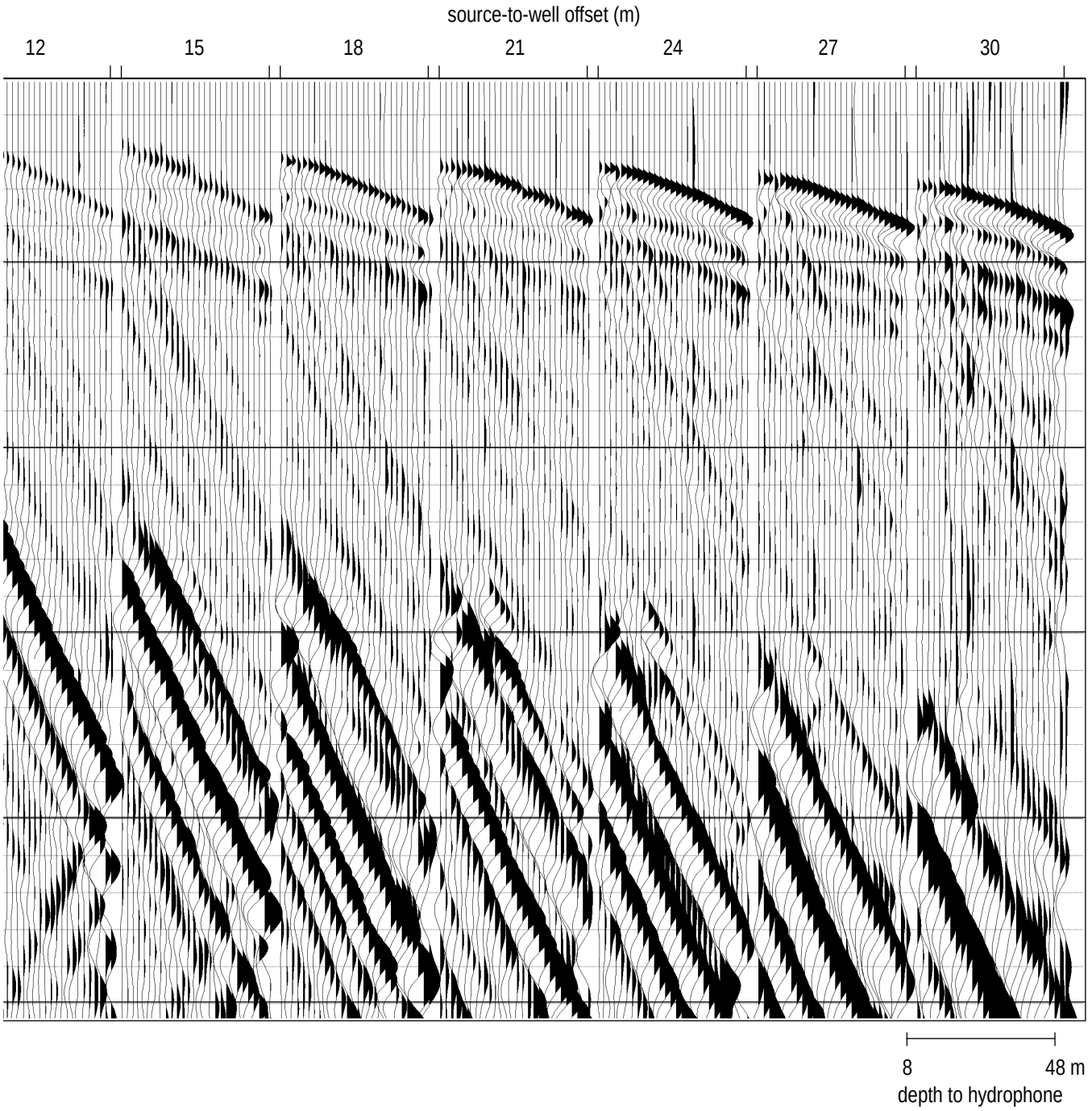
source-to-well offset (m)
12
15
18
21
24
27
30
8
48 m
depth to hydrophone

Figure B13b.

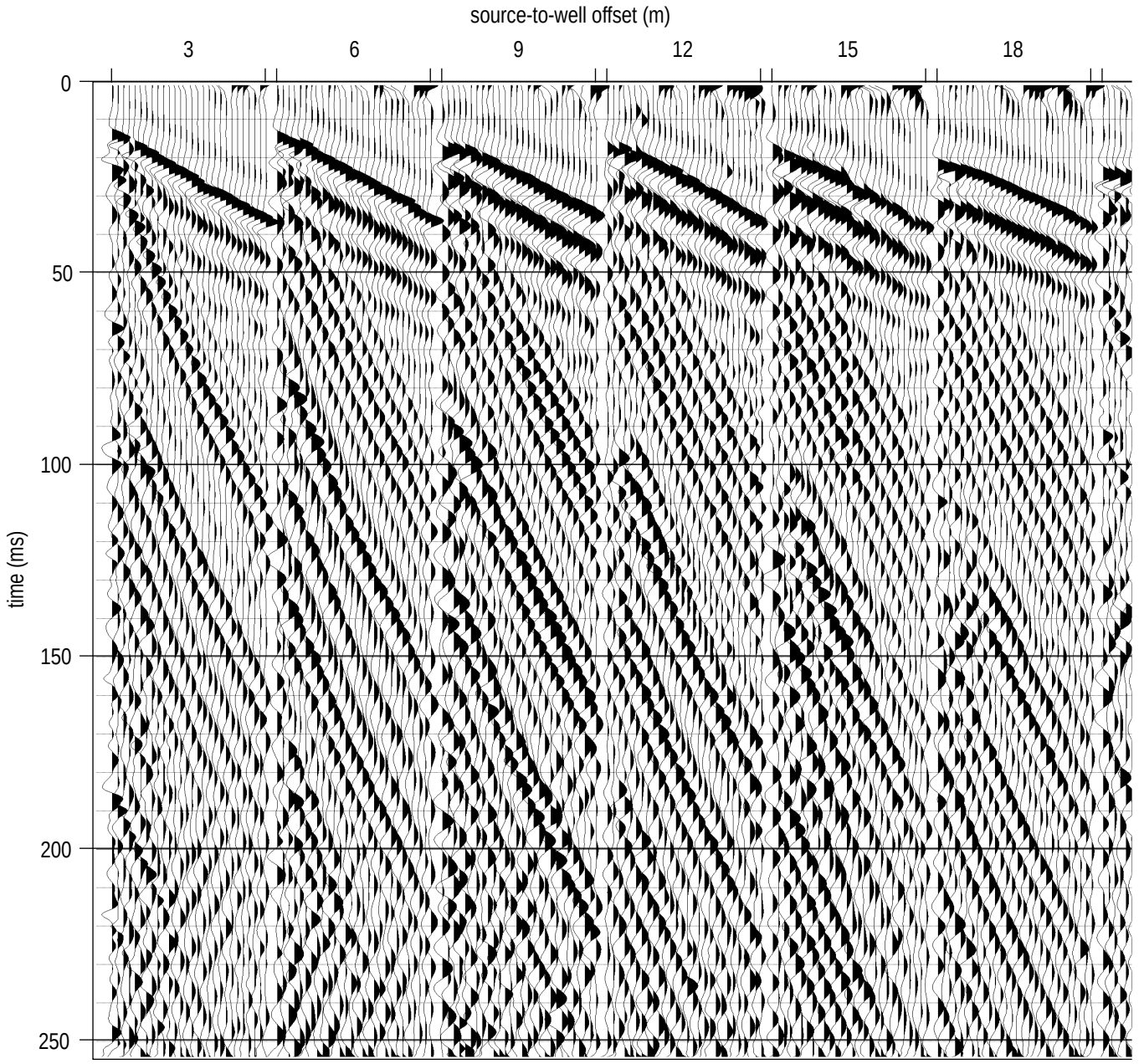

Figure B14a. VSP #1 hydrophone data (Figure B13) band-pass filtered (50 100 300 450) and AGC (50 ms) scaled.

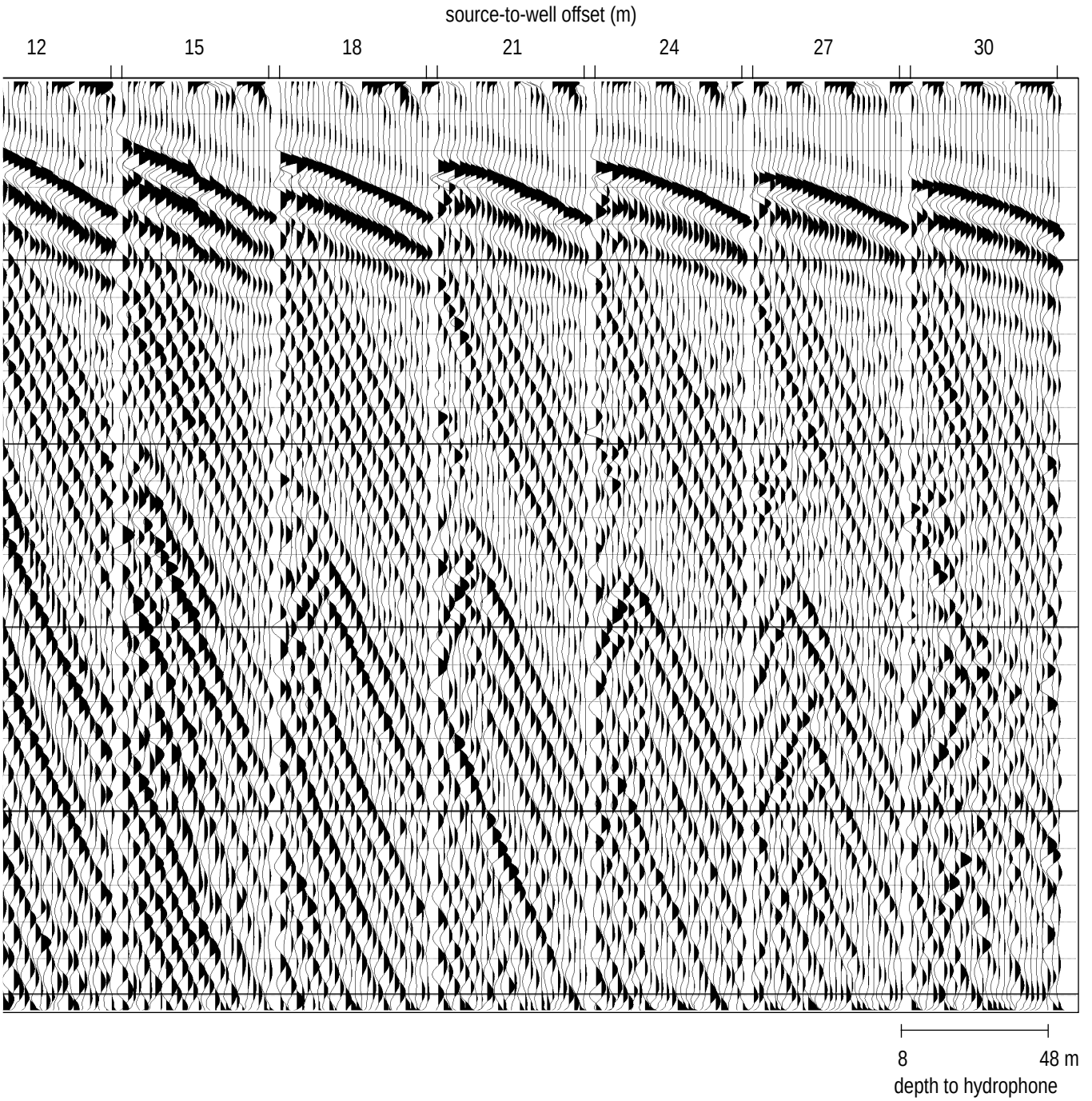
source-to-well offset (m)
12
15
18
21
24
27
30
8
48 m
depth to hydrophone

Figure B14b.

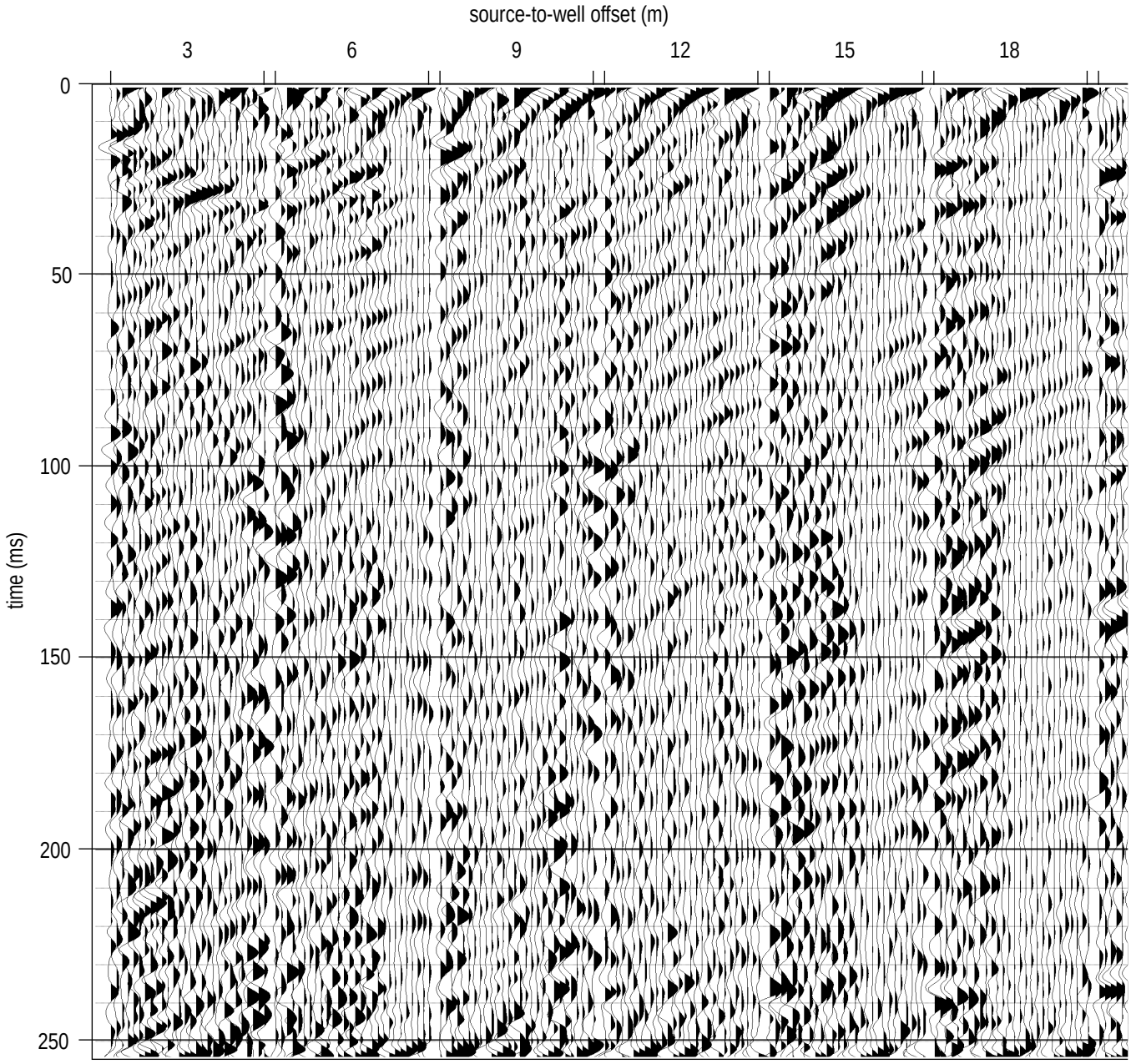

Figure B15a. VSP #1 up-coming waves. Two positive fan reject fk filters (0 – 1.5 ms/tr. and 2.0 – 4.0 ms/tr.) have been applied to filtered and scaled data (Figure B14) to eliminate down-going waves and one negative fan reject fk filter (-2.0 – -4.0 ms/tr.) has also been applied to the filtered data to take out strong up-coming tube waves.

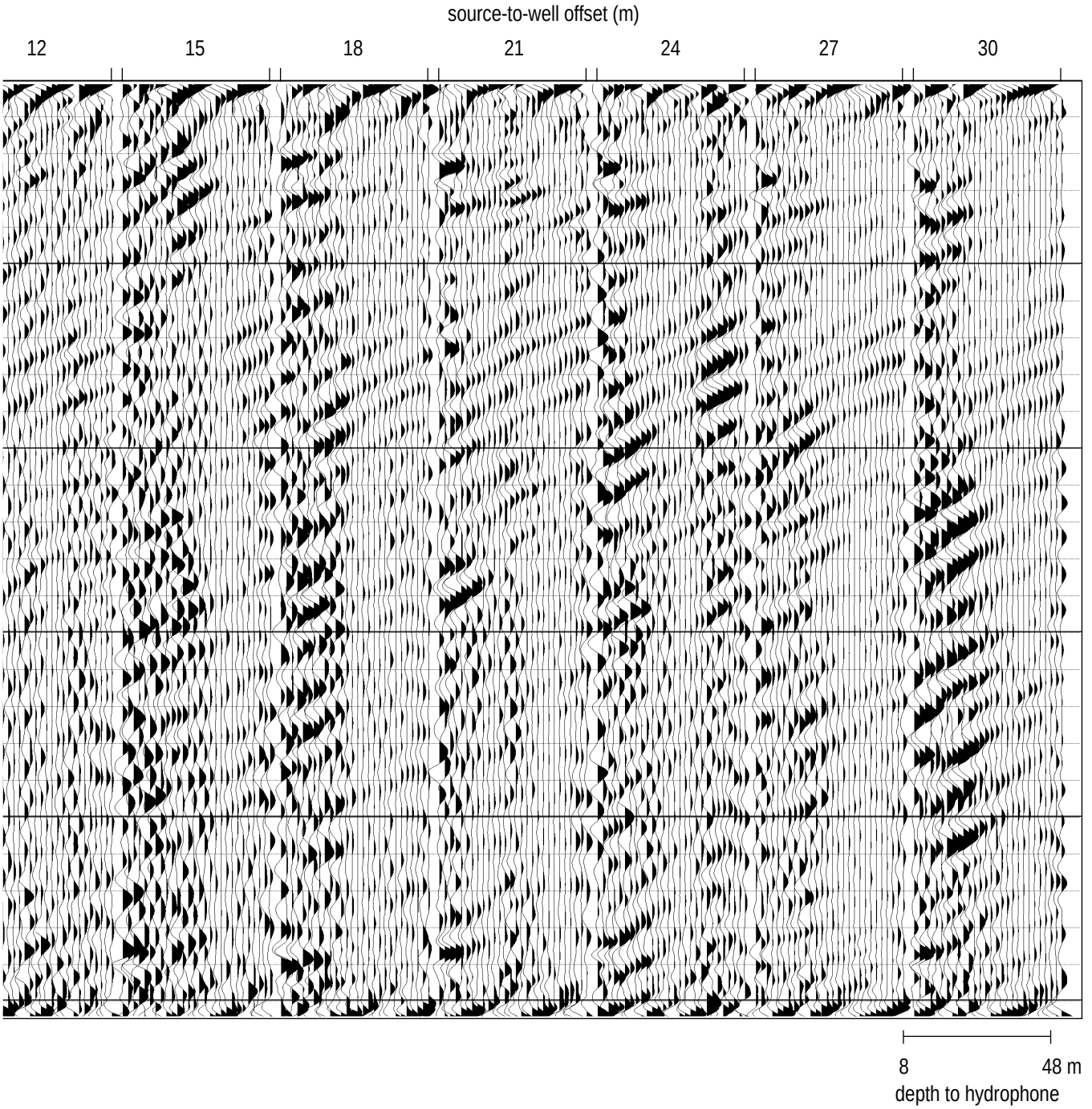
source-to-well offset (m)
12
15
18
21
24
27
30
8
48 m
depth to hydrophone

Figure B15b.

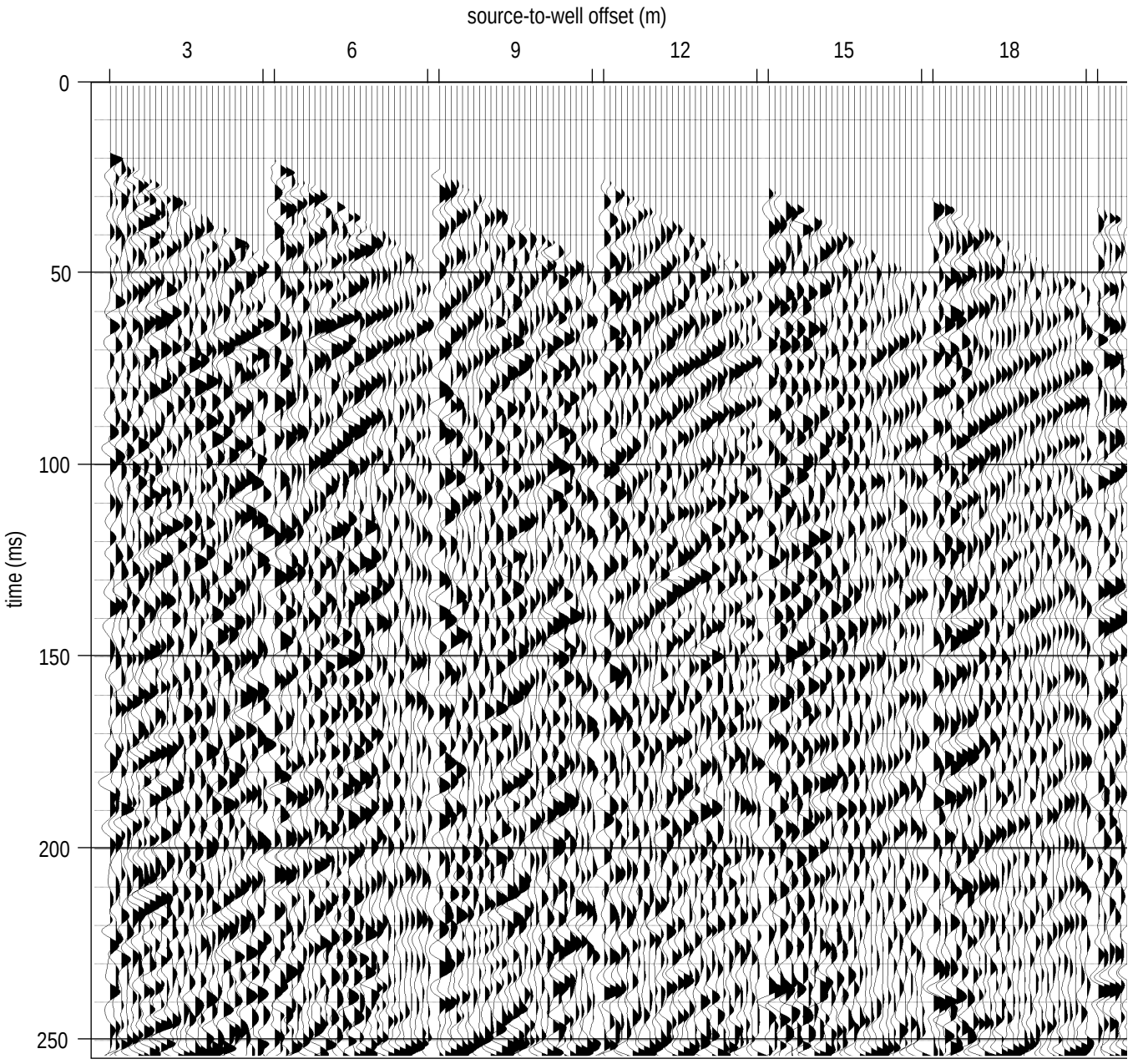

Figure B16a. VSP #1 hydrophone data first arrival muted. The first arrival mute is applied to fk filtered data (Figure B15).

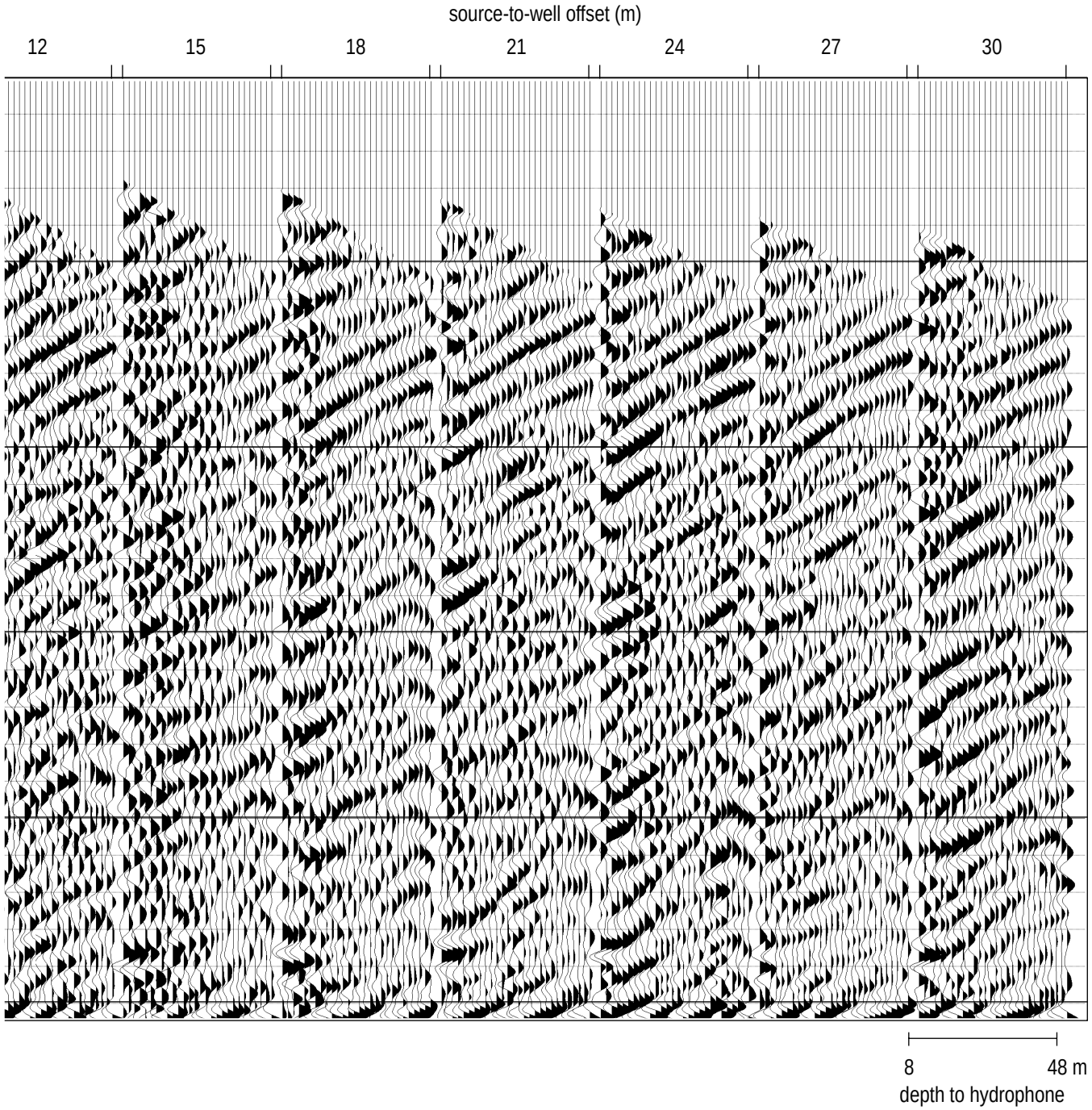
source-to-well offset (m)
12
15
18
21
24
27
30
8
48 m
depth to hydrophone

Figure B16b.

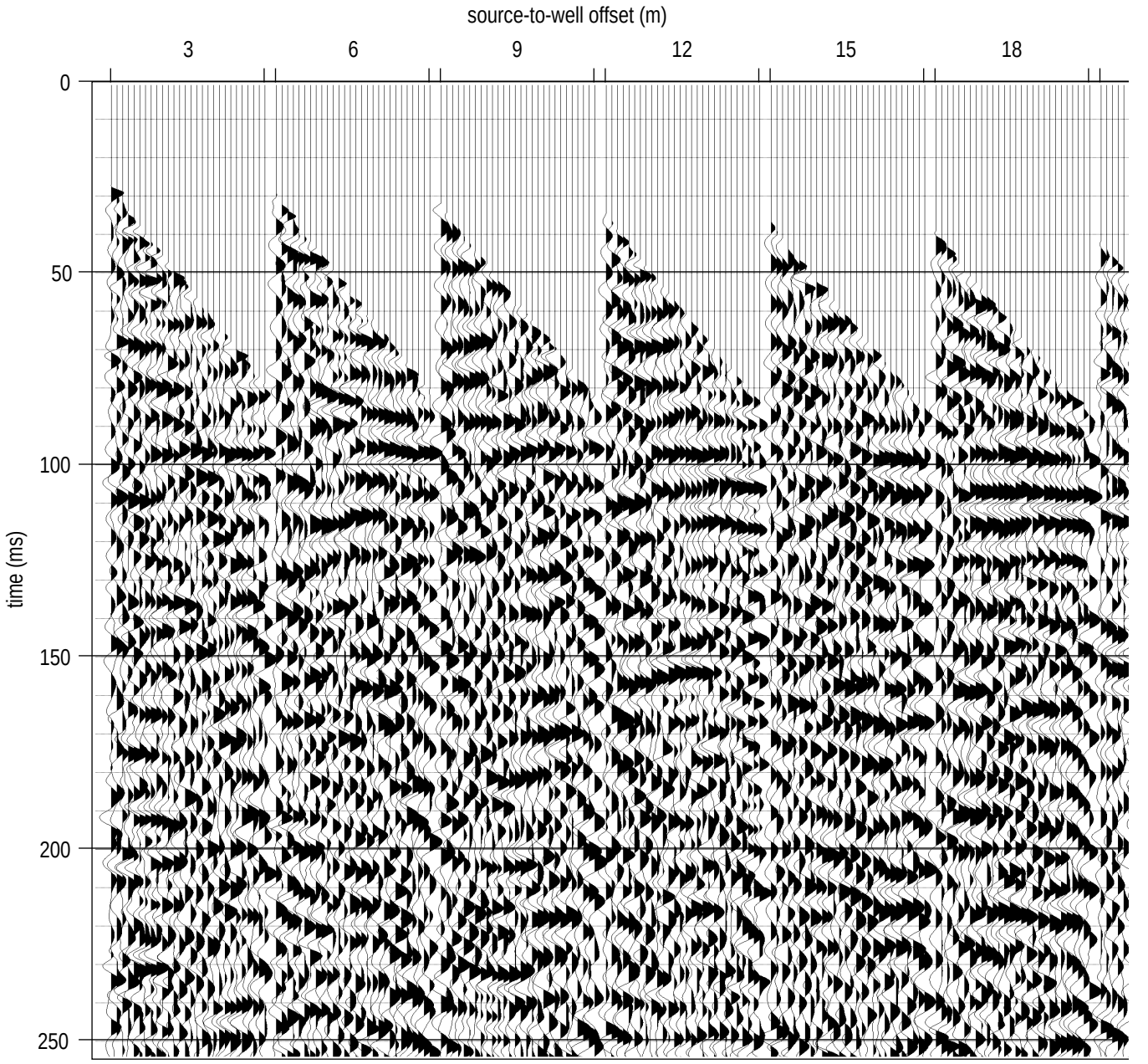

Figure B17a. VSP #1 hydrophone data static corrected to vertical incidence. The static correction is applied to first arrival data, datum correcting all hydrophones to the well head.

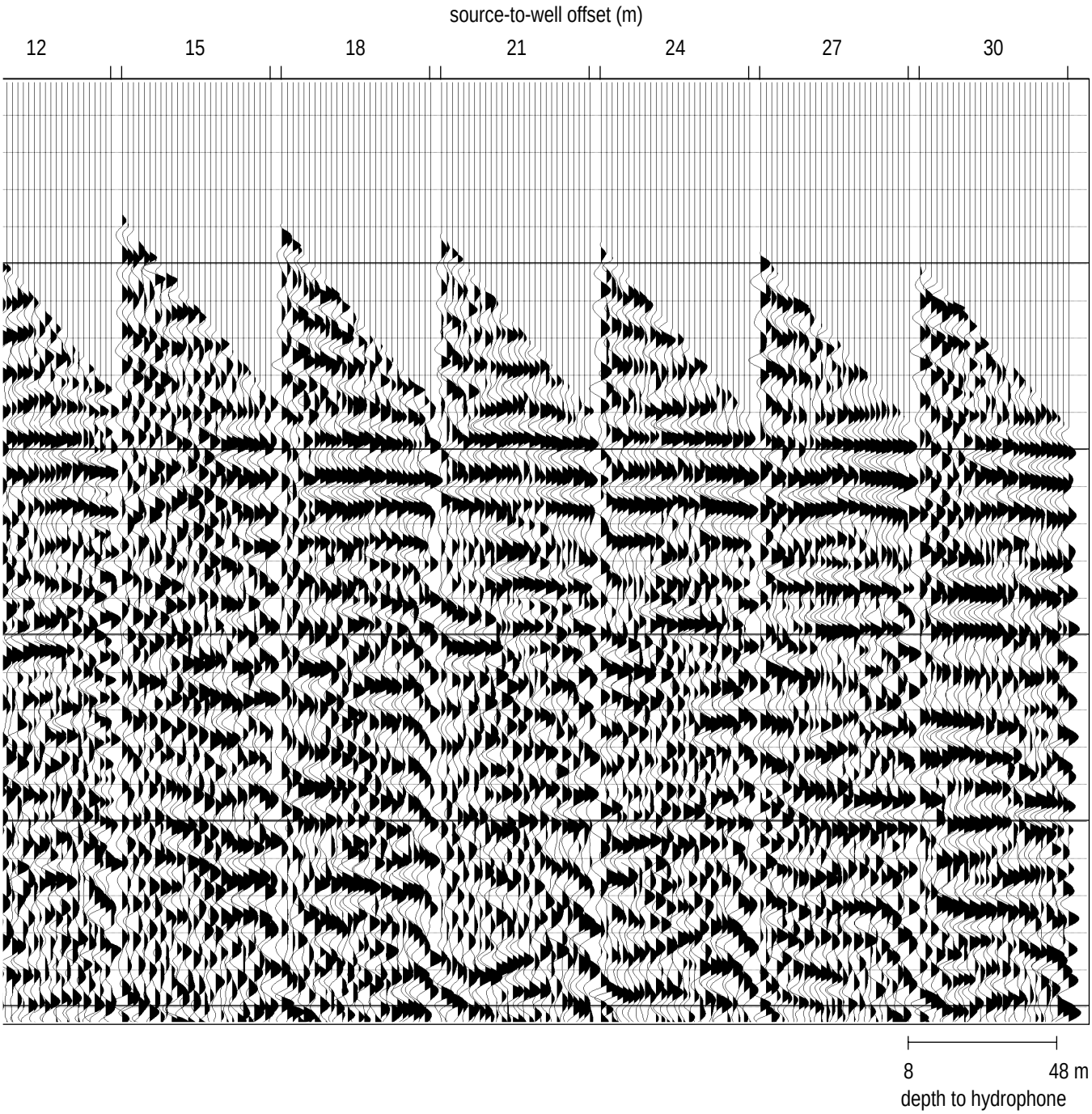
source-to-well offset (m)
12
15
18
21
24
27
30
8
48 m
depth to hydrophone

Figure B17b.

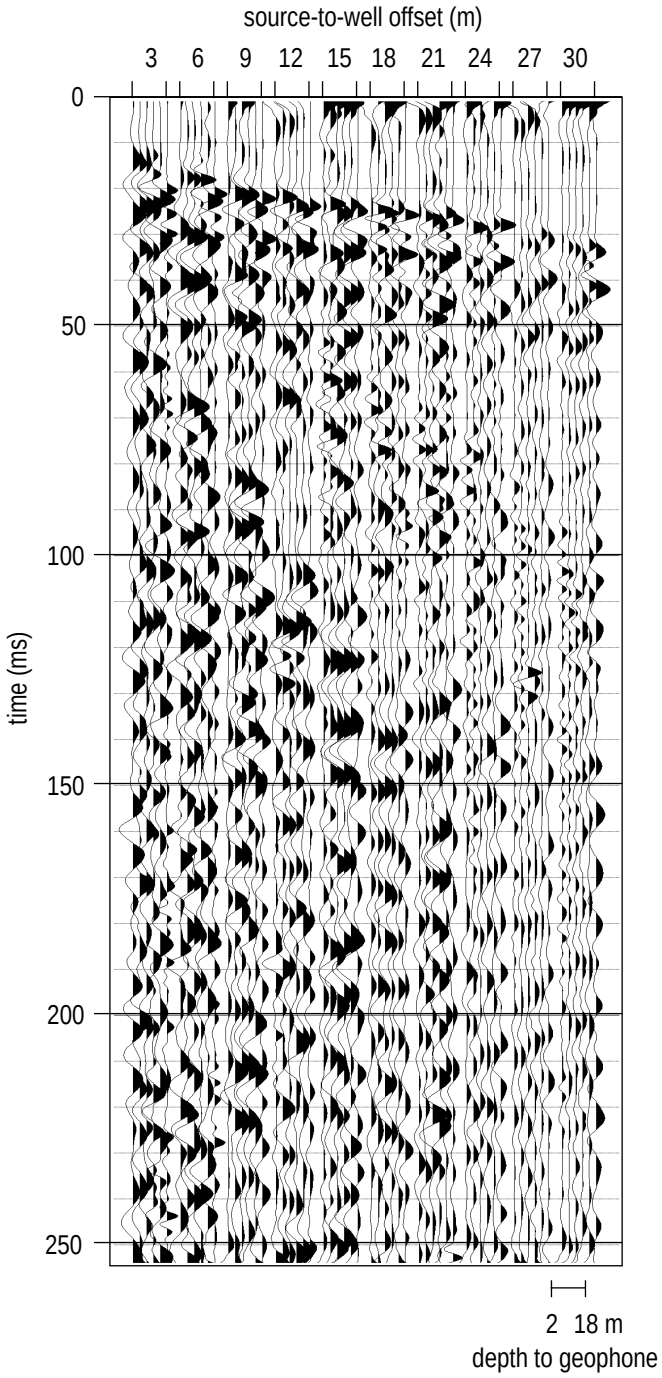

Figure B18. VSP #1 geophone data band-pass filtered (50 100 300 450) and AGC (50 ms) scaled. There are a total of 6 traces in each gather with depths from 2 m to 18 m.

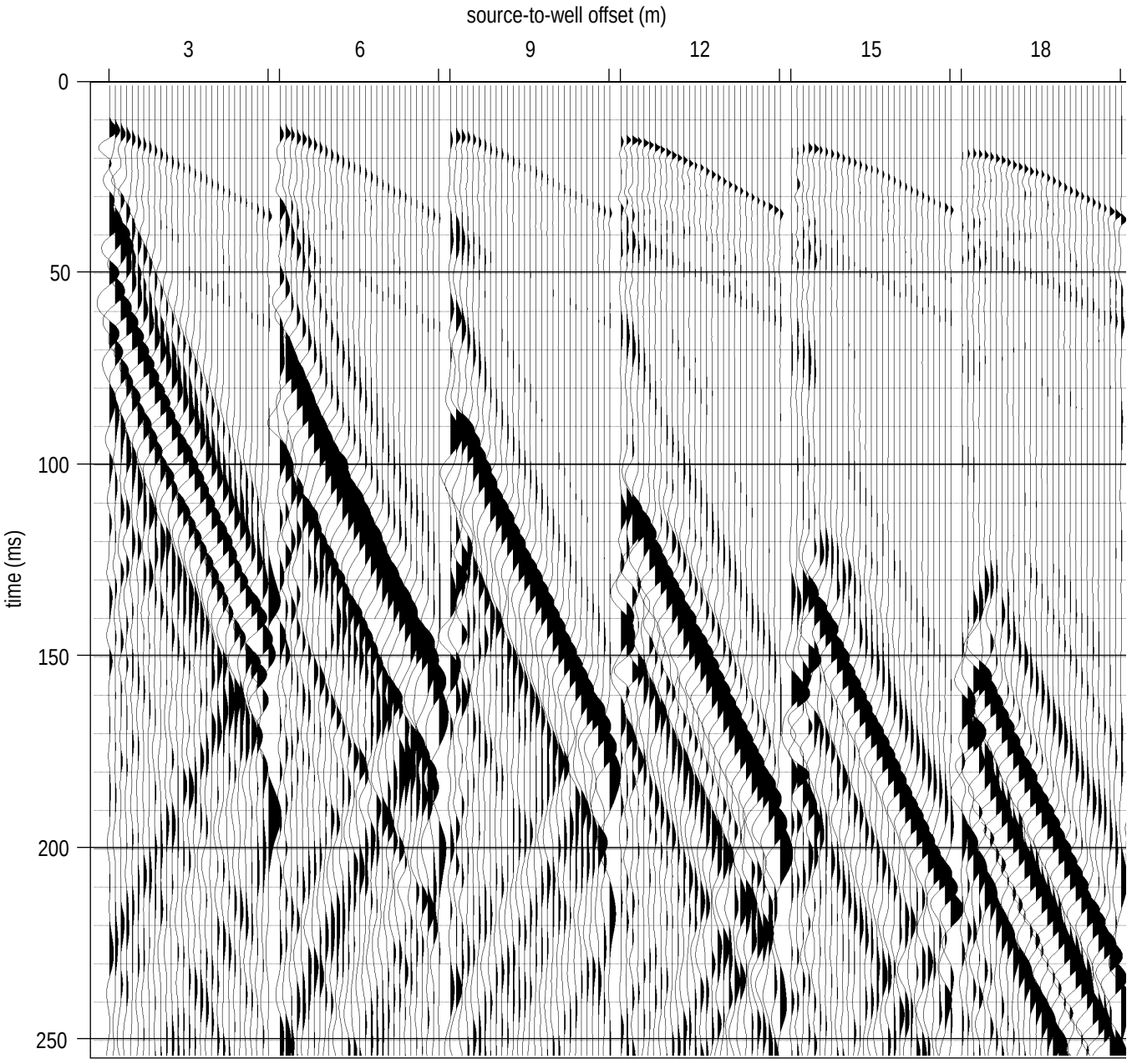

Figure B19a. VSP #2 raw hydrophone data. There are a total of 29 traces in each source offset gather with depths from 5 m to 47 m.

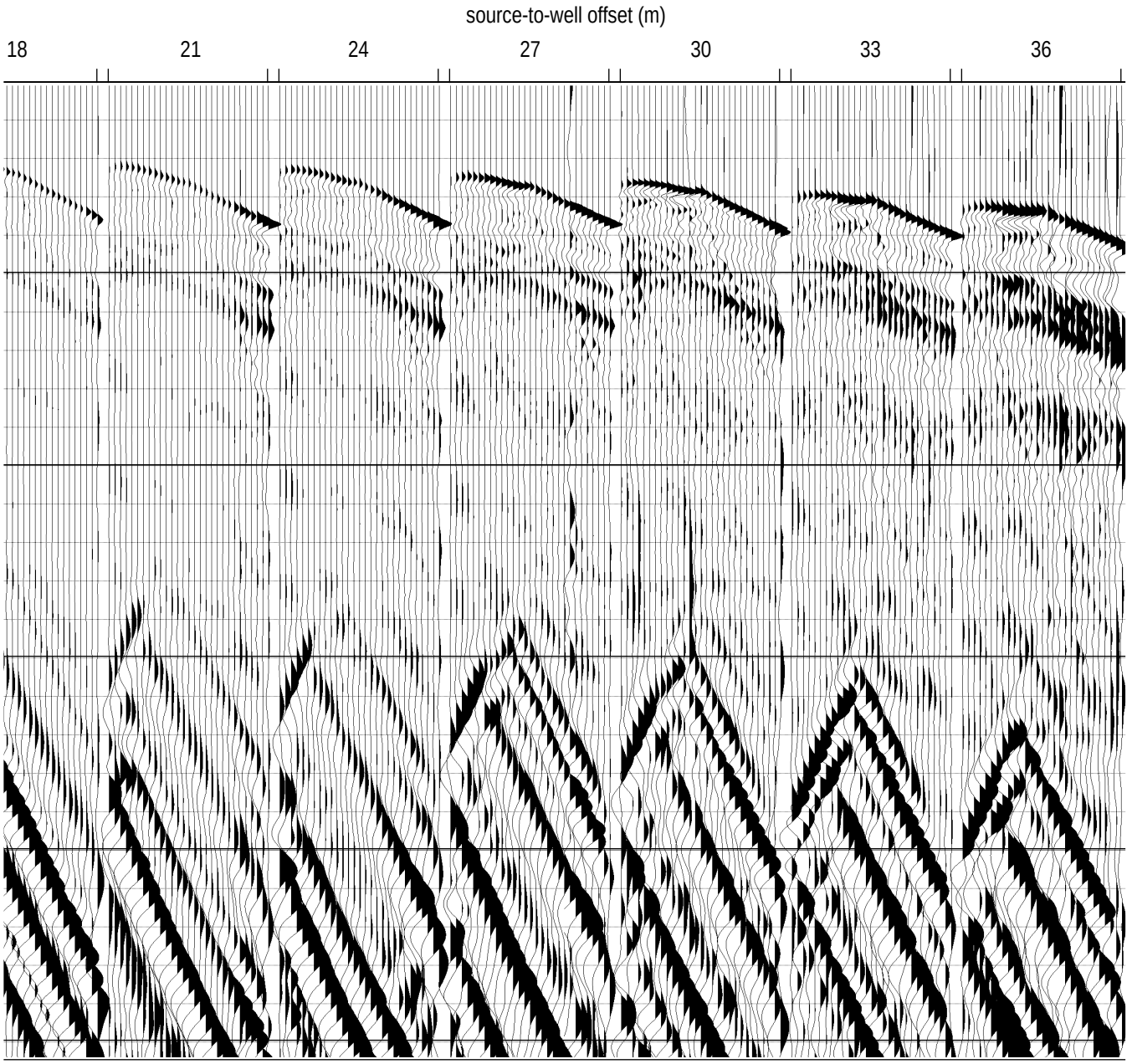

Figure B19b.

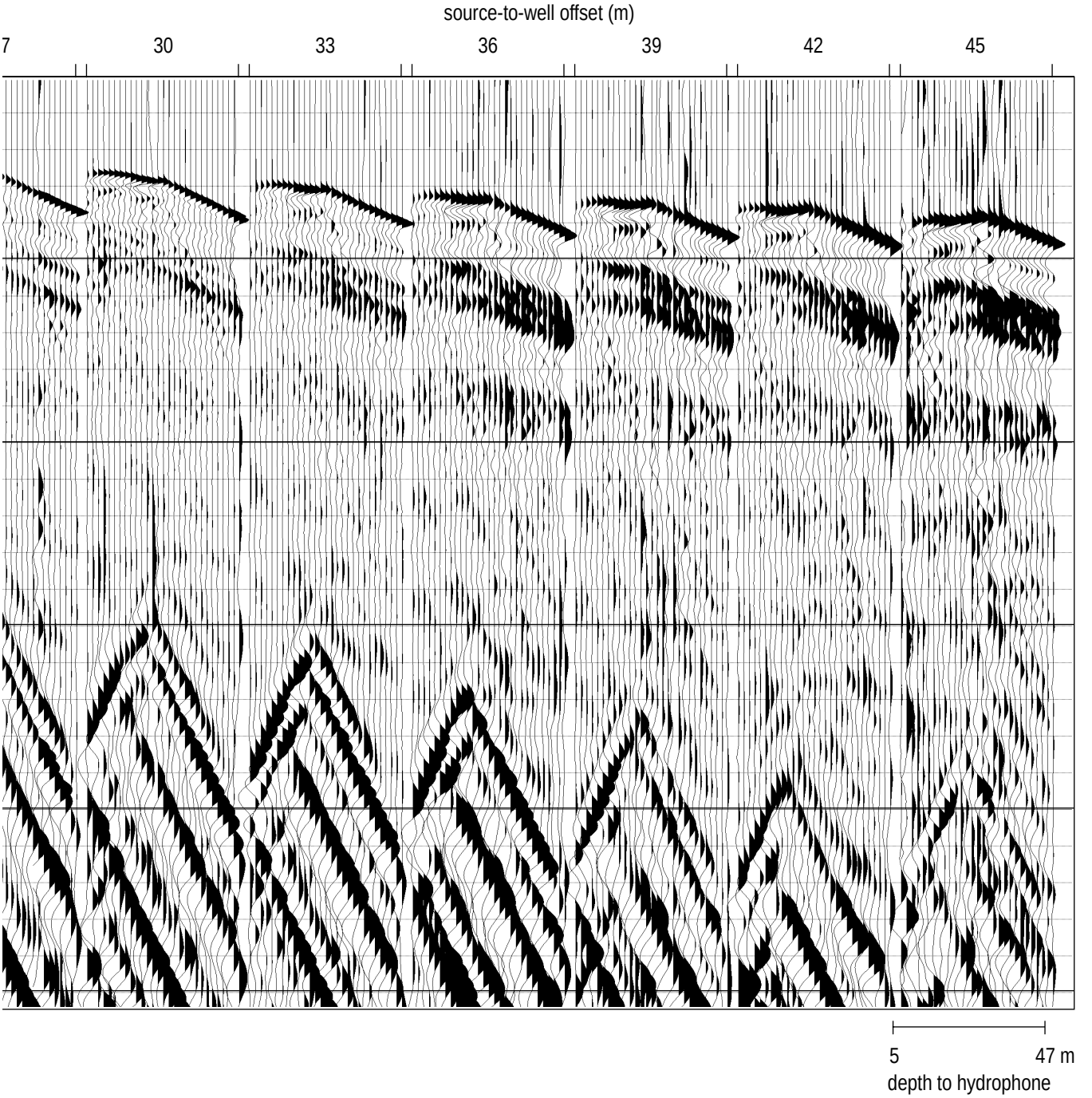
source-to-well offset (m)
7
30
33
36
39
42
45
5
47 m
depth to hydrophone

Figure B19c.

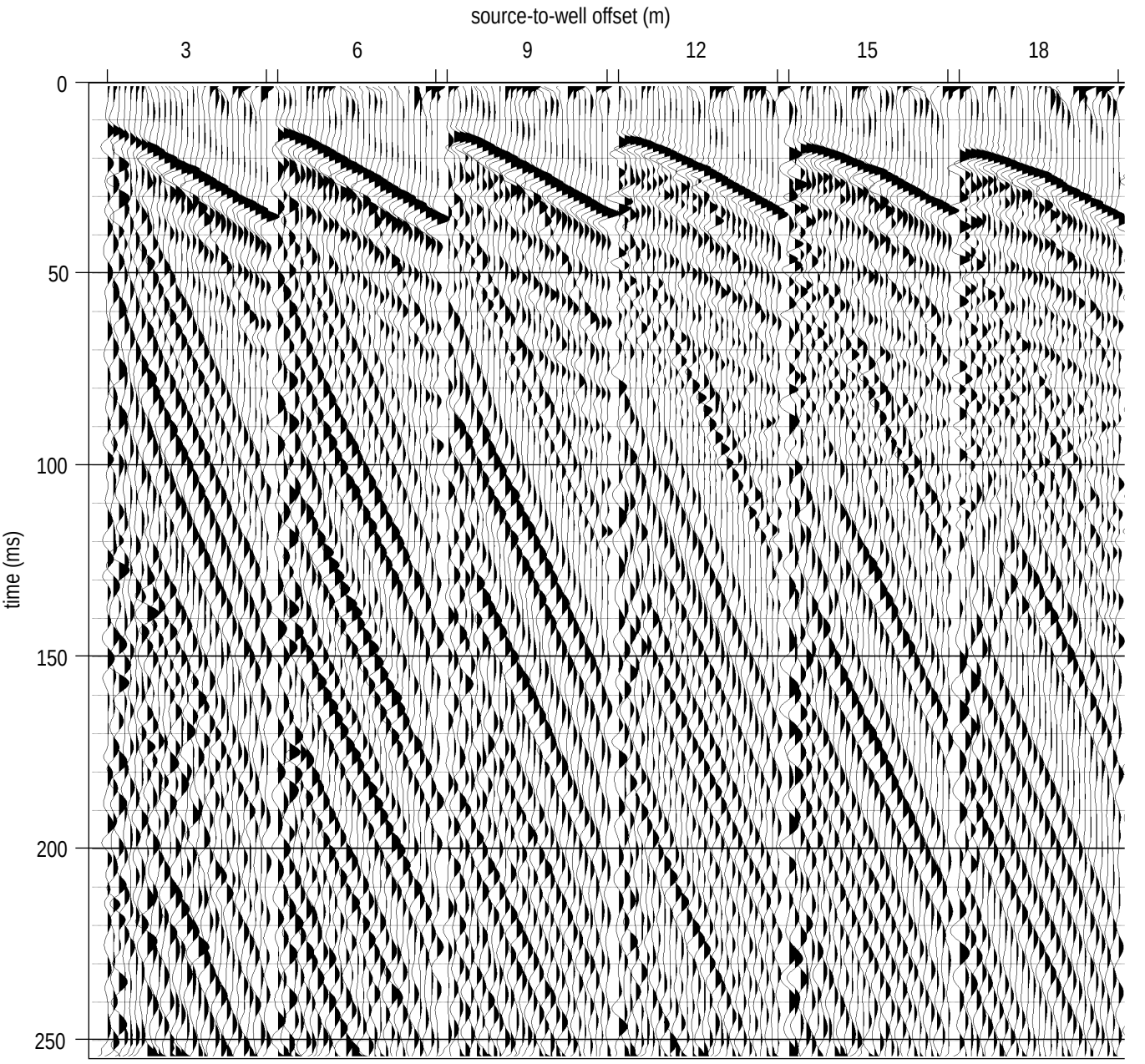

Figure B20a. VSP #2 hydrophone data (Figure B19) band-pass filtered (50 100 300 450) and AGC (50 ms) scaled.

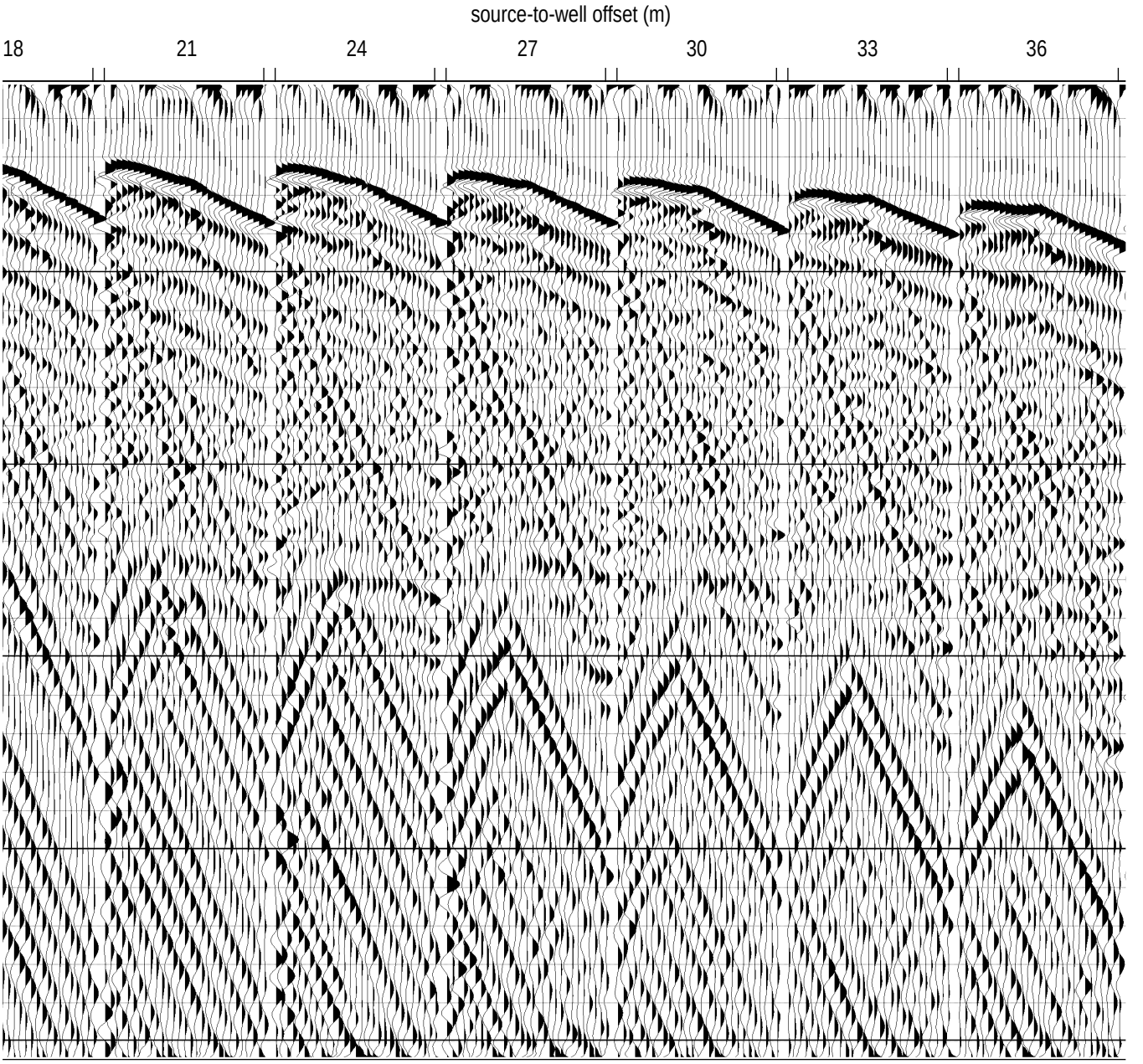

Figure B20b.

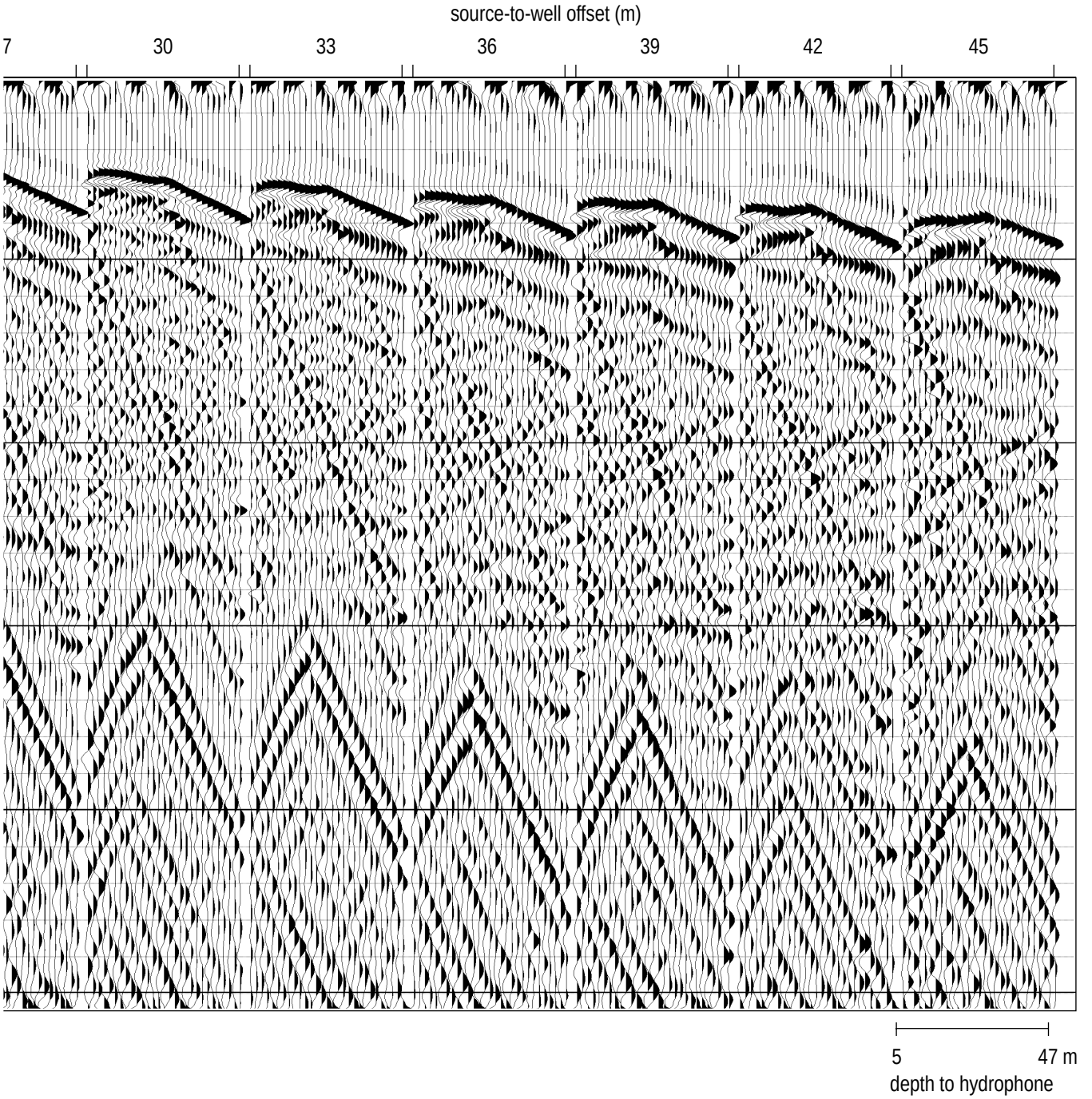
source-to-well offset (m)
7
30
33
36
39
42
45
5
47 m
depth to hydrophone

Figure B20c.

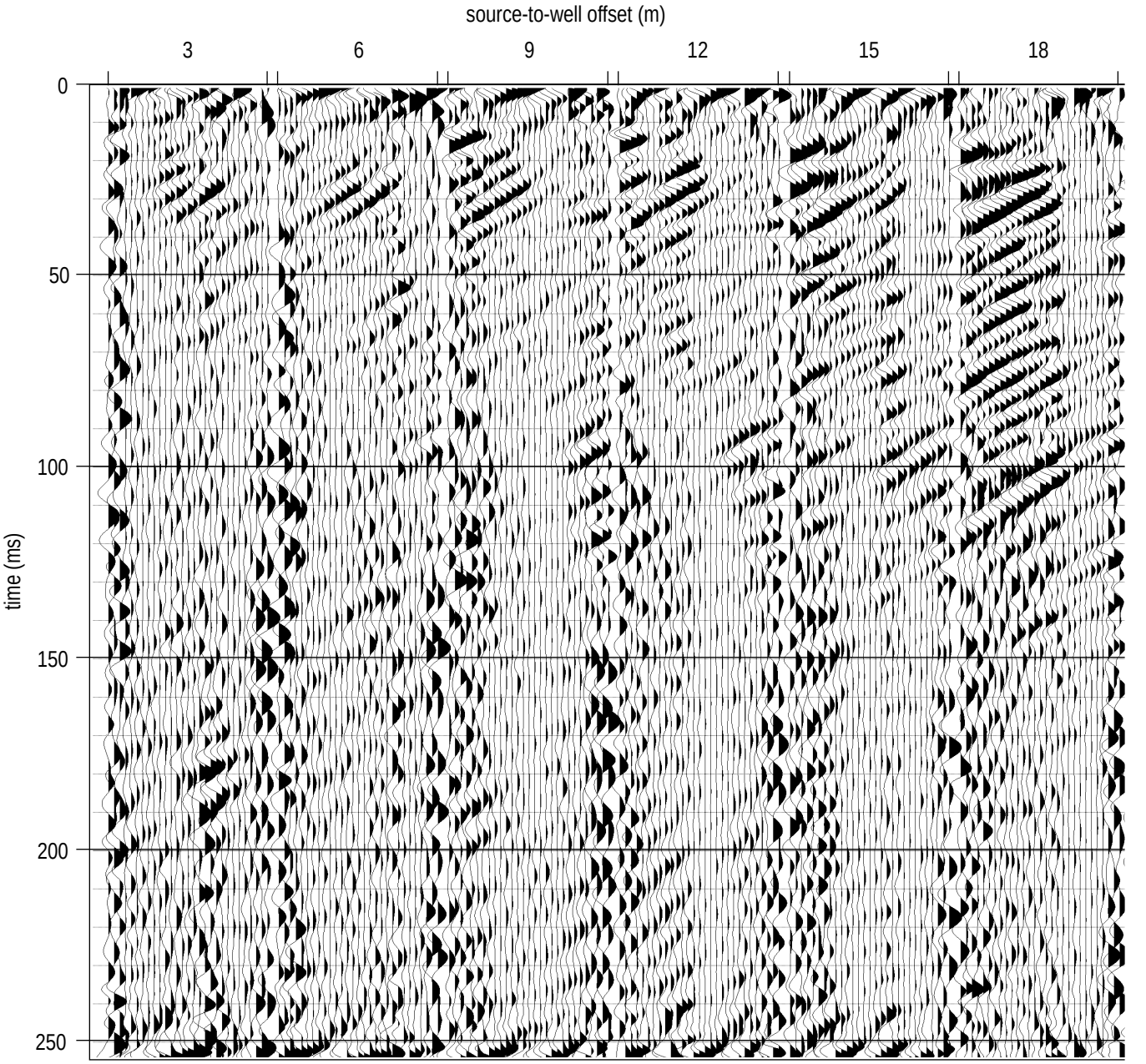

Figure B21a. VSP #2 up-coming waves. Two positive fan reject fk filters (0 – 1.5 ms/tr. and 2.0 – 4.0 ms/tr.) have been applied to filtered and scaled data (Figure B20) to eliminate down-going waves and one negative fan reject fk filter (-2.0 – -4.0 ms/tr.) has also been applied to the filtered data to take out strong up-coming tube waves.

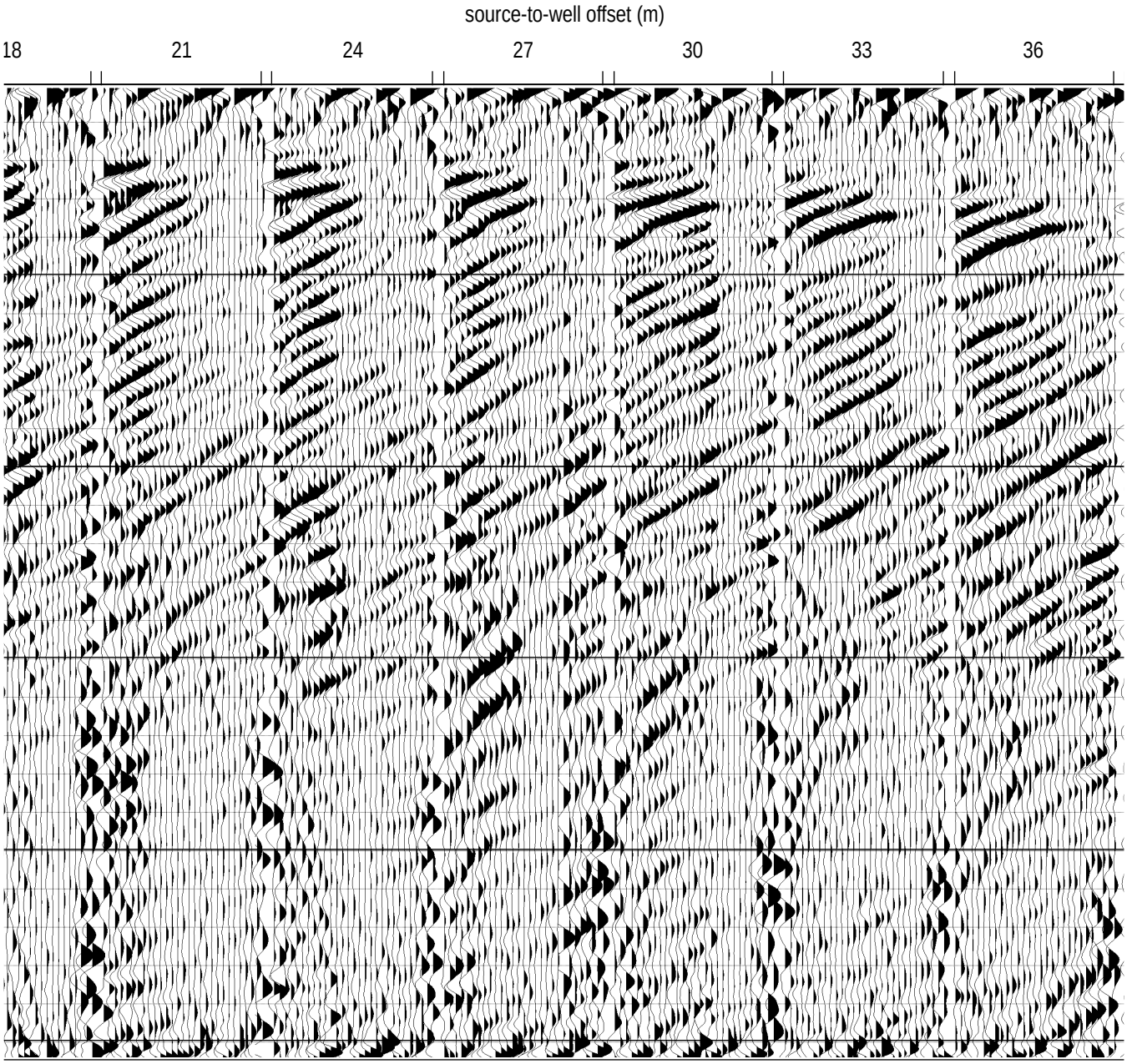

Figure B21b.

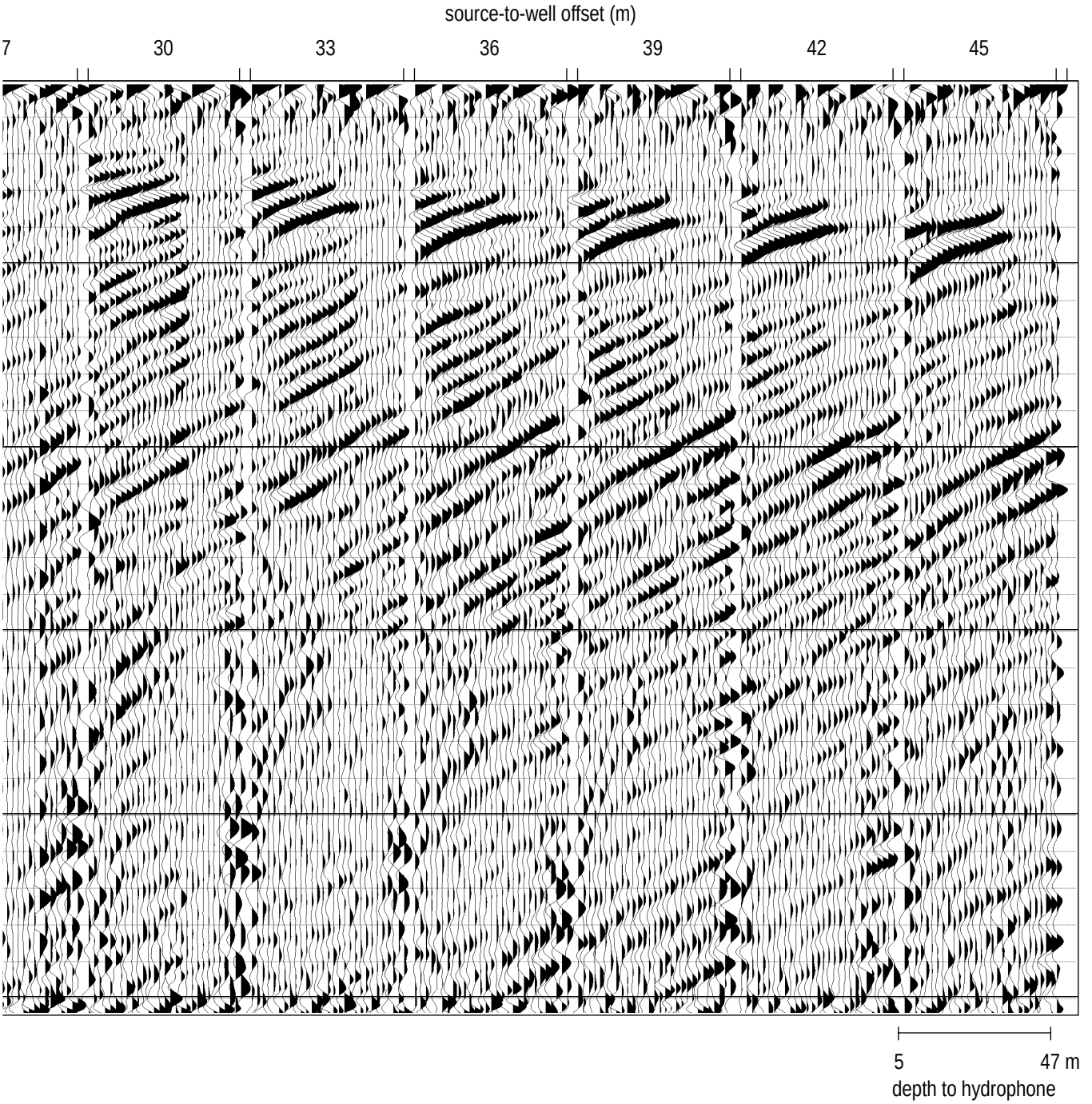
source-to-well offset (m)
7
30
33
36
39
42
45
5
47 m
depth to hydrophone

Figure B21c.

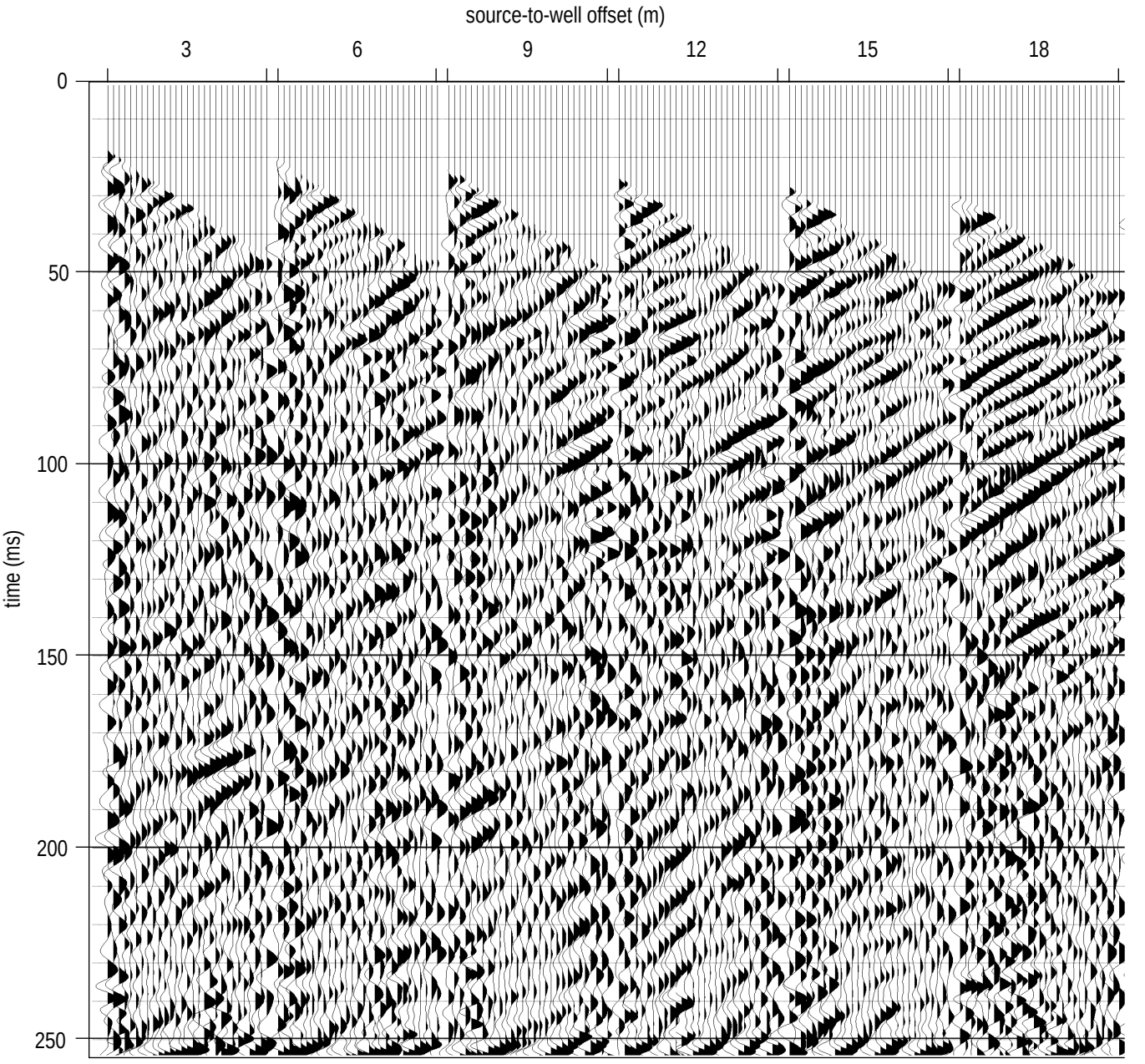

Figure B22a. VSP #2 hydrophone data first arrival muted. The first arrival mute is applied to fk filtered data (Figure B21).

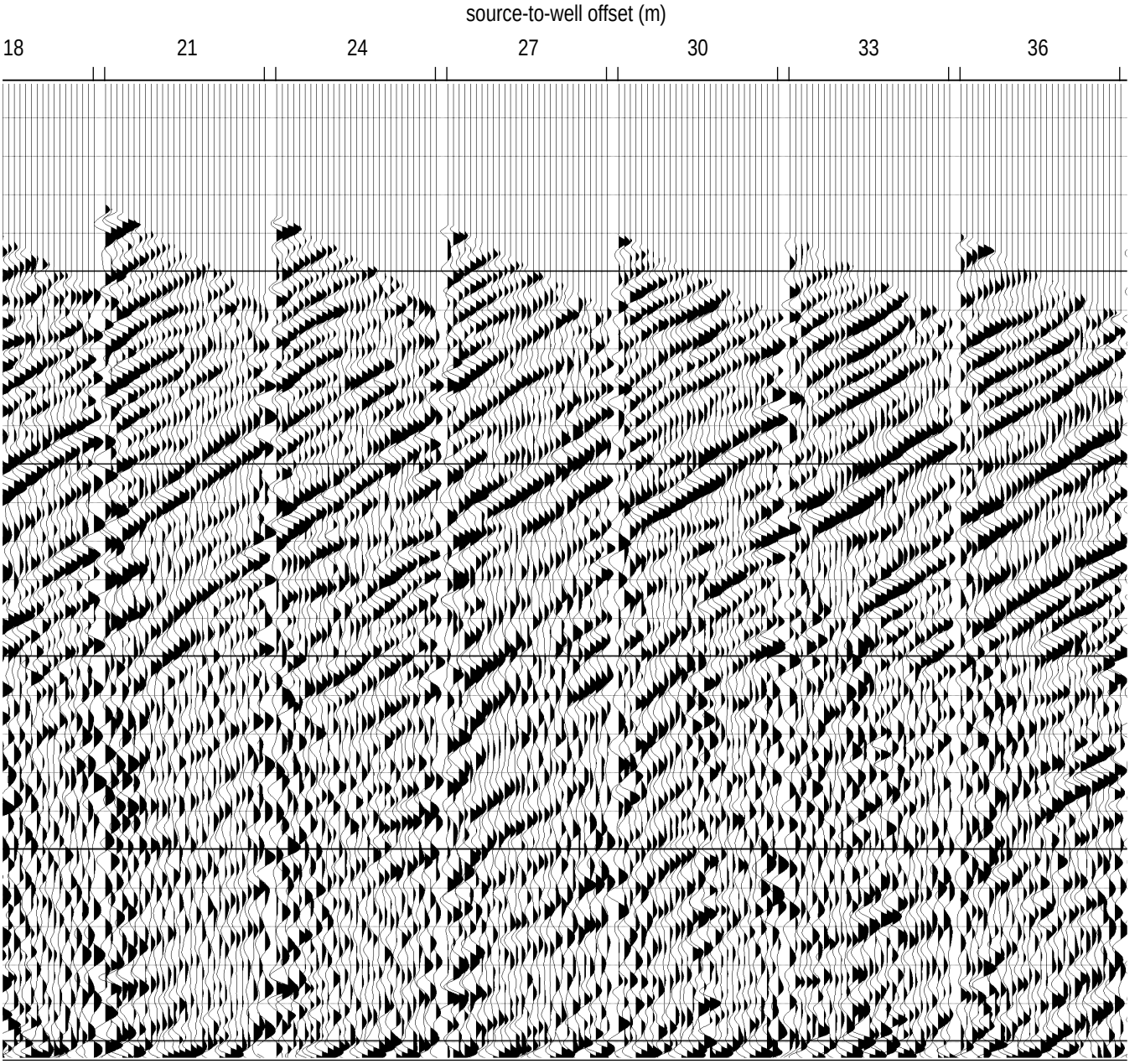

Figure B22b.

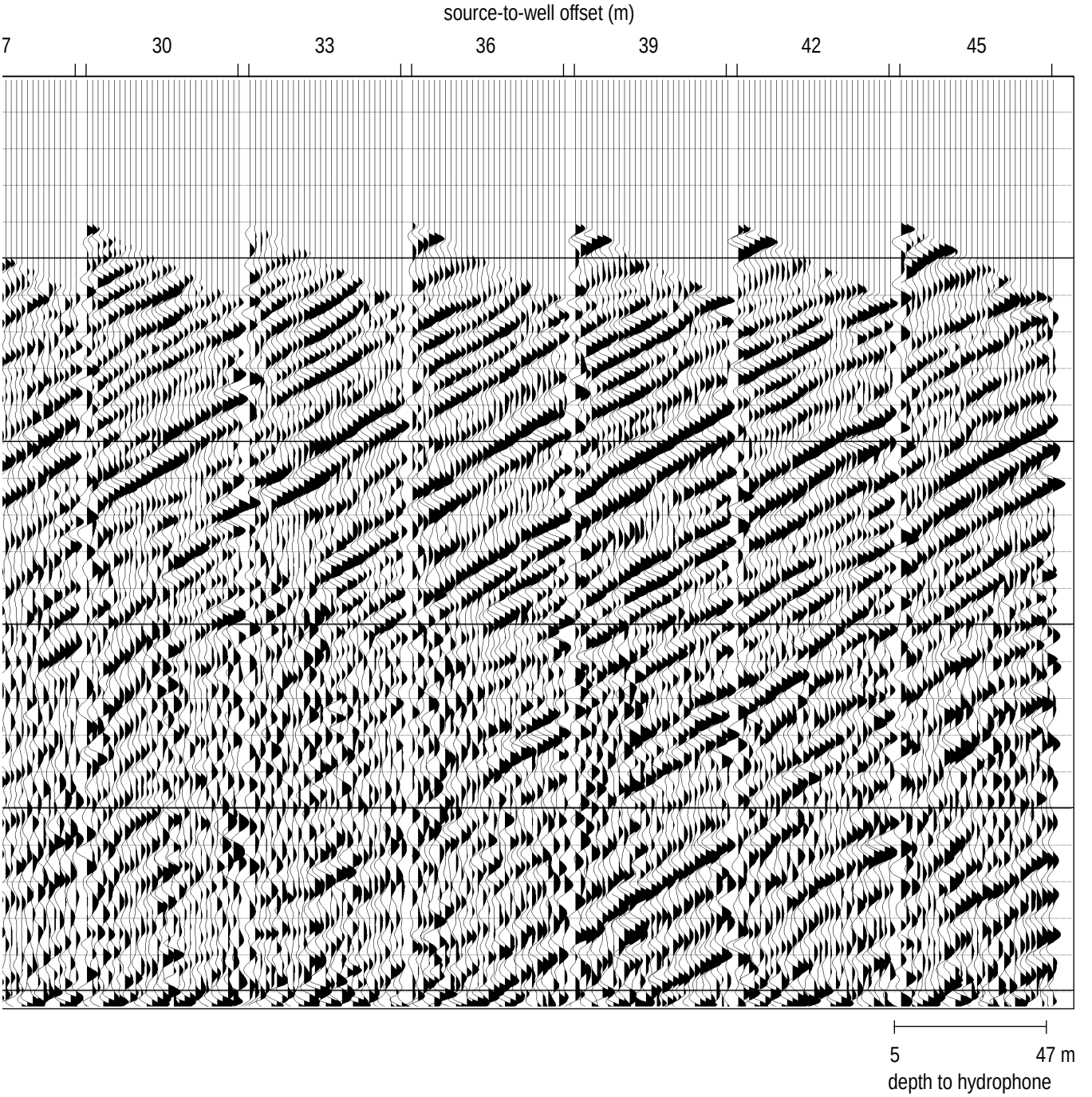
source-to-well offset (m)
7
30
33
36
39
42
45
5
47 m
depth to hydrophone

Figure B22c.

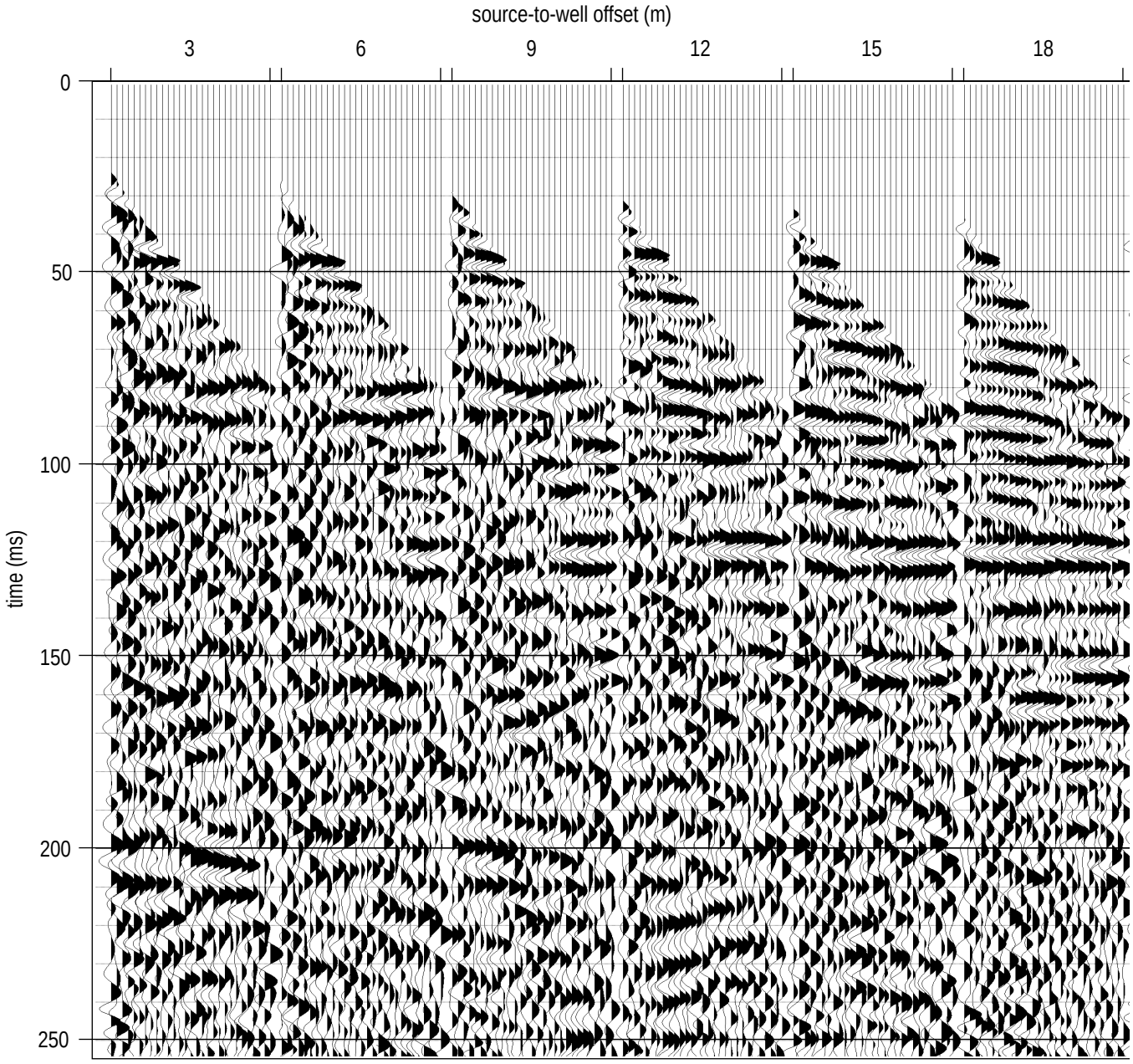

Figure B23a. VSP #2 hydrophone data static corrected to vertical incidence. The static correction is applied to first arrival data, datum correcting all hydrophones to the well head.

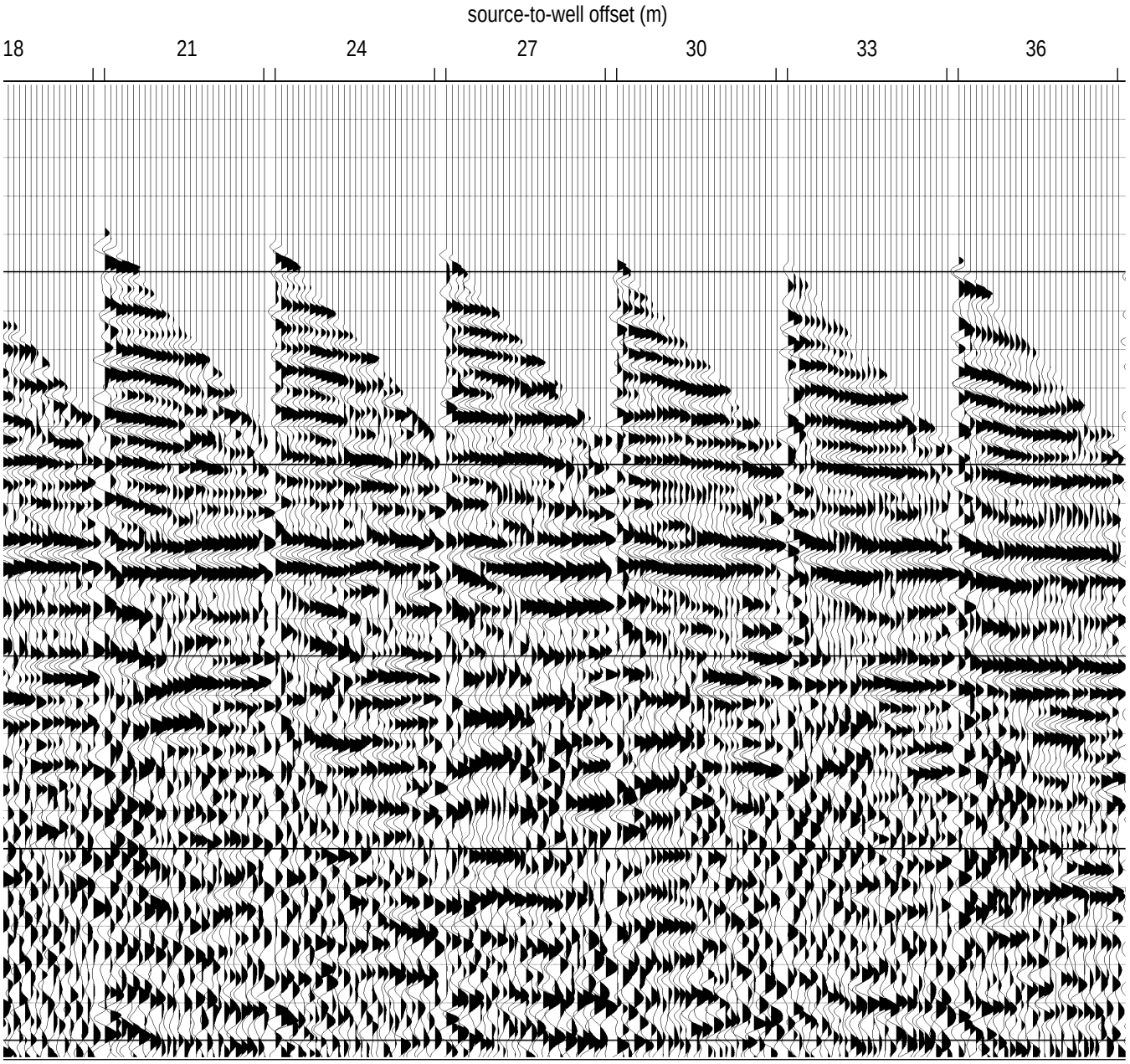

Figure B23b.

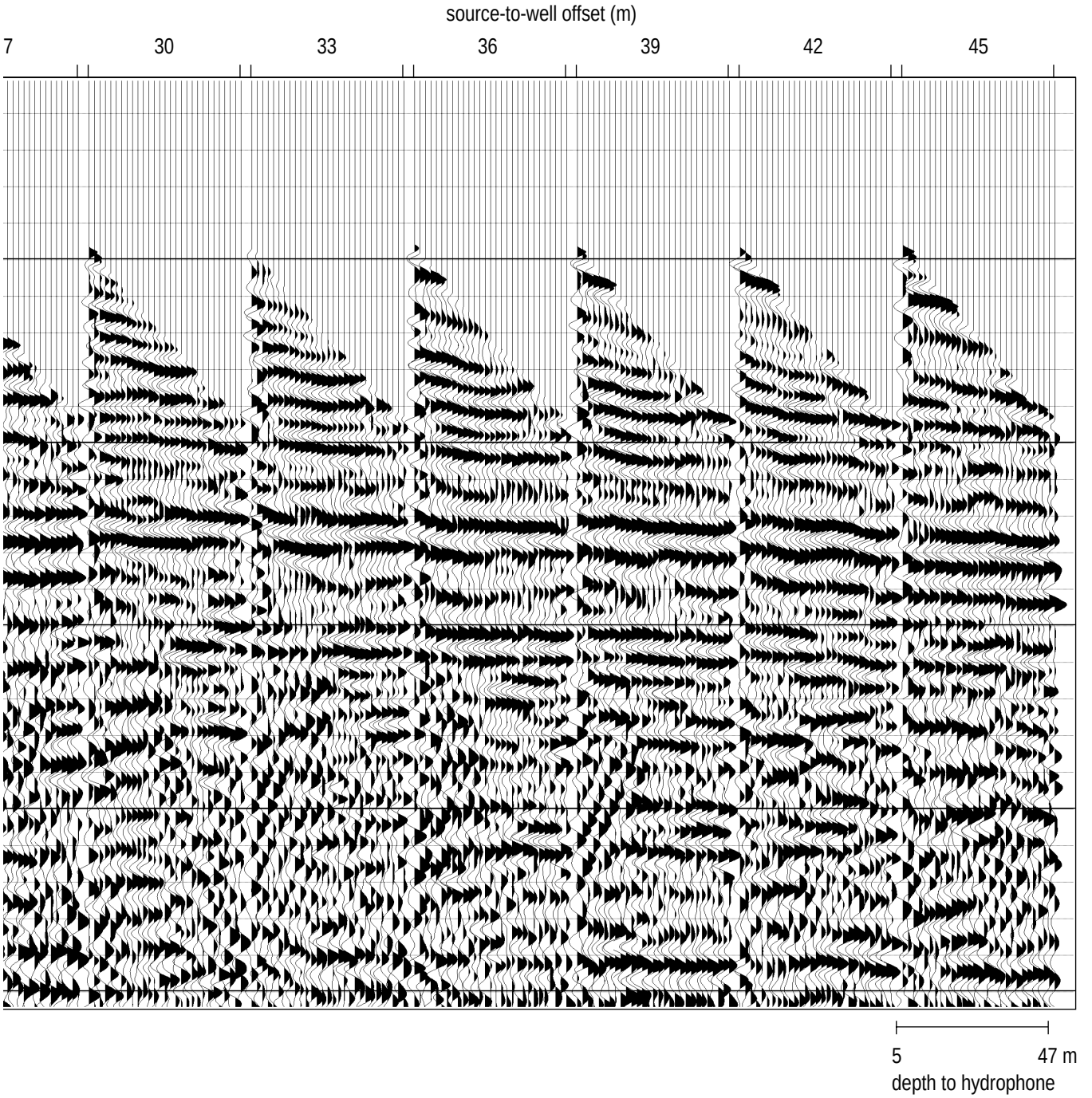
source-to-well offset (m)
7
30
33
36
39
42
45
5
47 m
depth to hydrophone

Figure B23c.

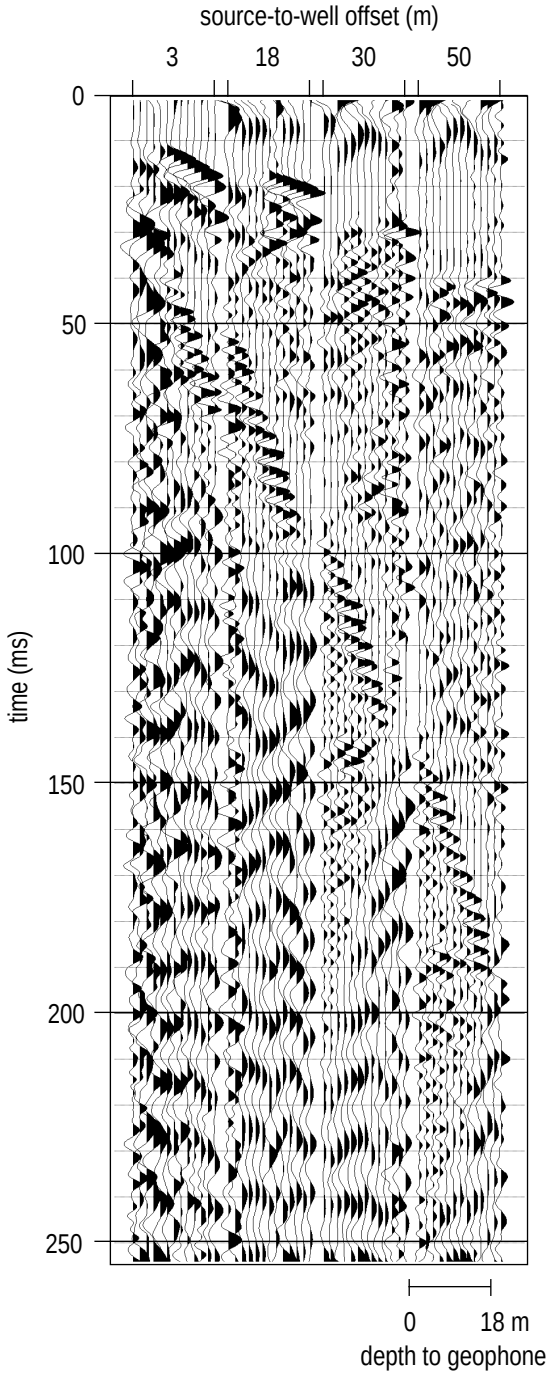

Figure B24. VSP #2 geophone data band-pass filtered (50 100 300 450) and AGC (50 ms) scaled. There are a total of 13 traces in each gather with depths from 0 m to 18 m.

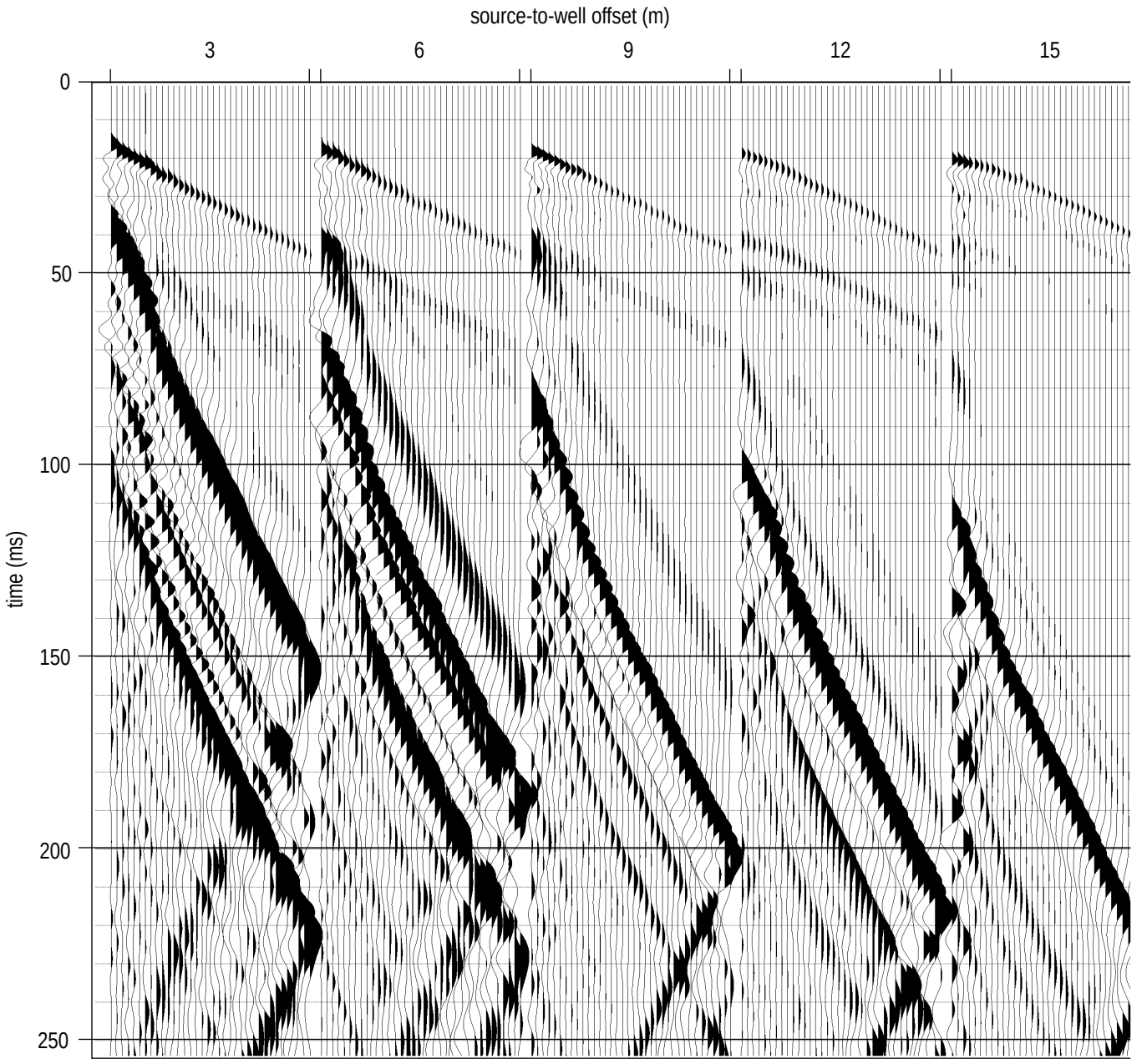

Figure B25a. VSP #3 raw hydrophone data. There are a total of 36 traces in each source offset gather with depths from 8 m to 60 m.

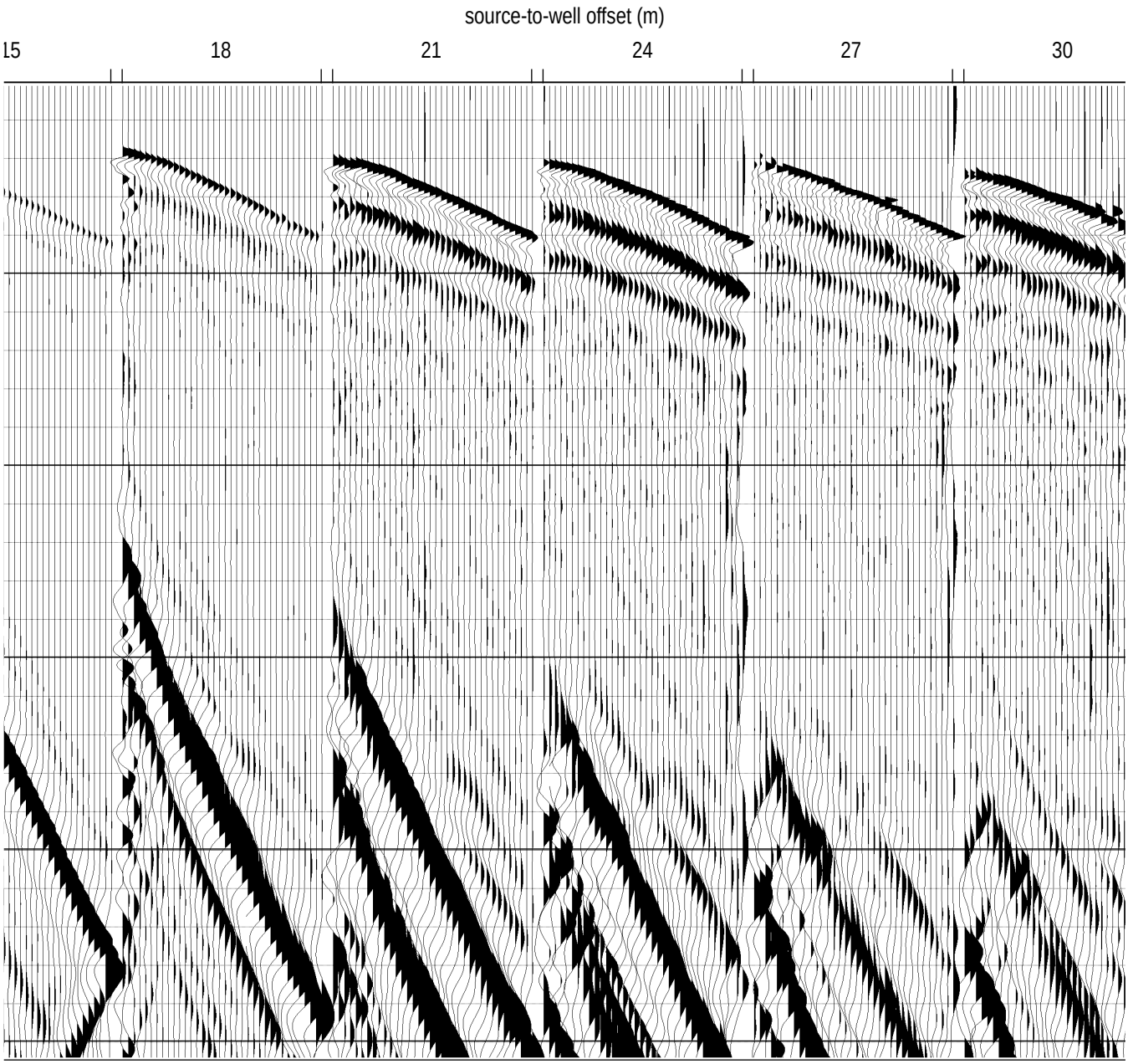

Figure B25b.

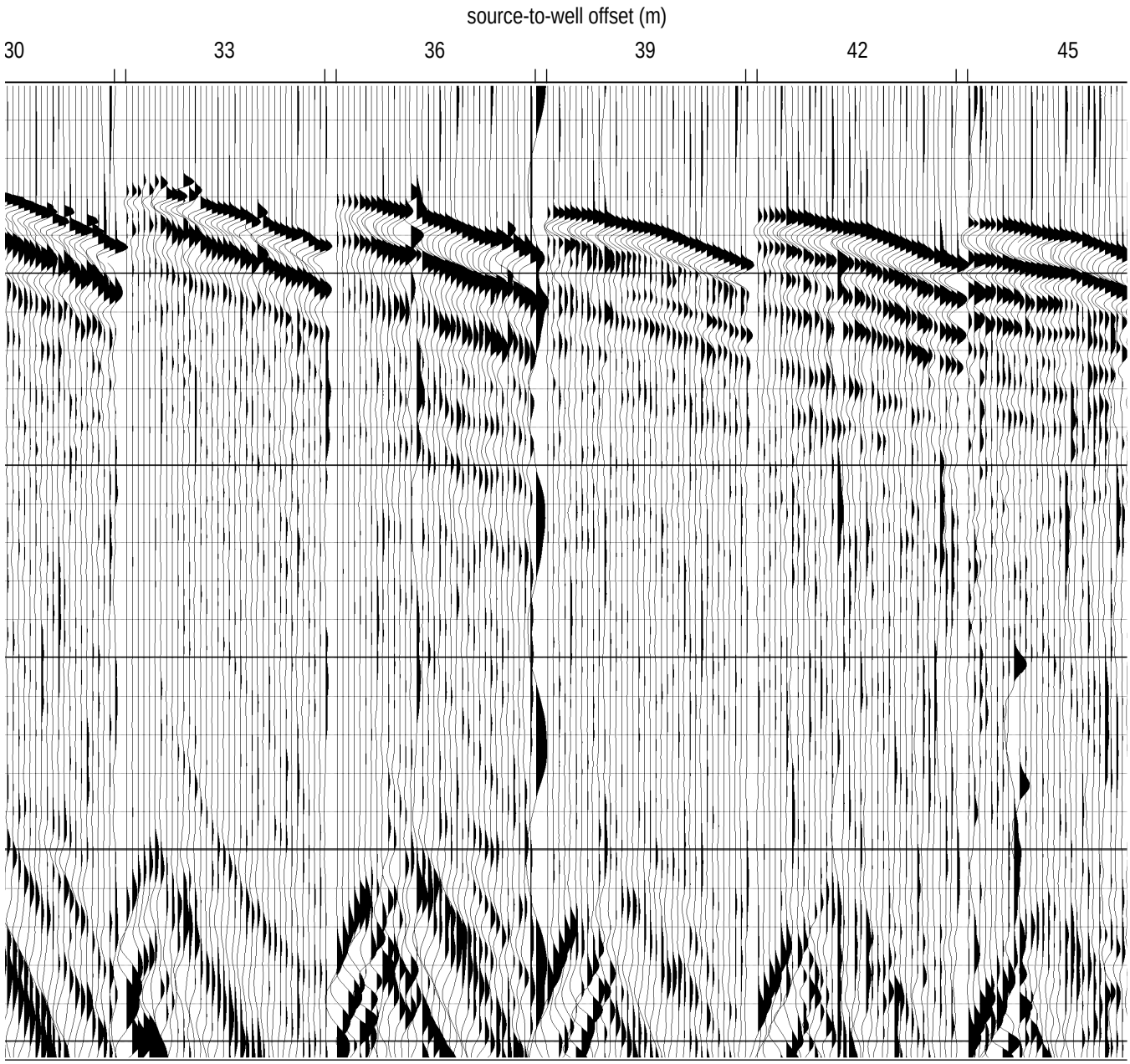

Figure B25c.

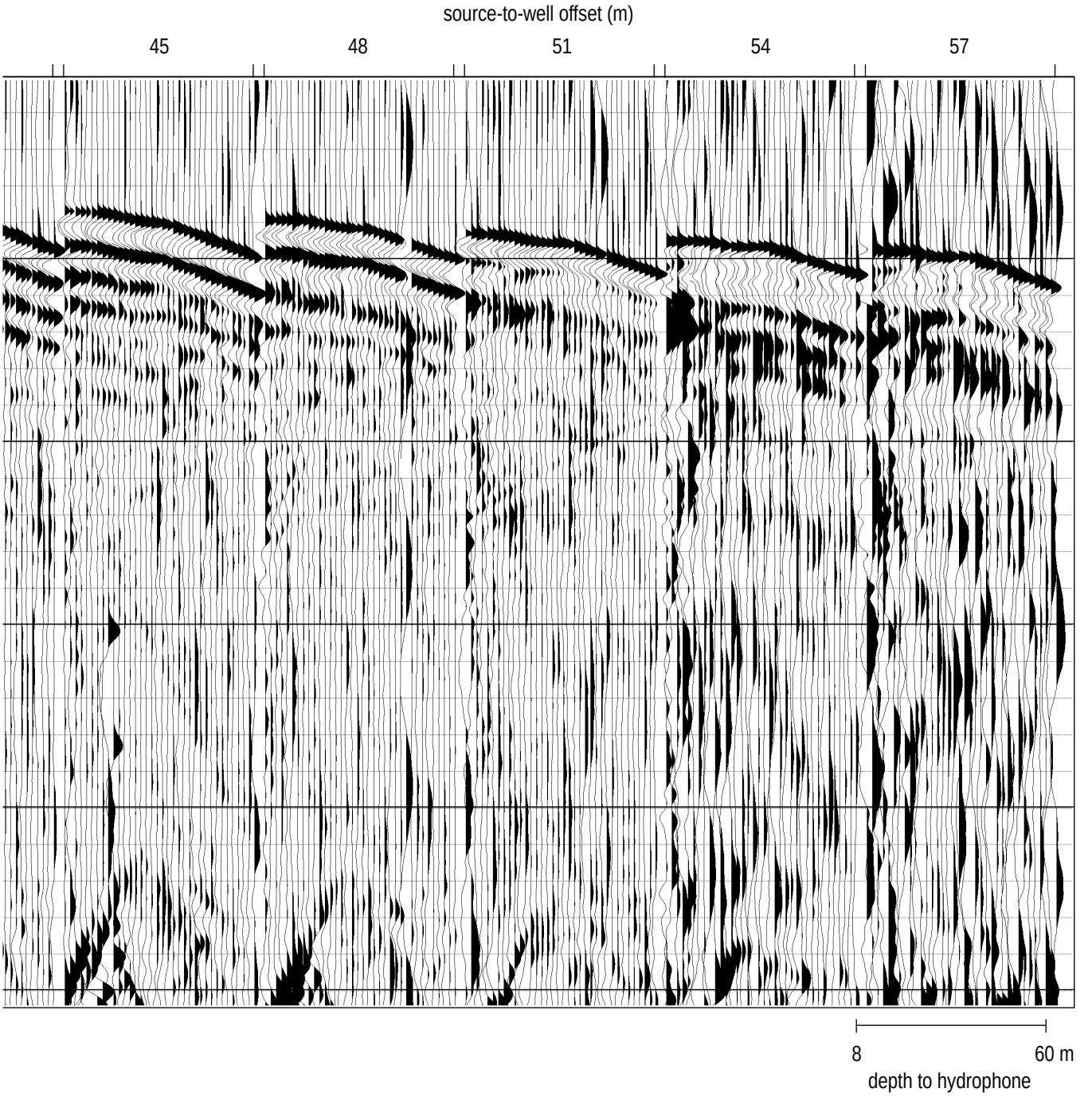
source-to-well offset (m)
45
48
51
54
57
8
60 m
depth to hydrophone

Figure B25d.

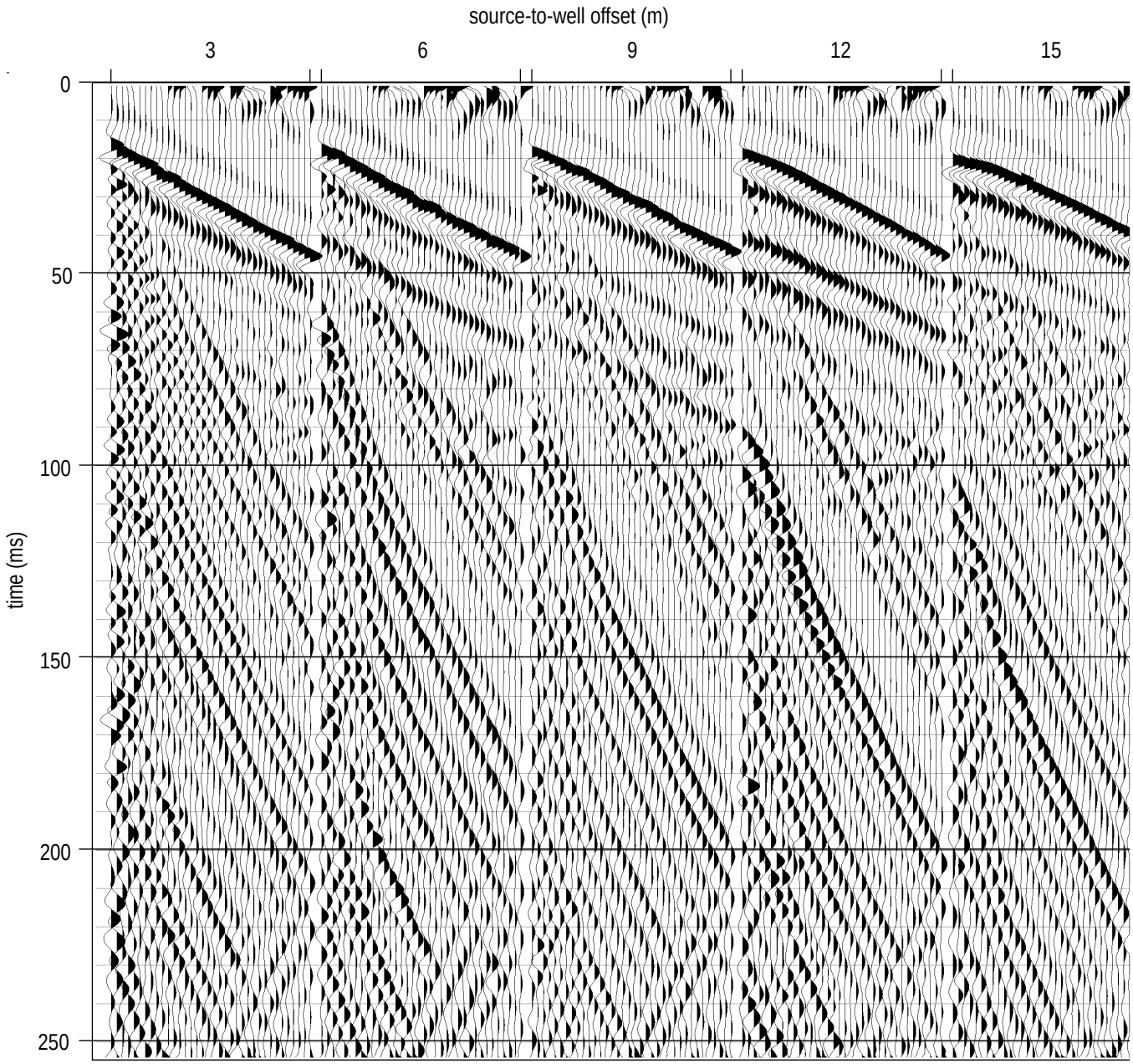

Figure B26a. VSP #3 raw hydrophone data. There are a total of 28 traces in each source offset gather with depths from 8 m to 60 m.

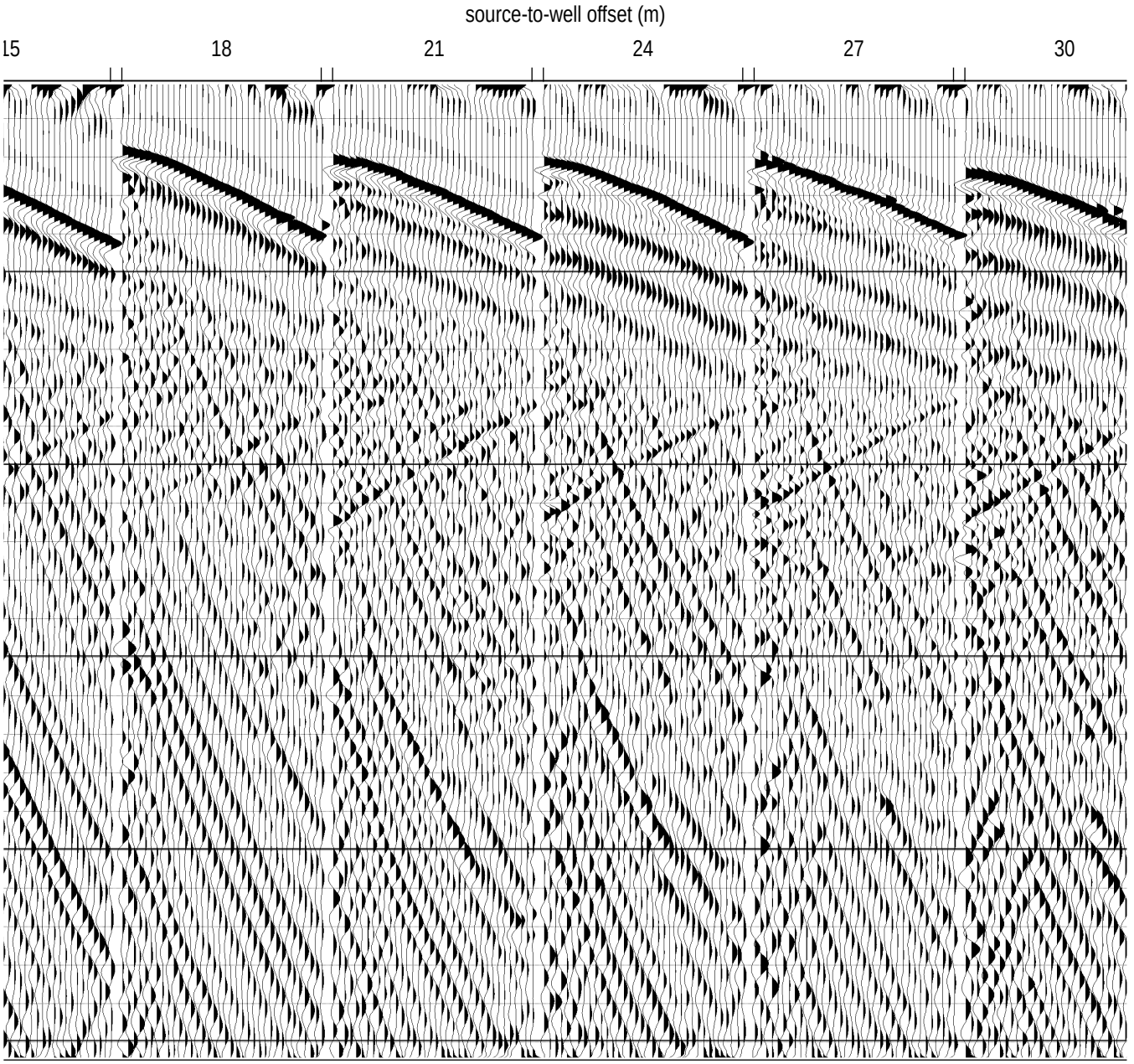

Figure B26b.

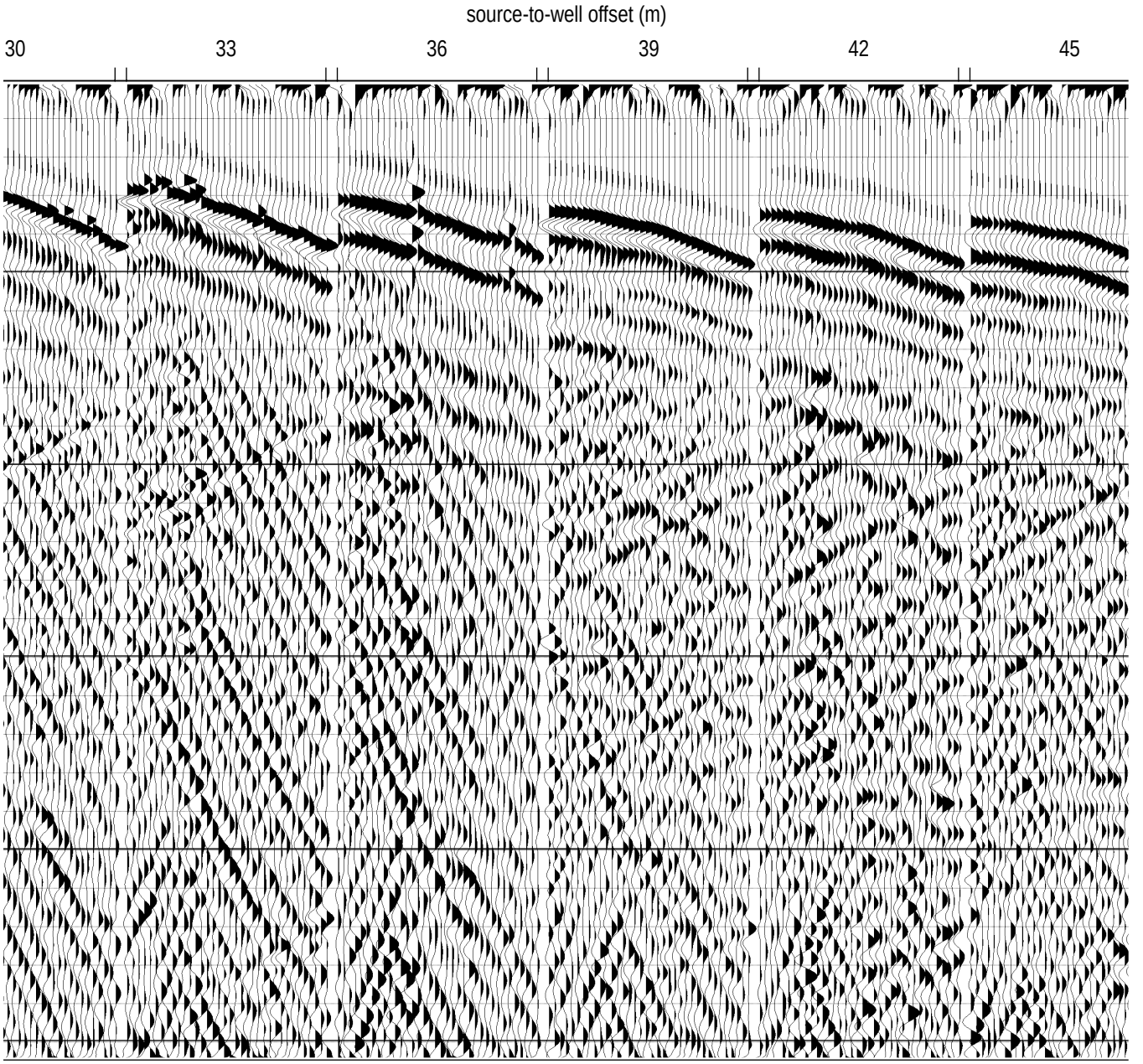

Figure B26c.

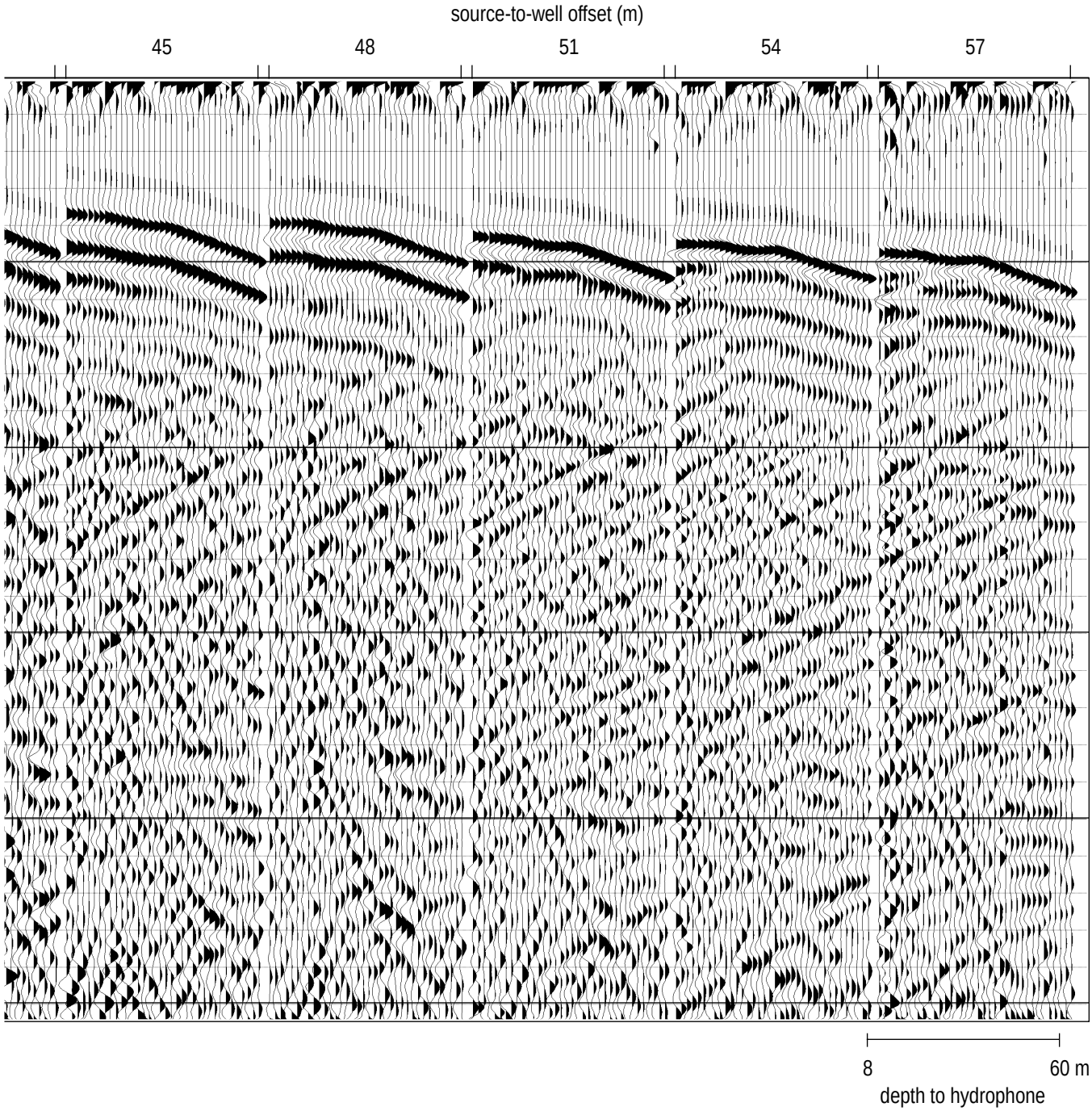
source-to-well offset (m)
45
48
51
54
57
8
60 m
depth to hydrophone

Figure B26d.

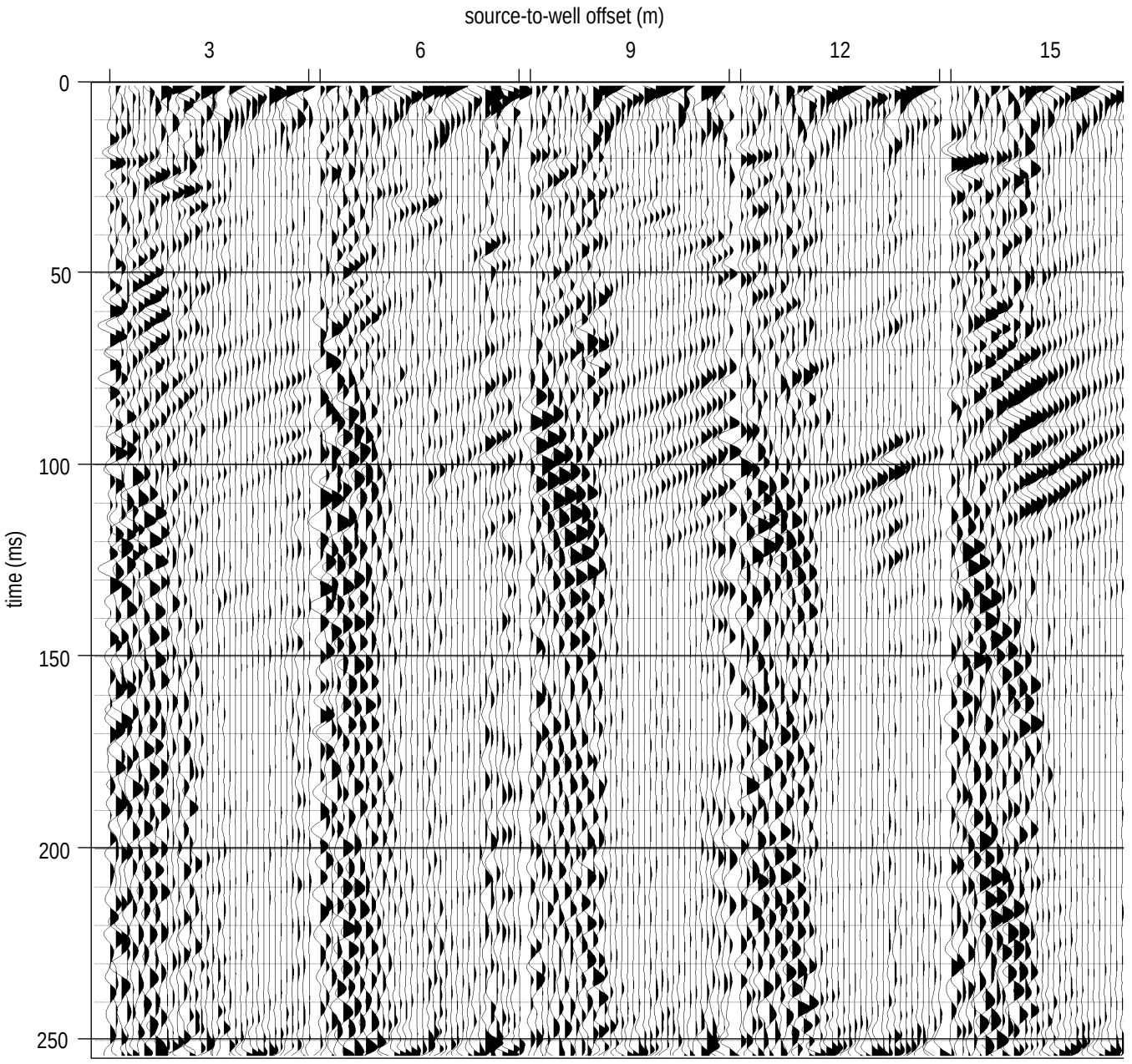

Figure B27a. VSP #3 hydrophone data (Figure B26) band-pass filtered (50 100 300 450) and AGC (50 ms) scaled.

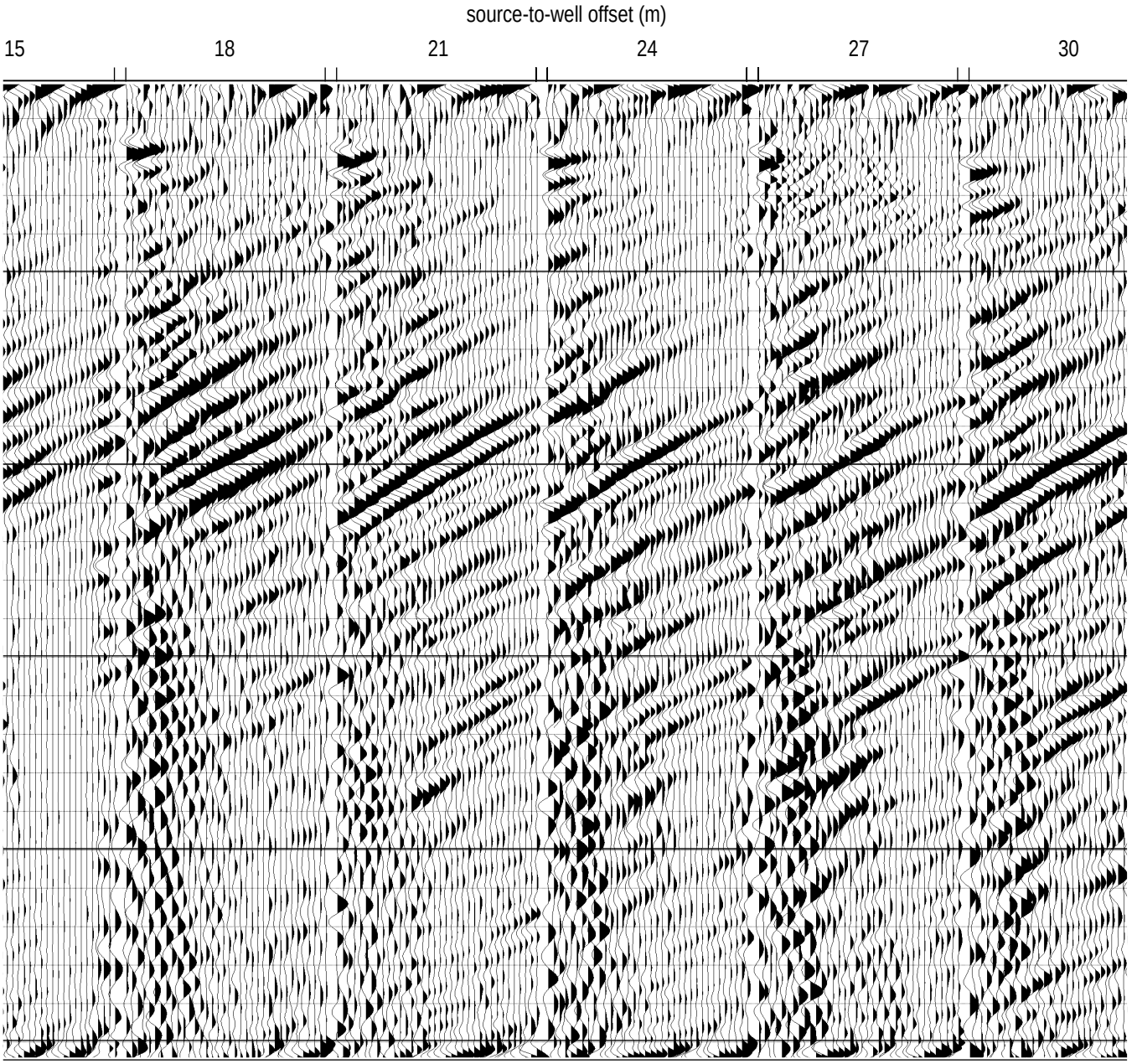

Figure B27b.

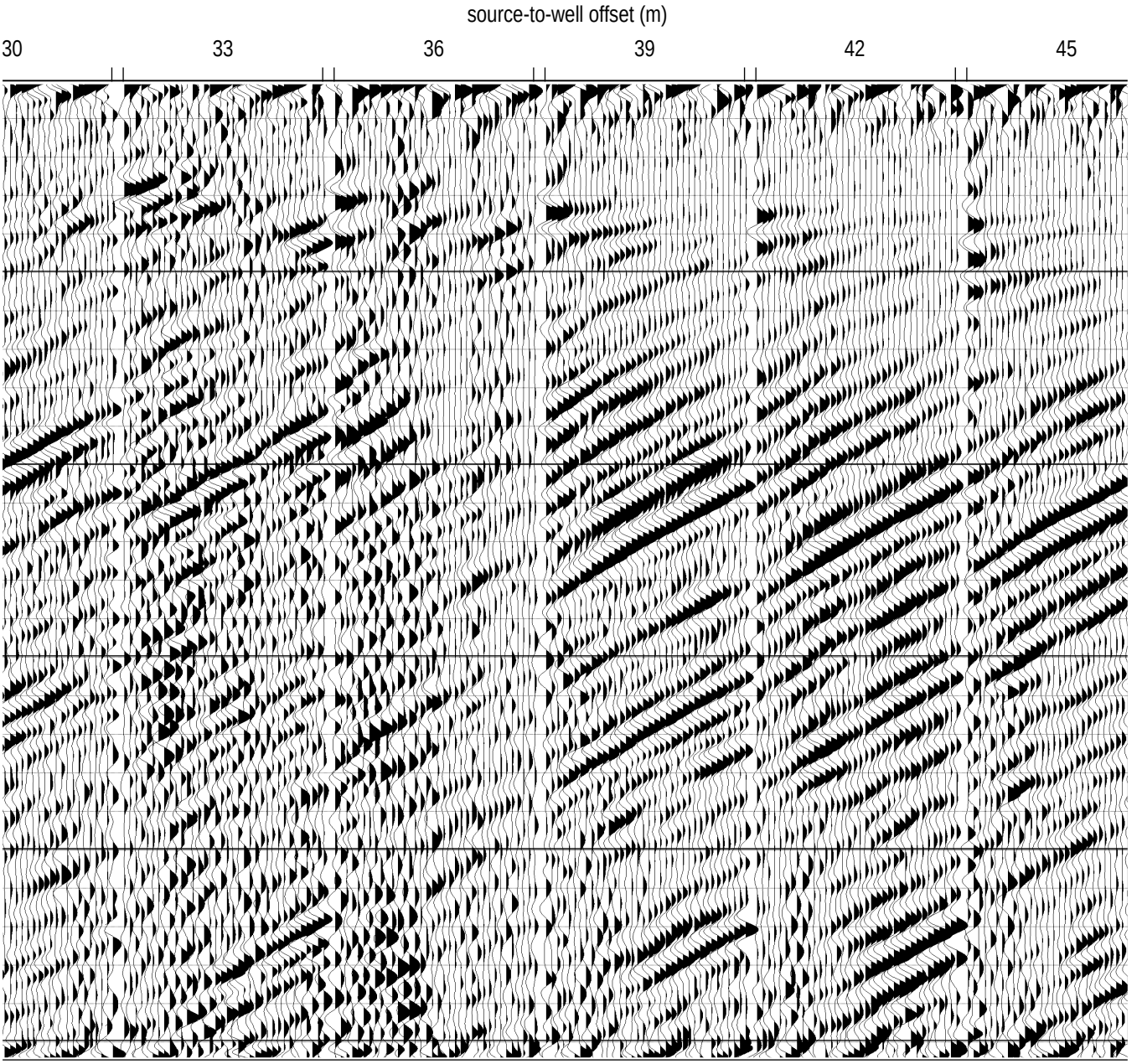

Figure B27c.

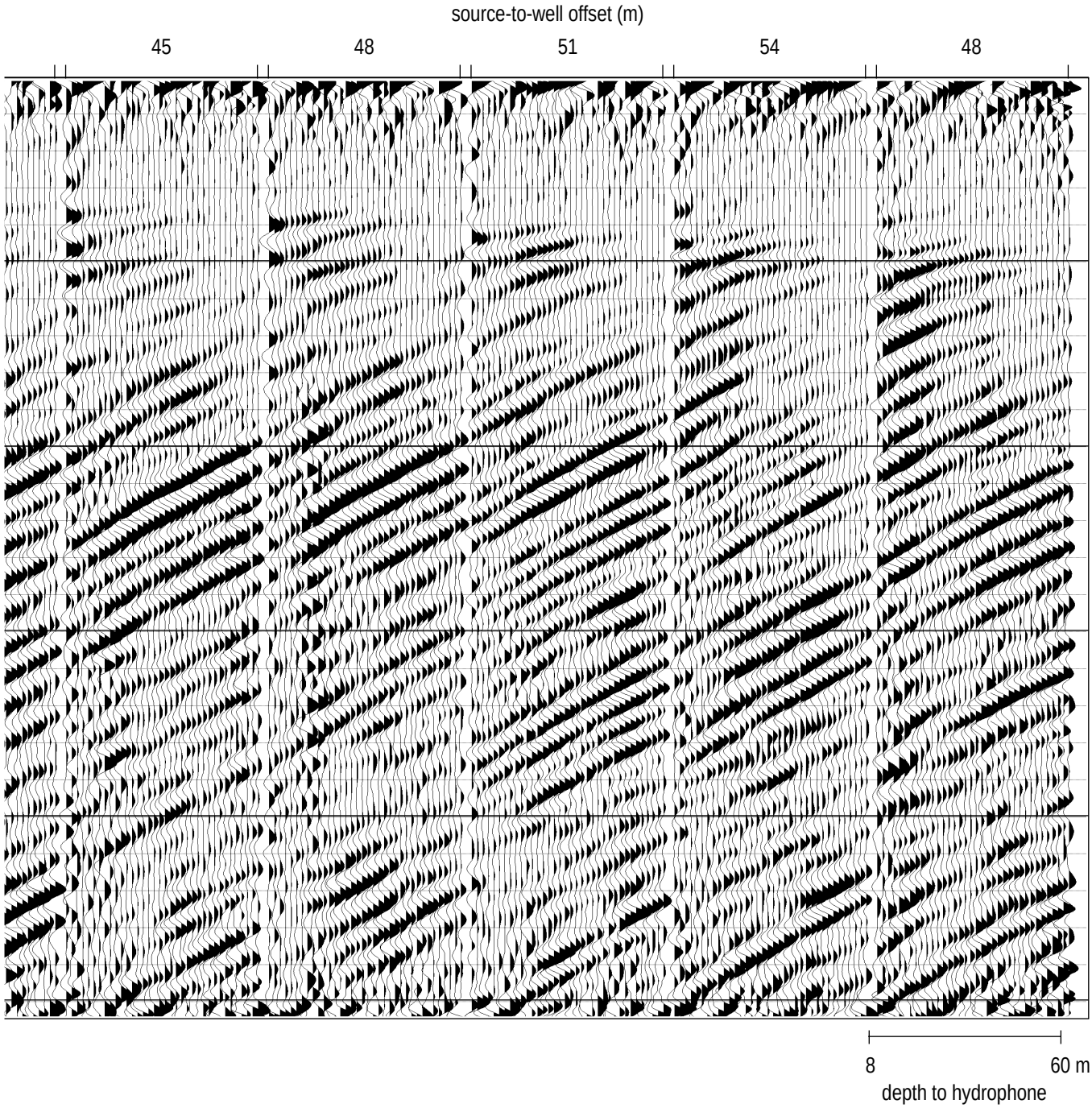
source-to-well offset (m)
45
48
51
54
48
8
60 m
depth to hydrophone

Figure B27d.

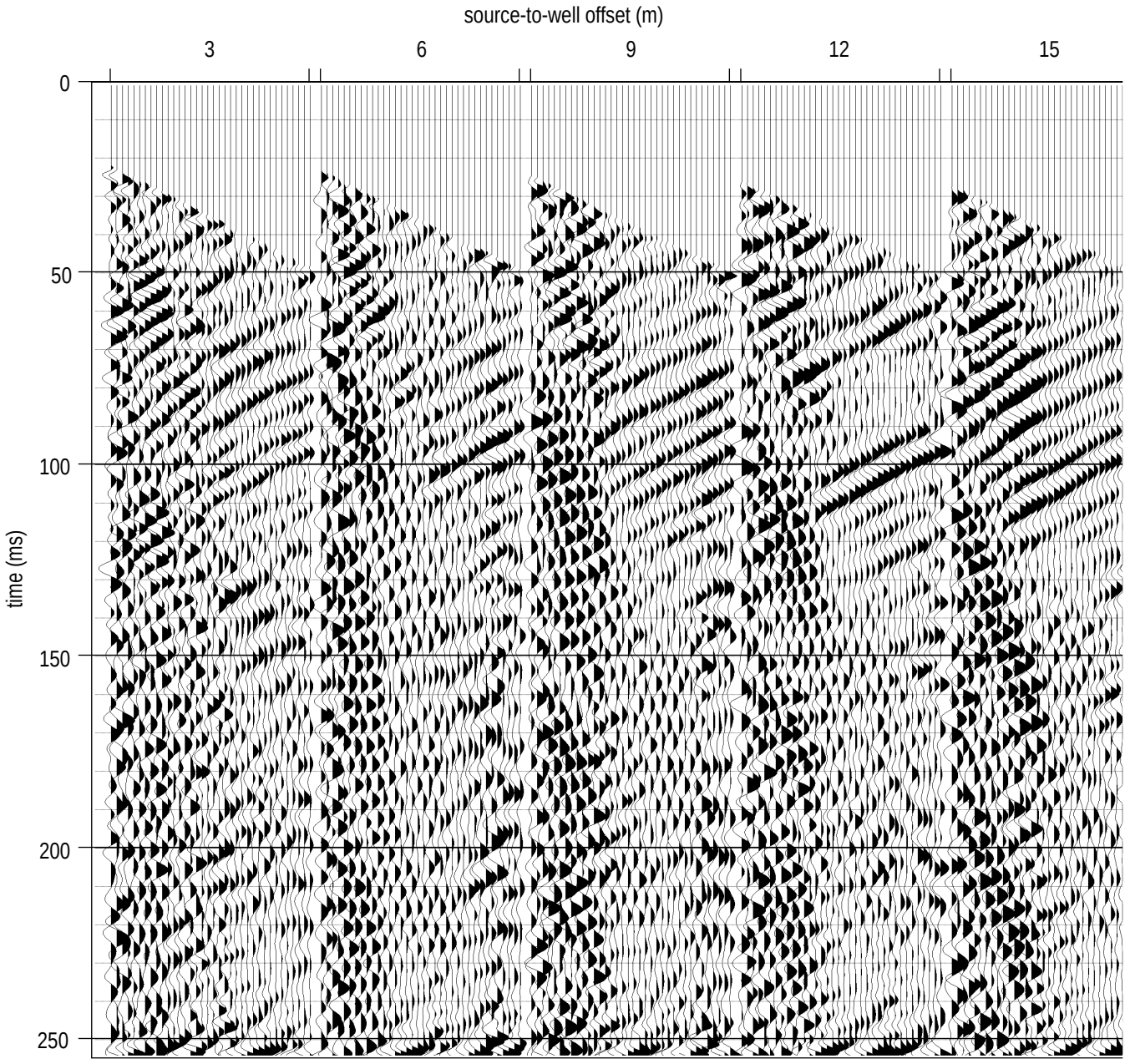

Figure B28a. VSP #3 up-coming waves. Two positive fan reject fk filters (0 – 1.5 ms/tr. and 2.0 – 4.0 ms/tr.) have been applied to filtered and scaled data (Figure B27) to eliminate down-going waves and one negative fan reject fk filter (-2.0 – -4.0 ms/tr.) has also been applied to the filtered data to take out strong up-coming tube waves.

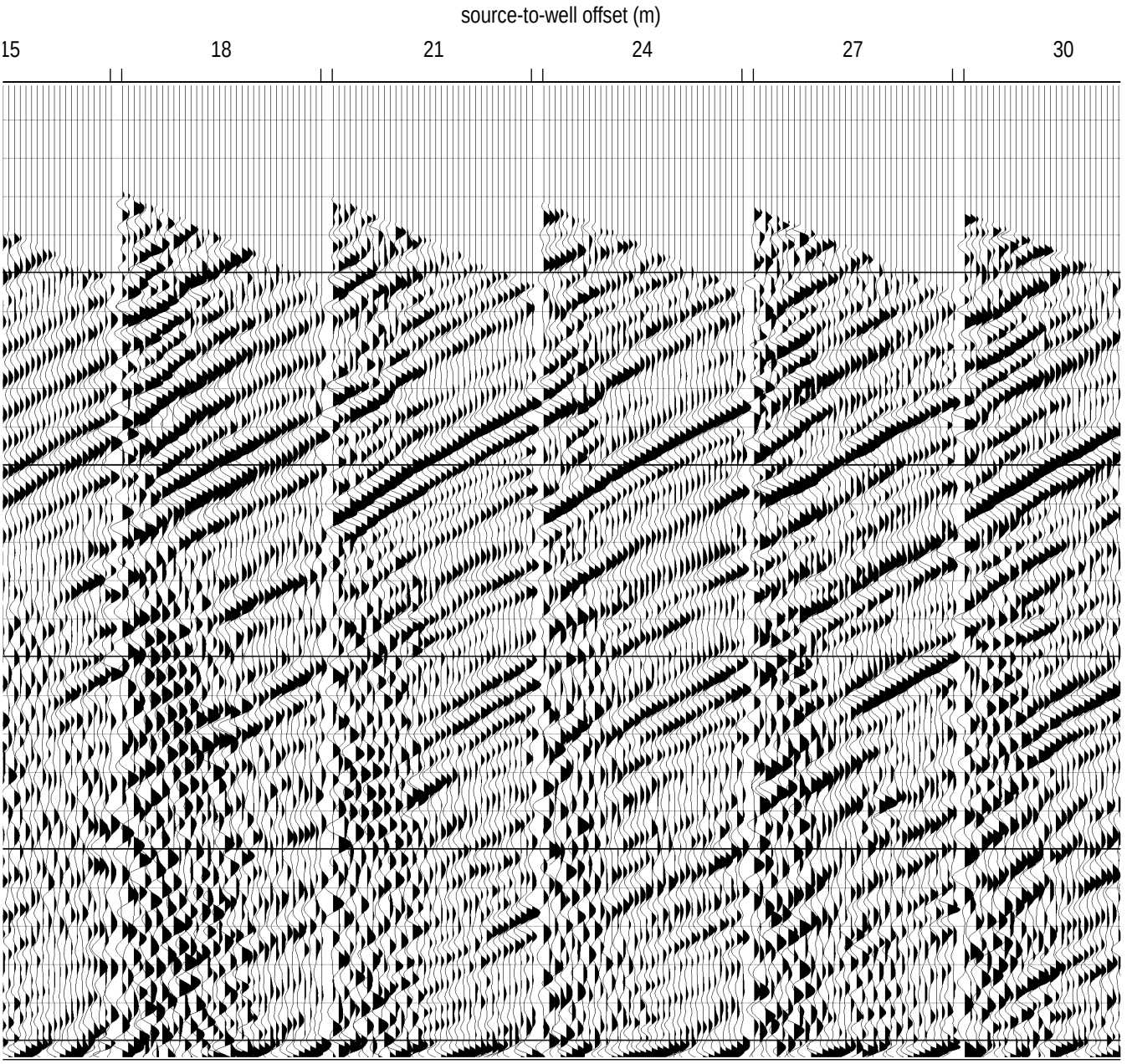

Figure B28b.

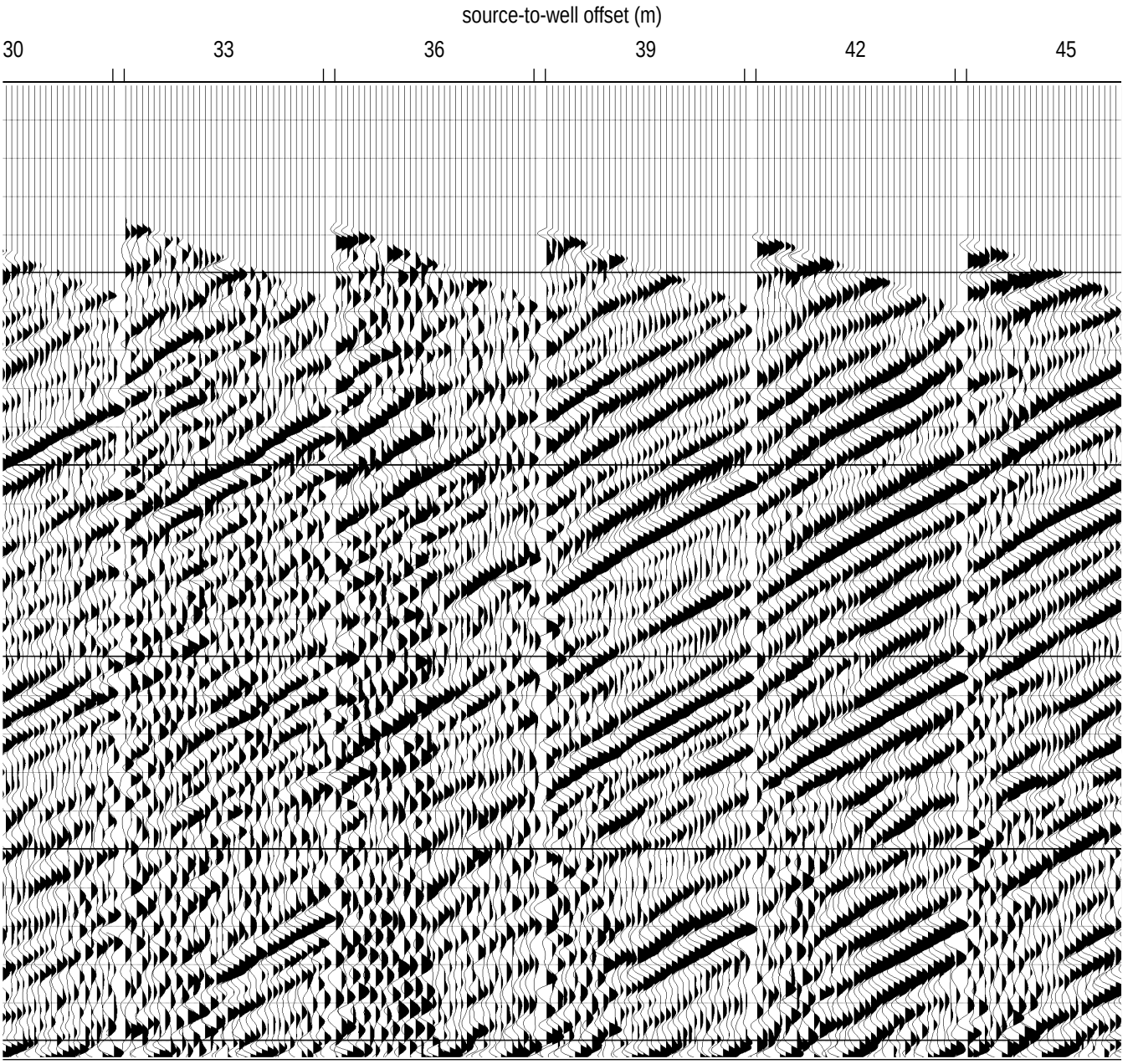

Figure B28c.

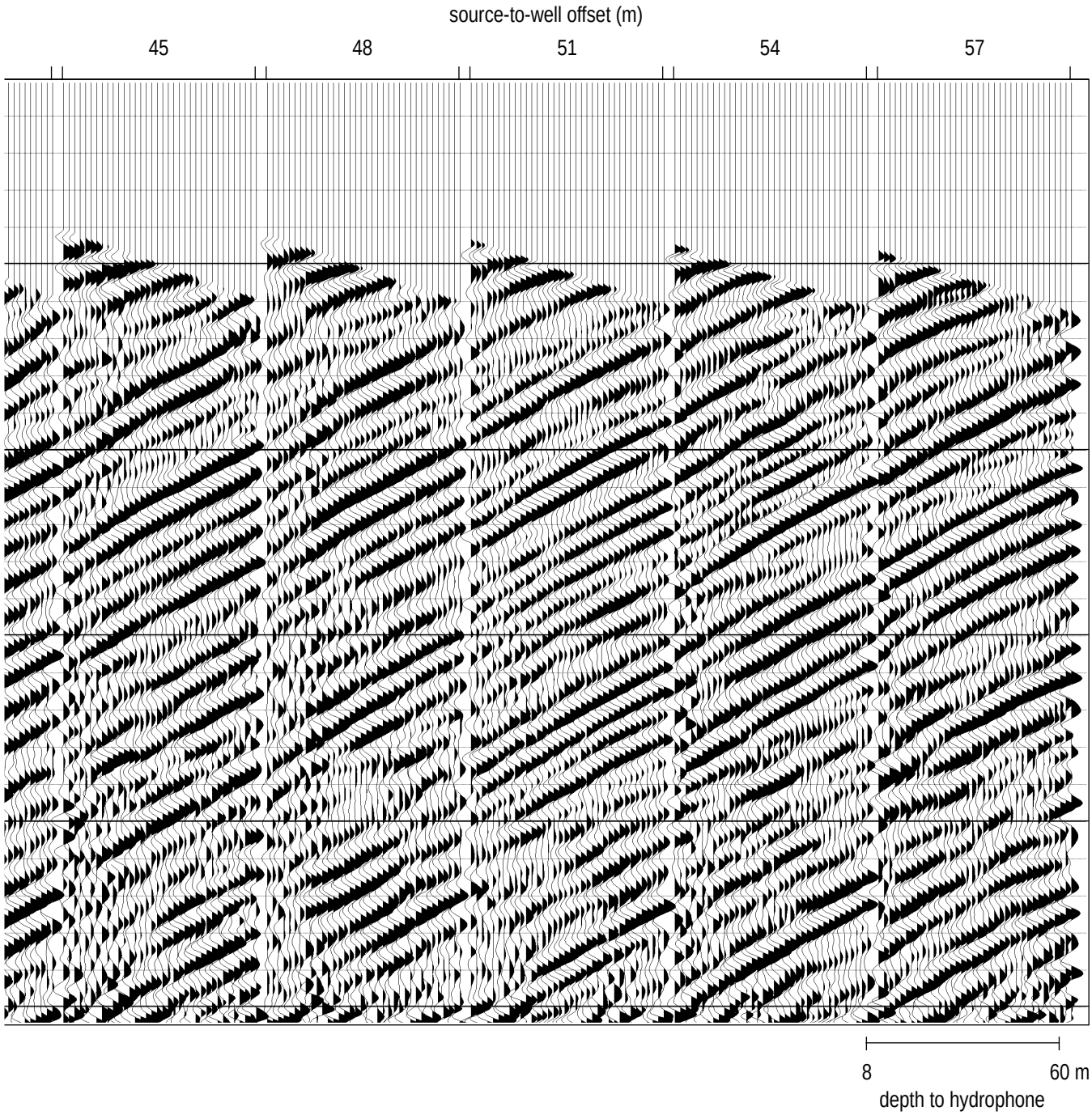
source-to-well offset (m)
45
48
51
54
57
8
60 m
depth to hydrophone

Figure B28d.

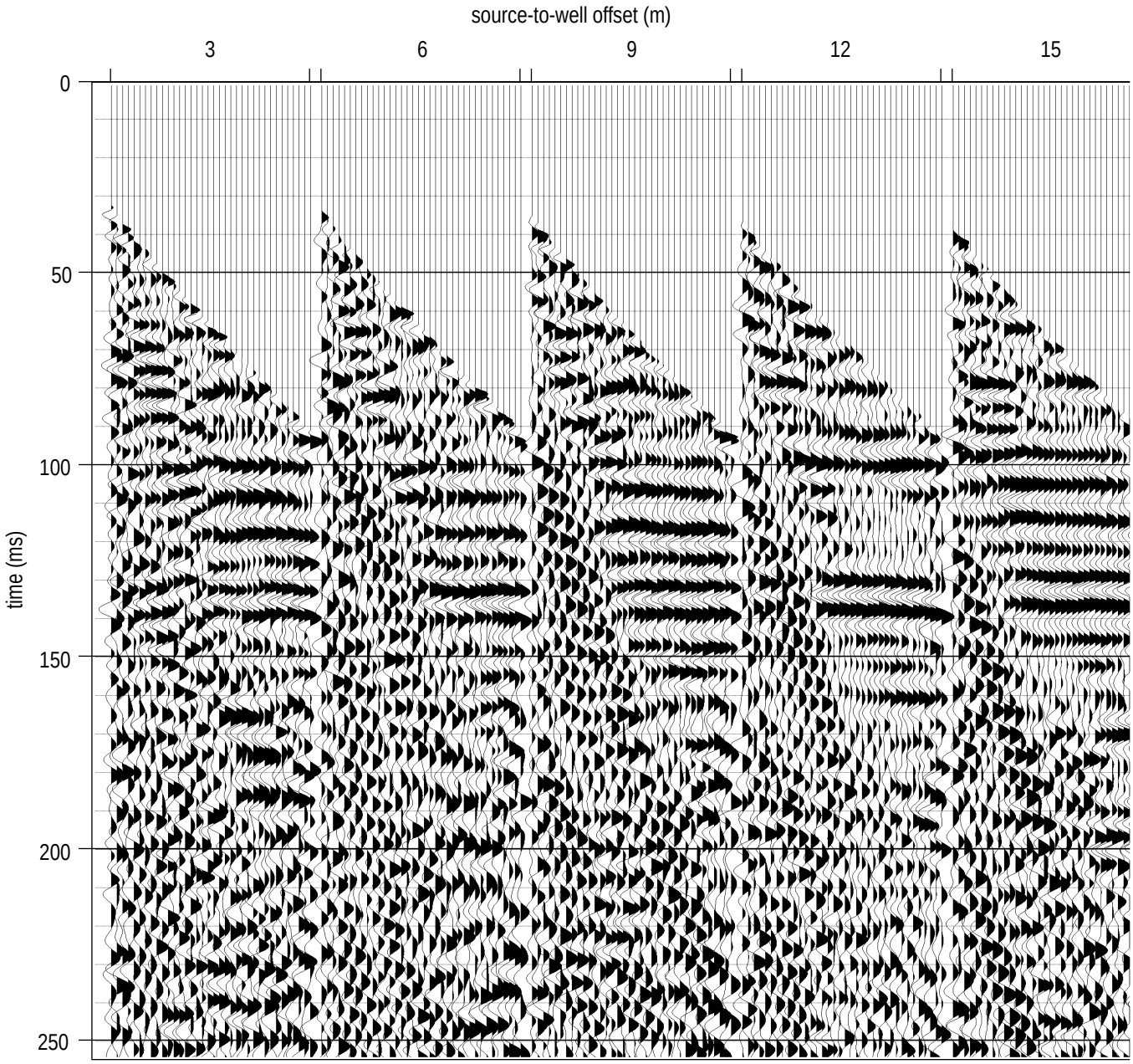

Figure B29a. VSP #3 hydrophone data first arrival muted. The first arrival mute is applied to fk filtered data (Figure B28).

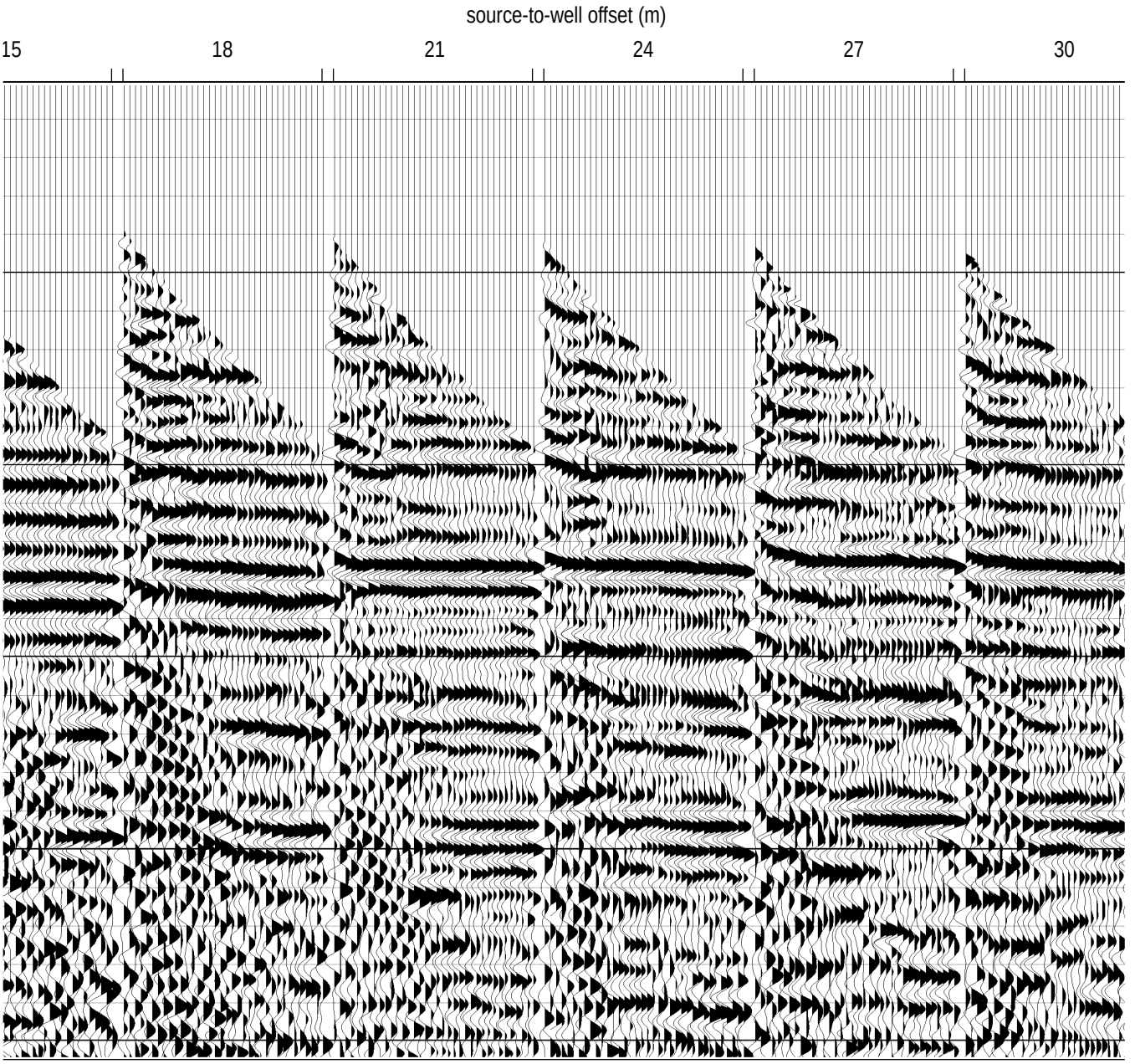

Figure B29b.

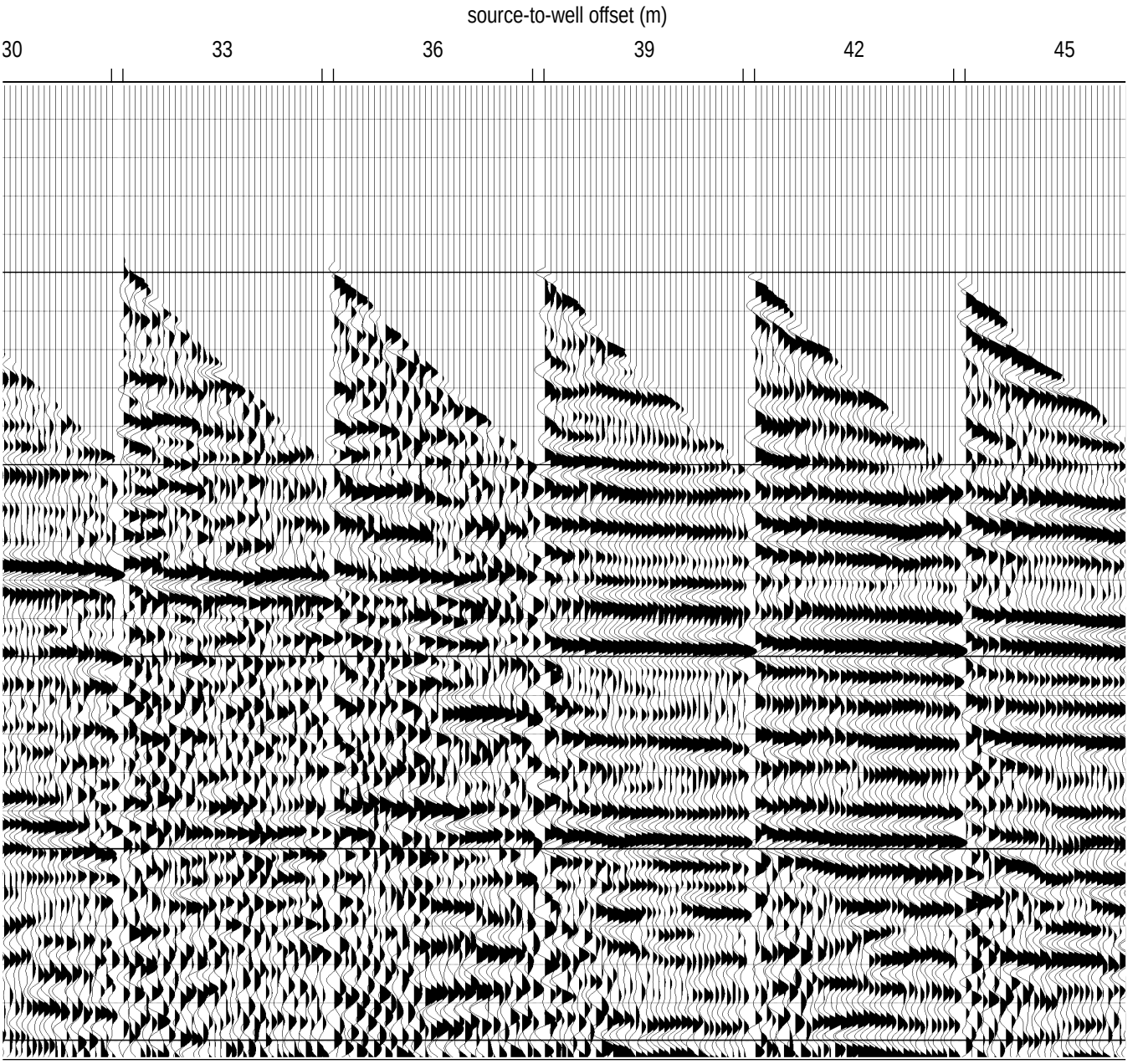

Figure B29c.

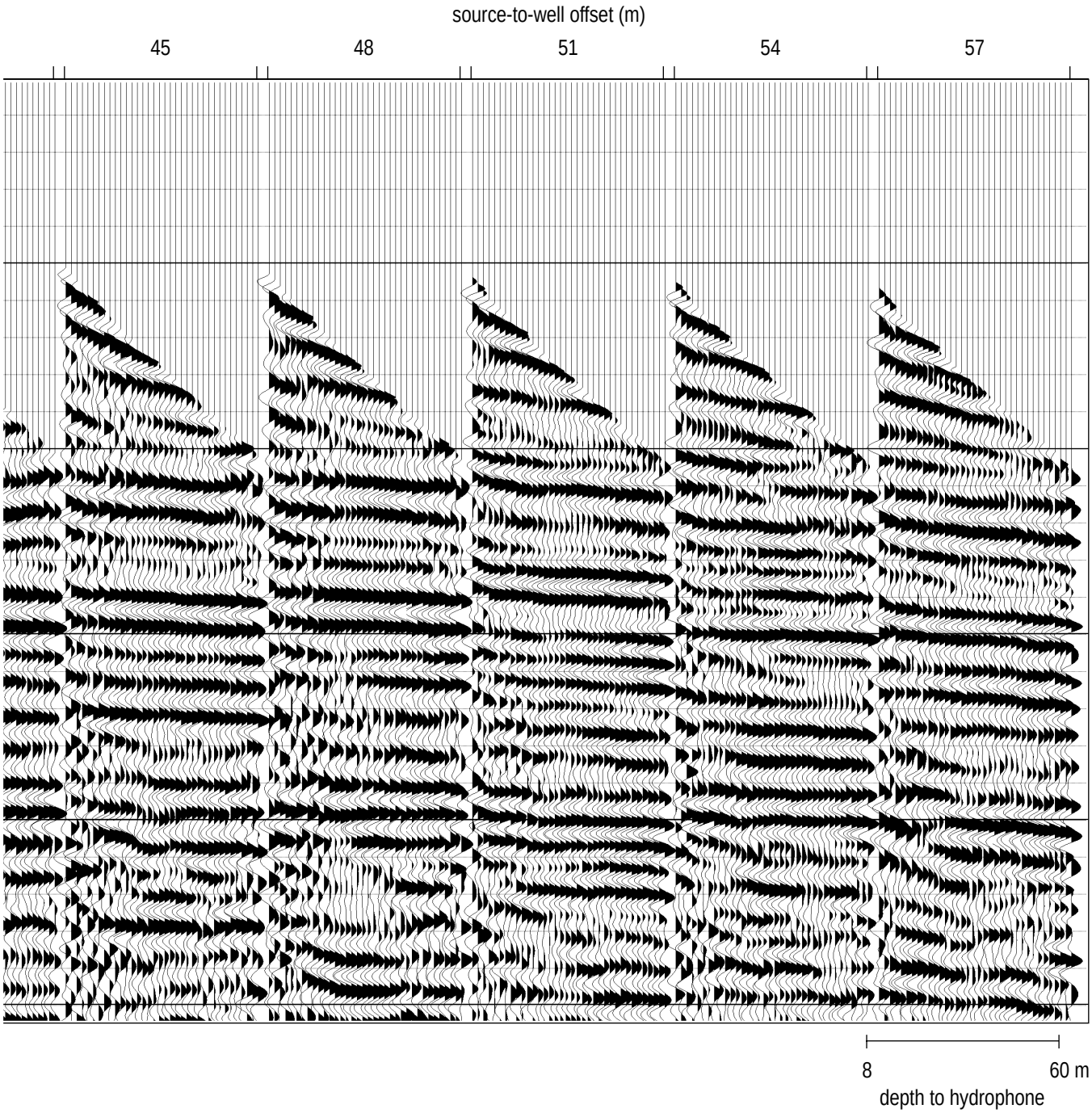
source-to-well offset (m)
45
48
51
54
57
8
60 m
depth to hydrophone

Figure B29d.

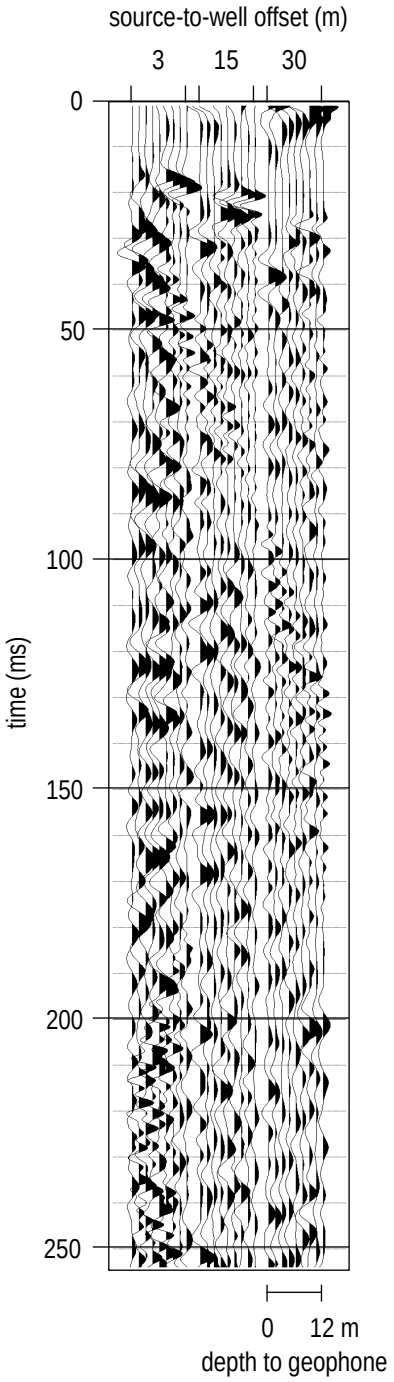

Figure B30. VSP #3 geophone data band-pass filtered (50 100 300 450) and AGC (50 ms) scaled. There are a total of 9 traces in each gather with depths from 0 m to 12 m.

Figure Captions

Figure 1. Site map of U.S. Marine Corps Air Station, Cherry Point, indicating the major roads, rivers, runways, seismic lines, and VSP wells.

Figure 2. Nominal 24-fold spot CDP stacked section of line 1 from site #1.

Figure 3. Nominal 24-fold spot CDP stacked section of line 2 from site #3.

Figure 4. Nominal 24-fold spot CDP stacked section of line 3. Section instrumental in location of VSP #2 well.

Figure 5. Interpreted nominal 24-fold spot CDP stacked section of line 3. Section instrumental in location of VSP #2 well.

Figure 6. Nominal 24-fold spot CDP stacked section of line 4.

Figure 7. Nominal 24-fold spot CDP stacked section of line 5.

Figure 8. Nominal 24-fold spot CDP stacked section of line 6.

Figure 9. Interpreted nominal 24-fold spot CDP stacked section of line 6.

Figure 10. Nominal 24-fold spot CDP stacked section of line 7.

Figure 11. Interpreted nominal 24-fold spot CDP stacked section of line 7.

Figure 12. Nominal 24-fold spot CDP stacked section of line 8.

Figure 13. Interpreted nominal 24-fold spot CDP stacked section of line 8.

Figure 14. Nominal 24-fold spot CDP stacked section of line 9.

Figure 15. Nominal 24-fold spot CDP stacked section of line 10.

Figure 16. Nominal 24-fold spot CDP stacked section of line 11. In part responsible for placement of VSP #1 well.

Figure 17. Interpreted nominal 24-fold spot CDP stacked section of line 11. In part responsible for placement of VSP #1 well.

Figure 18. Nominal 24-fold spot CDP stacked section of line 12.

Figure 19. Interpreted nominal 24-fold spot CDP stacked section of line 12.

Figure 20. Nominal 24-fold spot CDP stacked section of line 13.

Figure 21. Interpreted nominal 24-fold spot CDP stacked section of line 13.

Figure 22. VSP files with 18 m source offset showing (a) raw data, (b) filtered and scaled, (c) fk filtering, (d) filtering and muting, (e) static correction, and (f) corridor stack from well VSP #1.

Figure 23. VSP files with 18 m source offset showing (a) raw data, (b) filtered and scaled, (c) fk filtering, (d) filtering and muting, (e) static correction, and (f) corridor stack from well VSP #2.

Figure 24. VSP files with 18 m source offset showing (a) raw data, (b) filtered and scaled, (c) fk filtering, (d) filtering and muting, (e) static correction, and (f) corridor stack from well VSP #3.

Figure 25. AGC scaled field files from two different places on line 1A. The reflection arrivals are evident on both records. Evident from

Appendix A

Figure A12. Combined forward and reverse polarity S-wave field files with every other variable wiggle trace reversed to allow visual inspection of polarization and coherence of potential reflection events. The only potential reflection that can be identified with any degree of confidence has a zero offset time of about 180 msec. The S-wave mini block source was recorded with analog low-cut filters (a) out, (b) 50 Hz, and (c) 100 Hz.

Figure A13. S-wave shot gather of Figure A11 with a 25-50, 125-250 Hz digital filter and 100 msec AGC scale applied. Digital filtering did little to enhance potential reflection events evident with this display format.

Figure A14. S-wave shot gather of Figure A12 with a 25-50, 125-250 Hz digital filter and 100 msec AGC scale applied. Digital filtering did little to enhance potential reflection events evident on raw data. Some suggestion of reflections on data acquired with no analog low-cut are interpretable with vertical incident times between 150 and 250 msec.

Appendix B

Figure B1. Interval velocity plot of VSP #1 using the hydrophone receiver.

Figure B2. Average velocity plot of VSP #1 using the hydrophone receiver.

Figure B3. Interval velocity plot of VSP #1 using the hole-lock geophone.

Figure B4. Average velocity plot of VSP #1 using the hole-lock geophone.

Figure B5. Interval velocity plot of VSP #2 using the hydrophone receiver.

Figure B6. Average velocity plot of VSP #2 using the hydrophone receiver.

Figure B7. Interval velocity plot of VSP #2 using the hole-lock geophone.

Figure B8. Average velocity plot of VSP #2 using the hole-lock geophone.

Figure B9. Interval velocity plot of VSP #3 using the hydrophone receiver.

Figure B10. Average velocity plot of VSP #3 using the hydrophone receiver.

Figure B11. Interval velocity plot of VSP #3 using the hole-lock geophone.

Figure B12. Average velocity plot of VSP #3 using the hole-lock geophone.

Figure B13. VSP #1 raw hydrophone data. There are a total of 28 traces in each source offset gather with depths from 8 m to 48 m.

Figure B14. VSP #1 hydrophone data (Figure B13) band-pass filtered (50 100 300 450) and AGC (50 ms) scaled.

Figure B15. VSP #1 up-coming waves. Two positive fan reject fk filters (0 to 1.5 ms/tr. and 2.0 – 4.0 ms/tr.) have been applied to filtered and scaled data (Figure B14) to eliminate down-going waves and one negative fan reject fk filter (-2.0 – -4.0 ms/tr.) has also been applied to the filtered data to take out strong up-coming tube waves.

Figure B16. VSP #1 hydrophone data first arrival muted. The first arrival mute is applied to fk filtered data (Figure B15).

Figure B17. VSP #1 hydrophone data static corrected to vertical incidence. The static correction is applied to first arrival data, datum correcting all hydrophones to the well head.

Figure B18. VSP #1 geophone data band-pass filtered (50 100 300 450) and AGC (50 ms) scaled. There are a total of 6 traces in each gather with depths from 2 m to 18 m.

Figure B19. VSP #2 raw hydrophone data. There are a total of 29 traces in each source offset gather with depths from 5 m to 47 m.

Figure B20. VSP #2 hydrophone data (Figure B19) band-pass filtered (50 100 300 450) and AGC (50 ms) scaled.

Figure B21. VSP #2 up-coming waves. Two positive fan reject fk filters (0 to 1.5 ms/tr. and 2.0 – 4.0 ms/tr.) have been applied to filtered and scaled data (Figure B20) to eliminate down-going waves and one negative fan reject fk filter (-2.0 – -4.0 ms/tr.) has also been applied to the filtered data to take out strong up-coming tube waves.

Figure B22. VSP #2 hydrophone data first arrival muted. The first arrival mute is applied to fk filtered data (Figure B21).

Figure B23. VSP #2 hydrophone data static corrected to vertical incidence. The static correction is applied to first arrival data, datum correcting all hydrophones to the well head.

Figure B24. VSP #2 geophone data band-pass filtered (50 100 300 450) and AGC (50 ms) scaled. The numbers on the top of each panel are source-to-well offsets. There are a total of 13 traces in each gather with depths from 0 m to 18 m.

Figure B25. VSP #3 raw hydrophone data. There are a total of 36 traces in each source offset gather with depths from 8 m to 60 m.

Figure B26. VSP #3 raw hydrophone data. There are a total of 28 traces in each source offset gather with depths from 8 m to 48 m.

Figure B27. VSP #3 hydrophone data (Figure B26) band-pass filtered (50 100 300 450) and AGC (50 ms) scaled.

Figure B28. VSP #3 up-coming waves. Two positive fan reject fk filters (0 to 1.5 ms/tr. and 2.0 – 4.0 ms/tr.) have been applied to filtered and scaled data (Figure B27) to eliminate down-going waves and one negative fan reject fk filter (-2.0 – -4.0 ms/tr.) has also been applied to the filtered data to take out strong up-coming tube waves.

Figure B29. VSP #3 hydrophone data first arrival muted. The first arrival mute is applied to fk filtered data (Figure B28).

Figure B30. VSP #3 geophone data band-pass filtered (50 100 300 450) and AGC (50 ms) scaled. There are a total of 9 traces in each gather with depths from 0 m to 12 m.